DISSERTATION

ICE NUCLEATING PARTICLES IN THE ARCTIC: MEASUREMENT AND SOURCE TRACKING

Submitted by

Kevin Robert Barry

Department of Atmospheric Science

In partial fulfillment of the requirements

For the Degree of Doctor of Philosophy

Colorado State University

Fort Collins, Colorado

Summer 2024

Doctoral Committee:

Advisor: Sonia Kreidenweis
Co-Advisor: Paul DeMott

Susan van den Heever
Emily Fischer
Pankaj Trivedi

ABSTRACT

ICE NUCLEATING PARTICLES IN THE ARCTIC: MEASUREMENT AND SOURCE TRACKING

The Arctic landscape is rapidly changing in a warming climate, with sea ice melting and permafrost thawing. Its near-surface air temperature is warming 3.8 times faster than other regions around the world. This rapid warming is known as Arctic amplification. Clouds contribute to this amplification, with their presence and phase is important for determining the surface energy budget. Arctic mixed-phase clouds can last for several days but are not represented well in climate models. Special aerosols, called ice nucleating particles (INPs) trigger ice formation in the atmosphere at temperatures warmer than -38 °C, and thus are important for determining the initiation, lifetime, and radiative properties of these clouds. Observations of INPs, especially over the central Arctic, are limited, and many sources are unknown. This dissertation has the overarching goal of increasing understanding of Arctic INPs. This is achieved through first presenting a full year of INP measurements in the central Arctic, as well as a full year of their composition, using coincident sampling of bacteria and fungi to gain insight into airmass origin. Next, some of the potentially most active Arctic INP sources are explored. Permafrost, which was known previously to contain high levels of INPs, was tested for its activity and persistence in water, and ability to be aerosolized through bubble bursting over several weeks. Then, sources of INPs were surveyed in a region that is controlled by permafrost (a thermokarst landscape). This included field measurements of permafrost, vegetation, sediment, active layer soil, water, and aerosol samples. A high temperature heat test was developed as a diagnostic tool to differentiate sources. Coincidentally, clean working methods to

measure INPs were optimized, as efforts to reduce contamination are needed to accurately sample in this region. The main findings from this work suggest a regionally relatively homogenous population of Arctic INPs at most times of year, which is encouraging for efforts to represent them in numerical models across scales and understand their changes in the future. Permafrost-sourced INPs showed high activity and were enhanced near the coast. Unexpectedly, other components of the thermokarst landscape were found to be rich, organic INP reservoirs, emphasizing that the Arctic tundra is a diverse collection of potential contributors to the aerosol.

ACKNOWLEDGEMENTS

Words cannot express my fullest acknowledgements here. Over my time at CSU in the past 7 years, I have learned and continue to learn a lot, both in the fields of ice nucleation and microbiology, but also about myself. I am much more confident now presenting my research and writing, and in passing on some of what I learned to others. I came into CSU with no previous laboratory experience, and I have been fortunate to have been taught a lot. From my first field experience in WE-CAN, getting to work with, in particular Ezra Levin, he was very patient with me and helped me have confidence in operating the CFDC in wildfire plumes for my master's work. Emily, thank you for being a great PI in WE-CAN, setting the best example of leadership, approachability, and teamwork. Similarly, Jun Uetake provided me with patience and understanding as I started to learn microbiology methods and have confidence in sequencing samples. Jessie has been an influential part of my PhD work here, and I owe her a lot of gratitude for allowing me to work on her projects over the past several years and apply the foundations that I have learned to the Arctic environment. The coursework at CSU has also been exceptional. I will carry the knowledge I have learned from Pankaj's microbiome class, Sue's cloud physics, and Emily's atmospheric chemistry courses. I owe a lot of gratitude to Pankaj, as he was very patient with me that I came into his class with limited microbiology familiarity but was very interested in what I was doing, and this sparked my passion in making my research more broad and cross disciplinary. I will remember Sue putting aside a lot of time to help me succeed in her course.

To Sonia and Paul, my advisors from the first day I arrived at CSU, I owe significant thanks to where I am today, in pushing me to be a better researcher and scientist and to think critically about the research questions and hypotheses. Thank you for giving me the opportunity

to be here. And thank you to the rest of my committee for your time and helping me develop my research and providing guidance and feedback.

My largest gratitude to where I am today definitely goes to Tom. He has been a large part of my life, both in research and personally, and his calm demeanor, overflowing wealth of information, kindness, humor, and relatability has contributed to my life in more ways to count. I can't see myself doing a PhD if it wasn't for him.

I would additionally like to extend thanks to the Kreidenweis group, in particular Kathyrn Moore, Russell Perkins, Claudia Mignani, Marina Nieto-Caballero, Ryan Patnaude, Carson Hume, and Drew Juergensen for being so helpful and great to work with. Lastly, I would like to thank the department and office staff, especially Heidi Hammon, Adam Finefrock, Amanda Davey, Nate Gronlund, and Sarah Tisdale. I have done a lot of purchasing for the lab and travel in the last few years, and this would not have been possible without this amazing, exceptionally competent, and kind staff. Sarah has helped me with all of my graduate school questions with ease, and I have had the privilege of working with her on giving campus tours.

Chapter specific acknowledgements:

Chapter 2: Coauthors: Thomas Hill, Yutaka Tobo, Sonia Kreidenweis, Paul DeMott, Jessie Creamean

Chapter 3: Coauthors: Thomas Hill, Thomas Douglas, Kathryn Moore, Sonia Kreidenweis, Paul DeMott, Jessie Creamean. This work was supported by the National Science Foundation, Award No. 1946657. Kathryn Moore acknowledges support by a National Science Foundation Graduate Research Fellowship under Grant No. 006784. Thomas Douglas acknowledges the US Army Futures Command and the Assistant Secretary for the Army Acquisition, Logistics, and

Technology Basic and Applied Research programs. Special thanks to Jun Uetake (Now at National Institute of Polar Research, Tachikawa, Tokyo 190-8518, Japan) for help in sample collection of the 1,000-year-old core.

Chapter 4: Coauthors: Thomas Hill, Marina Nieto-Caballero, Thomas Douglas, Sonia Kreidenweis, Paul DeMott, Jessie Creamean. This work was supported by the National Science Foundation, Award No. 1946657. T. Douglas acknowledges the US Army Futures Command and the Assistant Secretary for the Army Acquisition, Logistics, and Technology Basic and Applied Research programs. Special thanks to Raelene Wentz, Cody Johnson, Matt Irinaga, Martin Edwardson, Harvard Brown, Jerry Brower, Eben Hopson, Ebony Brown, and Thomas Panningona (all from the Ukpeagvik Iñupiat Corporation) for the success of the ARCtic Study of Permafrost Ice Nucleation (ARCSPIN) campaign. Forest Banks and Rommel Zulueta from the National Ecological Observatory Network (NEON) Program/ Battelle are acknowledged for guidance and lending the SIPRE auger. Thank you to Amy Sullivan for use of her TOC instrument.

Chapter 5: Coauthors: Thomas Hill, Conrad Jentzsch, Bruce Moffett, Paul DeMott. This work was supported by National Science Foundation awards AGS-1650786 and AGS-1660486, and also partially supported by the U. S. Department of Energy's Atmospheric System Research, an Office of Science Biological and Environmental Research program, under grant DE-SC0018929. Conrad Jentzsch was supported by Deustche Forschungsgemeinschaft (Projekt STR 453/10-1). Special thanks to the two anonymous reviewers whose insights greatly improved this manuscript.

TABLE OF CONTENTS

1. Introduction

The Arctic has received considerable attention in recent years as the temperature near the surface is warming nearly 4 times faster than anywhere else globally (analyzed since 1979), called Arctic amplification (Rantanen et al., 2022). One feedback mechanism that affects amplification involves clouds, where the low-lying cloud fraction is expected to increase as the sea ice extent decreases, enhancing downwelling longwave radiation and leading to warmer temperatures at the surface (Previdi et al., 2021). In addition to fractional coverage, a change in cloud phase (increased liquid content/fraction) can also affect Arctic amplification by increasing downwelling longwave radiation, as has been previously shown in global climate model simulations (Tan & Storelvmo, 2019). Liquid and ice fundamentally have different properties; for a given water content and temperature, liquid clouds have a higher optical depth and emissivity. Mixed-phase clouds in the Arctic can have relatively long lifetimes, and have been observationally shown to last over 5 days (Morrison et al., 2012). Future mixed-phase clouds are expected to have more liquid water content due to surface warming, which could affect the amount of precipitation at the poles (Bintanja & Andry, 2017; Cesana & Storelvmo, 2017). Climate models struggle to accurately represent Arctic mixed-phase clouds. As discussed in Tan et al. (2022), the current parameterizations and limited observations lead to the clouds glaciating too quickly, underestimating the downwelling longwave radiation.

A special subset of aerosol, called ice nucleating particles (INPs), influences the phase of Arctic clouds, and thus indirectly impacts the surface energy budget. The presence of INPs in low- and mid-level clouds can lead to glaciation and reduced cloud lifetimes, called the ice indirect effect (DeMott et al., 2010; Lohmann, 2002). INPs are abundant in surface reservoirs (Schnell & Vali, 1976) but are very rare in the atmosphere. Rogers et al. (2001) found a median

of 20 INPs active at -20 °C out of 1,000,000 total particles in research flights conducted over the Arctic Ocean. INPs are necessary to commence ice formation in the atmosphere in clouds warmer than -38 °C. Since 90% of observed Arctic mixed-phase clouds occur at temperatures between -25 and -5 °C (Shupe et al., 2006), understanding the characteristics and abundances of INPs is therefore particularly important in the Arctic.

There are many sources of INPs, both in the Arctic and other latitude zones. These include desert and other soil dusts, volcanic ash, biomass burning, sea spray, and biological material (Kanji et al., 2017). Biological and organic INPs can originate from bacteria and fungi, plant tissues, pollen, and lichen (Hill et al., 2018; Huang et al., 2021) that are present over a variety of landscapes, such as arable midlatitude soils (Hill et al., 2016; Tobo et al., 2014), especially during harvesting (Suski et al., 2018), and even in the free troposphere, emitted from wildfires (Barry et al., 2021a). Traditionally, -15 °C was used as an empirical marker for INP temperature spectra, distinguishing between biological ice nucleators initiating freezing at warmer temperatures, and mineral dust dominating INP populations at colder temperatures (Murray et al., 2012). Recent work has revealed a more complicated picture, where organics can dominate down to the coldest measured temperatures, such as the observations at -28 °C reported in air samples above pastures in Argentina in Testa et al. (2021).

In the Arctic, work on quantifying atmospheric INPs has primarily centered on aerosol measurements from research cruises in the ocean, from fixed land sites, and during flight campaigns. Bigg (1996) found mean concentrations of 0.013 L^{-1} at -15 °C at the North Pole between August and early September. Bigg and Leck (2001) found median concentrations at -15 °C of up to 0.018 L^{-1} near the beginning of the ship measurements that extended between July and September. Flights that flew with a real-time ice nucleation instrument, the CSU Continuous

Flow Diffusion Chamber (CFDC), found variable concentrations. Rogers et al. (2001) found an impressive median INP concentration of 5 L^{-1} (median temperature of -20 °C) over the Arctic Ocean in May, while Prenni et al. (2007) found much lower concentrations in September and October near Utqiaġvik, Alaska, with 87% of the sampling times having no detectable INPs. A more recent flight-based campaign during March and April found concentrations as high as 0.018 L^{-1} at -15 °C near Villum Research Station, Greenland, using a high volume filter sampler (Hartmann et al., 2020). The observed variability could be attributed to different measurement sampling periods and locations within the Arctic, as well as measurement techniques.

Over the past decade there has been a greater emphasis on determining seasonal Arctic INP trends and the potential influence of terrestrial airmasses on INPs. Creamean et al. (2018) made measurements at Oliktok Point, Alaska, between March and the end of May, and found 100-fold higher maximum concentrations in airmasses with primarily terrestrial and open ocean transport pathways, compared with airmasses passing mainly over snow and ice. Šantl-Temkiv et al. (2019) measured higher INP concentrations in summer than spring in Greenland, which they suggested could be due to increases in terrestrial sources. This finding is consistent with Irish et al. (2019), who found higher INP concentrations in airmasses with lower latitude origins arriving in the Canadian Arctic. Most recently, Porter et al. (2022) found INP concentrations at the North Pole of up to 2 L^{-1} active at –15 °C during August and September, which were attributed to transport of aerosol from regions proximal to the Russian coast.

Longer-term measurements of Arctic INPs have also increased in recent years. Wex et al. (2019) noted similar seasonal trends from 4 fixed Arctic sites over a year, with a clear summer increase in Arctic INP concentrations. This summer peak in INPs has been corroborated by a year of central Arctic measurements by Creamean et al. (2022), over 2 years of measurements at

Villum Research Station, Greenland (Sze et al., 2023), and 4 years of measurements at Svalbard, Norway (Pereira Freitas et al., 2023). Unique observations from longer-term measurements include the abundance of likely proteinaceous INPs and primary biological aerosol particles in the summer, although influence of heat-labile INPs was found during all seasons (Pereira Freitas et al., 2023; Sze et al., 2023).

Although most measurements have focused on INPs in the free atmosphere, some recent studies have explored INP concentrations from potential Arctic sources. Creamean et al. (2019) found 100-3000 INPs mL^{-1} at -15 °C in seawater samples from the Bering Strait and Chukchi Sea (August and September), with the highest concentrations measured northwest of a phytoplankton bloom. Lower concentrations in bulk seawater have been observed with increasing distance from land (Hartmann et al., 2021; Wilson et al., 2015). Hartmann et al. (2021) attributed their observations to a local marine source. Some potential Arctic terrestrial sources of INPs have been hypothesized, including decaying leaves (Conen et al., 2016), glacial soil dust (Tobo et al., 2019), and thawing permafrost (Creamean et al., 2020). Recent parameterization of INP activity in glacial soil dust strongly improved comparability to observations when included in a global climate model (Kawai et al., 2023).

Clearly, significant effort has been focused on obtaining aerosol INP measurements in the Arctic during the last few decades at varying times of the year, and for annual cycles, but understanding potential sources of Arctic INPs, especially terrestrial-based, remains an open question. Additionally, measurements have mainly been focused on those close to land, leaving a large region of the Arctic relatively understudied. The key questions that this dissertation aims to cover, with new observations and analyses, are:

1) **Chapter 2[1]:** How do the composition and concentration of INPs vary and compare with previous Arctic observations in the central Arctic, far from coastal regions? Can we use microbial detection methods as tracers to better understand the origins of INPs? This study complements traditional meteorological trajectory approaches by using DNA to detect when the aerosol in a sample has been influenced by marine and terrestrial sources.
2) **Chapter 3[2]:** Can INPs from thawed permafrost persist in activity when entering thermokarst lakes? Can they persist under conditions of changing temperature and salinity in other water reservoirs including the Arctic Ocean? Can they be emitted and persist in the atmosphere, via emission from water sources under bubble bursting such as induced by wave action under wind stress? This study mimics these processes in the laboratory to address these questions.
3) **Chapter 4[3]:** What are the largest potential sources of INPs present in an active thermokarst region? Can we track INPs into the Arctic atmosphere from a ground-based approach? This study uses direct observations from an Arctic location to establish whether local sources of INPs appear to dominate the airborne INP population.
4) **Chapter 5[4]:** What are the best ways to eliminate INP contamination in the laboratory and the field, especially important for samples from regions with low INPs? This complementary chapter provides key protocol guidance for working with very low concentration samples and is provided to document methods and best practices for ongoing studies.

[1]Portions of this chapter are currently under review at *ISME Communications*

[2]This chapter has been published in *Environmental Science & Technology*: https://doi.org/10.1021/acs.est.2c06530

[3]This chapter has been published in *Atmospheric Chemistry and Physics*:

https://doi.org/10.5194/acp-23-15783-2023

[4]This chapter has been published in *Atmospheric Research*:

https://doi.org/10.1016/j.atmosres.2020.105419

2. Evaluating the seasonal cycle of central Arctic ice nucleating particles

2.1 Introduction

The Arctic surface temperature is warming at 3.8 times faster than the rest of the world, due to a phenomenon called Arctic amplification (Rantanen et al., 2022). Cloud properties are known to affect Arctic amplification, with enhancement after replacement of ice with liquid in global climate model clouds due to increased downwelling radiation reaching the surface (Tan & Storelvmo, 2019). Climate models of all scales struggle with properly representing Arctic clouds. Cloud microphysical parameterizations are a main factor for differences between global climate models when it comes to simulating Arctic clouds. In particular, ice parameterizations are important for determining the variability in the annual low-level cloud fraction, as low and thin ice clouds drive seasonal cloud amounts (Taylor et al., 2019). Another reason climate models struggle to represent Arctic clouds is that they have long lifetimes, with previous observations showing that mixed-phase clouds can persist for multiple days (Morrison et al., 2012).

A special subset of aerosol, INPs, influence the Arctic cloud phase feedback (increased liquid with warming, making the clouds more reflective), with different INP parameterizations changing the strength of the feedback (Tan et al., 2022). INPs trigger ice formation at temperatures warmer than the level of homogenous freezing (-38 °C), and have a variety of sources, including biological material such as bacteria and fungi, marine organics, and mineral dust (Hill et al., 2018; Kanji et al., 2017; Murray et al., 2012). In the Arctic, mixed-phase clouds have been found to occur 41% of the time during the year, with most having temperatures between -25 and -5 °C, within the range impacted by many of these INP sources (Shupe et al., 2006).

Recent work has discussed issues with climate model representation of Arctic aerosol sources in general, with models struggling in particular with local emissions (Schmale et al., 2021). The Arctic annual cycle can be divided into two main time periods with transitions between them. The Arctic haze season lasts typically from January to April, which is impacted by anthropogenic air transported from lower latitudes, while the summer between June and September typically is characterized by increased local influence and limited long-range transport (Schmale et al., 2021). Long term trends of aerosol within these time periods (Schmale et al., 2022) have revealed that the winter is still influenced by the Arctic haze, despite reduction of emissions since 1970. Schmale et al. (2022) found no clear trends in long term measurements during the summer, but strong natural aerosol influence persisted. Some natural local sources of aerosols that are active as INPs include permafrost, glacial soil dust, and leaf litter (Conen et al., 2016; Creamean et al., 2020; Tobo et al., 2019). A recent study showed that when glacial soil dust was included as the basis for a model parameterization to represent Arctic dust INP sources, Arctic dust accounted for virtually all of the dust INPs between June and November (Kawai et al., 2023). A potential large future perturbation in summer INP sources influencing the Arctic is INPs that could be released from thawing permafrost, as demonstrated by Barry et al (2023a). Thermokarst regions contain many active, unrepresented potential sources of Arctic INPs (Barry et al., 2023b). The impact of this source, via emissions from water sources, has yet to be modeled.

There have been several previous measurements of INPs in the Arctic, including ship, aircraft, and fixed site campaigns. Long-term measurements in the Arctic have mostly occurred at fixed sites. Wex et al. (2019) reported on data from 4 coastal sites that spanned multiple years, Sze et al. (2023) analyzed over two years of measurements at Villum Research Station in

Greenland, and Pereira Freitas et al. (2023) analyzed four years of measurements at Mount Zeppelin in Svalbard, Norway. All of these studies have provided valuable information, picking up seasonal trends in the Arctic, with high temperature INPs (>-15 °C) generally more abundant in the summer at coastal locations. However, observations in the central Arctic have been confined to specific months, such as Porter et al. (2022) measuring shipborne INPs during August and September, Bigg and Leck (2001) measuring from July to September, Bigg (1996) measuring from August to October, and Hartmann et al. (2021) measuring up to 83.7° N between May and July.

Thus, there has been a lack of seasonal or long term measurements in the central Arctic to provide a framework to compare and integrate results from other sites. This changed with the Multidisciplinary drifting Observatory for the Study of Arctic Climate (MOSAiC) campaign, which provided the first full year of INP measurements in the central Arctic. The seasonal cycle from one collection and analysis method of INPs, resulting in size-resolved measurements, has been published (Creamean et al., 2022). They found the highest concentrations in the summer, with most of the INPs in the 1-3 µm size range, but lower concentrations and smaller INPs in winter. They hypothesized that the main source of the winter INPs was long-range transport, while summer may be dominated by emissions from local melt ponds, leads, and the marginal ice zone. The work presented here also includes results from the MOSAiC campaign, but extends the findings of Creamean et al. (2022) by presenting seasonal results from whole aerosol filters (not behind a size-segregating inlet), as well as providing a more detailed analysis of INP characteristics. Additionally, to identify the sources of INPs, we provide the first seasonal cycle of Arctic aerosol bacteria and eukaryotes, and sequence select local sources to see if they may be contributing to the aerosol.

2.2 Methods

2.2.1 Sample collection during the MOSAiC expedition

The MOSAiC campaign took place from October 2019 to September 2020 in the central Arctic aboard the R/V *Polarstern*, separated into 5 legs with changing personnel. The vessel drifted passively in ice between: October 4-December 13 (Leg 1); December 13-February 24 (Leg 2); February 24-May 16 (Leg 3); June 19-July 31 (Leg 4); and August 21-September 20 (Leg 5). The other periods are when the *Polarstern* was in transit. Overviews of this campaign have been provided in depth in several recent articles (Nicolaus et al., 2022; Rabe et al., 2022; Shupe et al., 2022).

Aerosols for INP and DNA analyses were collected onboard the *Polarstern's* P-deck during MOSAiC, on filter samplers mounted about 15 m above sea level with the U.S. Department of Energy Atmospheric Radiation Measurement (DOE ARM) AMF2 facility. This was about 3 m below the Aerosol Observation System (AOS) inlet. Polycarbonate filters for INP analyses (0.2 µm Whatman Nuclepore track-etched hydrophilic membranes) were precleaned by brief ultrasonication in methanol (2-10 s pulses) followed by 0.1 µm filtered deionized (DI) water rinses (Barry et al., 2021b). For DNA analyses, polycarbonate filters (0.4 µm Whatman Nuclepore track-etched hydrophilic membranes) were precleaned by soaking in 10% H_2O_2 followed by 0.1 µm filtered DI water rinses (Uetake et al., 2020). Filters for both INP and DNA analyses were precleaned and preloaded in disposable Nalgene units in a laminar flow cabinet at Colorado State University (CSU). Identically cleaned 10 µm polycarbonate filters were loaded underneath the 0.2 and 0.4 µm filters to provide a barrier for the sample filter. Filters were typically collected for 3-day periods, with an average total volume of air filtered of 88,800 standard Liters (sL: 0 °C; 1013.25 mb) for INP filters and 139,500 sL for DNA filters. All filters

were stored colder than -20 °C for the duration of the campaign, during transport, and at CSU until analysis. Size resolved aerosol for INP analyses were also collected with a 4-stage Davis Rotating-drum Unit for Monitoring cascade impactor (DRUM) with the AOS inlet (Creamean et al., 2022). These data are included for comparison purposes to the polycarbonate filters.

Samples of seawater, sea ice, snow, melt pond water, and open lead ice were collected and used to identify potential local sources of biological aerosols. All sample metadata, including types, collection dates and times, latitudes/longitudes, and depths are provided in Table A.1.1. Protocols for collection of seawater, sea ice and snow are discussed in detail in Nicolaus et al. (2022) and Rabe et al. (2022), but are described here briefly. Seawater includes samples from *Polarstern's* flowthrough seawater tap system (FT) collected approximately daily and those collected from a CTD (conductivity, temperature, depth) rosette approximately once per week. The flowthrough system on *Polarstern* collects seawater at 11 m depth. CTD samples presented here were collected at 4-7 depths within the upper 400 meters of the ocean surface. Sea ice cores were collected approximately weekly from both first and second year ice using a Kovacs II coring system. Ice cores were sectioned into 5-10-cm segments while on the pack ice, melted on *Polarstern*, then diluted with filtered seawater (0.22 µm Sterivex filters) under red-light-only conditions in a cold laboratory container for preservation of microorganisms. Ice core samples analyzed for the current work were from various sections of each core (predominantly the bottom 0-10 cm). Snow pit samples were typically collected approximately weekly from the surface, middle, and bottom (near the snow-ice interface) of the snow pits. Melt pond and newly formed lead ice samples were collected during intensive observational periods throughout the expedition but focused mostly during the summer months. These samples were collected by hand, which involved triple-rinsing 50-mL centrifuge tubes then filling to ~40 mL from the edge of these

open water features. All samples were stored and transported at –20 °C or less prior to INP and DNA analysis.

2.2.2 INP sample analysis

For INP sample processing, 8 mL of 0.1 µm filtered DI water were added to a filter in a prerinsed 50 mL centrifuge tube to create a suspension and shaken for 20 min in a Roto-Torque rotater (Cole Parmer). Corresponding 11-fold dilutions were made (400 µL sample and 4000 µL 0.1 µm filtered DI water) and pipetted out in 32-50 µL aliquots into PCR trays (Optimum Ultra). A 32-50 µL block of 0.1 µm filtered DI water was included with each sample as a negative control. The PCR trays were placed into the aluminum blocks of the CSU Ice Spectrometer (IS) and cooled at 0.33 °C min^{-1}. The current setup of the IS is further described in DeMott et al. (2018). Based on the number of frozen wells, the INPs were first converted to concentration per mL of suspension, before conversion to INPs per L of air by considering the total volume of air filtered (Vali, 1971). 95% confidence intervals are from Agresti and Coull (1998). 74 samples were processed in all. For blanks, 4 filters were transported and processed identically to the INP samples (without airflow), and they were combined to create a regression of INPs per filter as a function of temperature for subtraction from the INPs per sampled filters before conversion to numbers per L of air. The blank corrections had virtually no effect on INP concentrations, as there was only an average of 11 INPs per blank filter at -25 °C, while filters typically had >1000 INPs at this temperature. Thermal and chemical treatments were performed on 26 of the remaining portions of filter suspensions. These treatments have been used extensively in previous work to infer the basic INP composition (e.g., Barry et al., 2023; Hill et al., 2016; McCluskey et al., 2018; Suski et al., 2018). Heat treatment at 95 °C removes heat labile INPs (such as proteins), and hydrogen peroxide (H_2O_2) digestion at 95 °C removes all organics.

Thereby, heat labile and heat stable organic fractions can be derived, with the remaining presumed mineral.

2.2.3 DNA sample analysis

Samples for DNA analyses were processed similarly to previous work (Barry, Hill, Moore, et al., 2023; Uetake et al., 2020). Starting with the aerosol filters, 54 were extracted and sequenced. 47 followed the previous protocol, starting with cutting up the filter in several pieces, 30 s ultrasonication in 2 mL of nuclease free water, and concentration with a Microcon DNA Fast Flow Centrifugal Filter. Extraction was done with the DNeasy PowerLyzer Microbial Kit (Qiagen). A different protocol was employed for 79 source samples and 7 additional aerosol filters (to get more data in certain months), which were also cut into pieces as for the others. Ice, seawater, melt pond, flowthrough, and snow filters were pre-processed identically, by first thawing the sample and filtering approximately 30 mL through a Sterivex (Millipore) 0.22 µm pore filtering unit. Snow had less liquid volume when it melted, so approximately 15 mL went through a Sterivex unit. The Sterivex was separated with a PVC pipe cutter (Cruaud et al., 2017), and filter detached with a sterile scalpel and cut into pieces. For the water and 7 additional aerosol samples, pieces were then placed directly into the extraction tubes of the DNeasy PowerSoil Pro Kit (Qiagen). This kit and method were chosen for the latter batch to remove the concentration pre-step where losses may occur, and directly proceed with extraction from the filter. Extraction for both batches followed their respective Qiagen protocol, with two elutions used in the final step to improve recovery (Hill et al., 2014).

All samples were then treated identically for amplification and library preparation. For 16S rRNA, the V4-V5 region was targeted with the 515yF/926pfR primers (Parada et al., 2016) with cycling conditions following (Uetake et al., 2020) and using the UCP Multiplex PCR master

mix (Qiagen). Every sample was amplified for 16S rRNA. A subset of aerosol samples (29) were amplified for both ITS and 18S rRNA to look at the seasonality of the eukaryotes in the air. For ITS, the primers followed Walters et. al. (2015), and cycling conditions were: 95 °C for 2 min; 37 cycles of 95 °C for 30 s, 55 °C for 60 s, 72 °C for 60 s; followed by a 72 °C hold for 5 min and a hold at 4 °C until sample removal. For 18S, we used the Euk1391f-EukBr primer pair detailed on the Earth Microbiome Project (Thompson et al., 2017). Cycling conditions were also adapted from the Earth Microbiome Project: 94 °C for 3 min; 37 cycles of 94 °C for 45 s, 57 °C for 60 s, 72 °C for 90 s; followed by a 72 °C hold for 10 min and a hold at 4 °C until sample removal. All primers contained the Illumina adapters and were purified with AMPure XP (Beckman Coulter) two times: once after 1st amplification and once after 2nd amplification that added sample barcodes (IDT for Illumina Nextera DNA UD Indexes). This 2nd PCR step had cycling conditions of 95 °C for 5 min; 12 cycles of 95 °C for 30 s, 60 °C for 30 s, and 72 °C for 30 s; followed by a 72 °C for 7 min and a hold at 4 °C until sample removal. This step used the AmpliTaq Gold LD DNA Polymerase (Applied Biosystems). After 2nd purification, samples were quantified with the Quant-iT™ 1X dsDNA Assay Kits (Invitrogen) on an Enspire Plate Reader, to create an equimolar library. This library was sequenced at the CSU Next Generation Sequencing (NGS) Core with the Illumina MiSeq Reagent Kit v3 (600-cycle).

Next, sequences were demultiplexed in the Illumina BaseSpace Sequence Hub, before being imported into QIIME2 Version 2023.5 for processing (Bolyen et al., 2019). Reads were denoised with DADA2 (Callahan et al., 2016) to create an amplicon sequence variant table. For 16S, preformatted reference sequence and taxonomy files were based on SILVA 138 (Quast et al., 2012; Robeson et al., 2020). For 18S, reference sequence and taxonomy files were from the PR^2 (Protist Ribosomal Reference) database, version 5.0.0 (Guillou et al., 2012; Vaulot et al.,

2023). For ITS, reference sequence and taxonomy files were from UNITE Community database, version 9.0 (Abarenkov et al., 2022). Taxonomy assignment used the feature-classifier plugin in QIIME2 (Bokulich et al., 2018; Pedregosa et al., 2011). For 16S, any non-bacterial reads (mitochondria, chloroplast, archaea) were removed. Negative controls were included for later correction with the decontam package prevalence method with a threshold of 0.5 (Davis et al., 2018). For aerosol filters, this included 3 field controls that were prepared and handled identically as the samples, minus airflow. For water samples, this included 2 laboratory controls that put 30 mL of nuclease free water into a 50 mL centrifuge tube and subsequently through a Sterivex unit before extraction. Additionally, 7 PCR and 4 extraction negatives were included.

For relation of the aerosol to the potential sources sequenced, 16S rRNA data were used in SourceTracker2 (Knights et al., 2011). Categories were initially narrow (e.g., the separation of flowthrough from CTD seawater samples). However, those categories showed large proportions of similarity (>50%), so we composited the samples into three categories (Fig. A.1.1) that contained over 70% unknown during class prediction. The exact sample category breakdown used for source tracking is given in Table A.1.1. For both source tracking and taxonomy, aerosol samples with less than 1000 reads were removed, resulting in the loss of 5 samples. For sources, samples were rarefied at 5000 reads for source tracking, which resulted in the loss of 12 samples, but were included in relevant taxonomy plots (Fig. A.1.2; the lowest sample included was 1912 reads). For ITS aerosol data, only 10 samples amplified, but those amplified well (minimum of 41506 reads). For 18S aerosol data, there was better success in that 19/29 amplified (after removal of one sample with 104 reads).

To get a better understanding of the bacterial seasonal cycle, filters were pooled by month of filter start date for taxonomic plots, using a sum to combine the ASV frequency. There

was only one successful sample in March (filter start date of 3/16/2020), which was included with February. There was also only one successful sample in October (filter start date of 10/27/2019), which was included with November. Additionally, filters collected on a ship that was drifting in sea ice presented a major challenge in identifying and removing contamination. Any bacterial contamination from the ship community would not be represented on a blank aerosol filter that did not have airflow. To provide a more accurate representation of the Arctic bacterial community, the top 60 abundant aerosol ASVs were put through the National Center for Biotechnology Information (NCBI) Basic Local Alignment Search Tool (BLAST) tool and the isolation source was checked for the sequences having the top scores. In total, 17 ASVs were removed, based on isolation sources having obvious contamination sources (e.g., skin, stool, waste).

2.3 Results and Discussion

2.3.1 Seasonal cycle of INPs

First, we present INP results from the MOSAiC campaign (Fig. 2.1). Creamean et al. (2022) reported the annual cycle of size-resolved INPs during MOSAiC from 24-hour samples, while here, we present new INP concentration and augmented composition data from total aerosol sampled at 72-hour intervals on filters. The longer duration sampling in this remote, low-aerosol region was intended to permit characterization of the rarer, warm temperature biological INPs. INP concentrations varied as a function of season, with higher average concentrations during the summer (-15 °C: 0.19 L^{-1}; -20 °C: 0.44 L^{-1}), and mean concentration similarities in the other seasons. The lowest average concentrations at -15 °C were in the winter and spring/melt transition season (0.0011 L^{-1}), while the lowest average concentrations at -20 °C were in the fall (0.016 L^{-1}). In addition to having the highest concentrations, the summer samples had the most

variability, with the highest standard deviation (0.35 L^{-1} at -15 °C). The winter samples had the lowest standard deviation at -15 °C, at 0.0013 L^{-1}. Summer INP concentrations of up to 1.4 L^{-1} at -15 °C were found on the filter collected on July 3-6. The highest values are consistent with up to 2 L^{-1} seen near the North Pole in August of 2018 (Porter et al., 2022). The trends observed in MOSAiC, with the highest concentrations in the summer months and lower concentrations in the winter and spring, have been seen before in the Arctic, most recently in long-term measurements in Svalbard, Norway, and Villum Research Station in Greenland (Pereira Freitas et al., 2023; Sze et al., 2023), as well at several other fixed Arctic sites (Wex et al., 2019). Partial year sampling also supports higher concentrations in summer (Creamean, et al., 2018; Šantl-Temkiv et al., 2019).

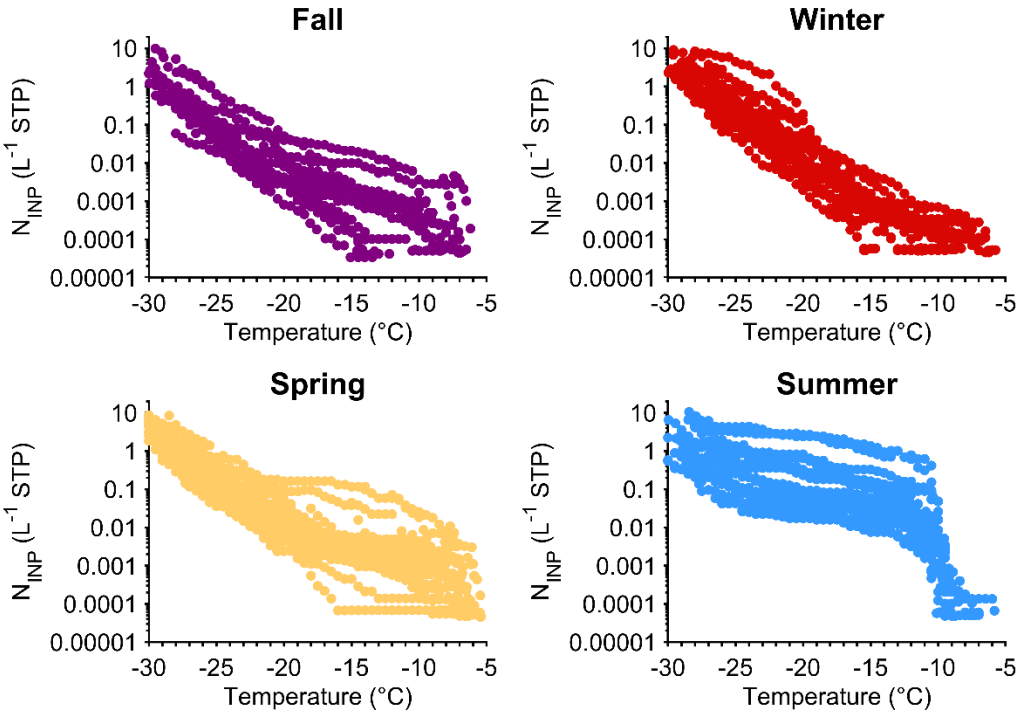

Figure 2.1: Cumulative INP-temperature spectra, colored by season. Fall (Purple: September, October, November), Winter (Red: December, January, February), Spring (Yellow: March, April, May), Summer (Blue: June, July, August).

The concentrations and seasonal cycle observed in MOSAiC agree quite well with those at the Zeppelin Observatory (474 m above sea level) in Svalbard (Fig. 2.2: Pereira Freitas et al., 2023), suggesting a basin-wide commonality of INP concentrations in the general Arctic. This is a bit surprising, considering the conclusions of Pereira Freitas et al. (2023), made on the basis of single particle fluorescence spectroscopy, that local terrestrial sources in Svalbard were the source of INPs. Mean concentrations varied by approximately a factor of 2 in the fall, winter, and spring, but were as much as an order magnitude lower in summer, which is mostly attributable to not apparently having experienced the event responsible for the highest concentrations found at the ship site in early July. Some differences are also expected with varied averaging times (the Zeppelin filters were collected over one week), and locations (with influence from local sources expected at both locations). The filter material was the same (polycarbonate). By -25 °C, the concentrations were nearly identical over the whole year in the two data sets.

Also shown in Fig. 2.2 (and Fig. A.1.2) is a direct comparison between coincident MOSAiC INP methods. For the DRUM data that represent an integration of all size stages, average concentrations at -15 °C were in the fall=$1.8x10^{-5}$ L^{-1}; winter=$6.1x10^{-5}$ L^{-1}; spring=$6.3x10^{-5}$ L^{-1}; summer=$1.1x10^{-3}$ L^{-1} compared to the polycarbonate filters which had 0.0044 L^{-1}, 0.0011 L^{-1}, 0.0011 L^{-1}, and 0.19 L^{-1}. Similar seasonality trends were detected (with 1-3 orders of magnitude lower concentrations); however, seasonality was less evident or nonexistent in the DRUM data at colder temperatures like -20 and -25 °C. It is seemingly perplexing that the highest average concentrations (at -20 °C) from the DRUM are in the winter, which is inconsistent with what the polycarbonate filters or Zeppelin Observatory data indicate (Pereira Freitas et al., 2023). There are several potential explanations for the discrepancies

observed, such as inefficient particle collection, removal, and variability of cooling rate, further discussed in Text A1.

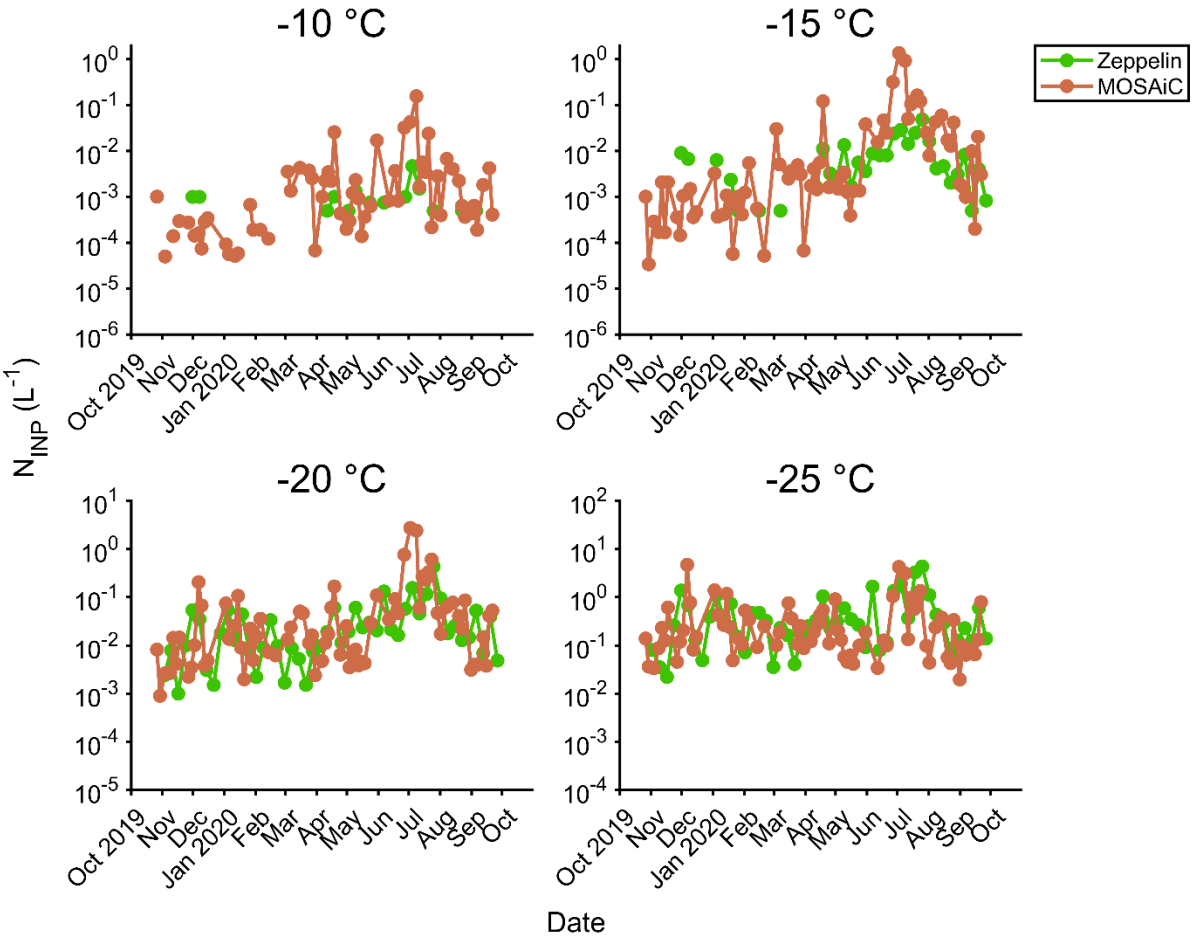

Figure 2.2: INP concentration time series during the MOSAiC campaign at -10 °C, -15 °C, -20 °C, and -25 °C. Zeppelin (green) refers to data taken at Zeppelin Observatory in Svalbard (Pereira Freitas et al., 2023); MOSAiC (orange) refers to data taken on the R/V *Polarstern* and analyzed with the Ice Spectrometer.

Next, we present the seasonal cycle of the INP composition, initially partially presented in the supplemental material of Creamean et al. (2022). Based upon heating to 95 °C and H_2O_2 digestion, we were able to separate samples into heat labile organics (likely proteinaceous), heat

stable organics, and mineral fractions (Fig. 2.3). Although the summer had the highest standard deviation for cumulative INP concentrations, it was the most stable time for INP composition, as June through August had virtually 100% heat labile organics at both -15 and -20 °C. Heat stable organics were seen periodically throughout the remainder of the year, concentrated in the fall and spring. Mineral influence was seen occasionally from late October to early February, with minor contributions lasting into May, consistent with the Arctic haze time period. Out of the 26 samples tested, all but one had at least some proportion of heat labile organics at -15 or -20 °C. We conclude that heat labile INPs are in the central Arctic nearly all times of the year, with the largest fractions occurring during the summer. This agrees with enhanced summer biological productivity and sunlight, decreasing sea ice, and less snow on land. This finding is consistent with those from recent work showing heat labile fractions of over 90 percent in summer, and 50-85% in winter, at -12 °C at Zeppelin Observatory (Pereira Freitas et al., 2023), heat labile fractions over 75% at -12 °C in months with snow at Villum Research Station (Sze et al., 2023), and all heat-labile INPs above -20 °C near the North Pole in August and September (Porter et al., 2022).

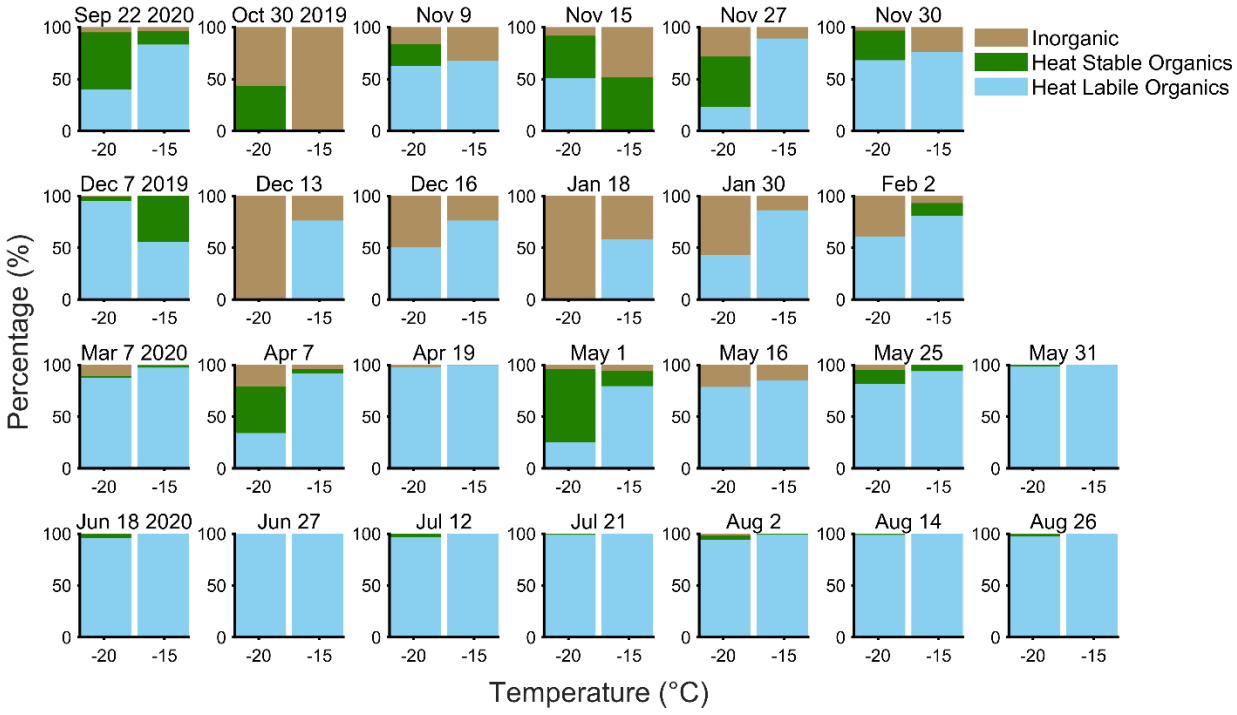

Figure 2.3: Seasonal cycle of the INP composition in the temperature regime at -15 and -20 °C measured on the R/V *Polarstern* during MOSAiC. Date refers to the aerosol filter start date, with blue denoting the heat labile organic fraction (from heating to 95 °C), green denotes the heat stable organic fraction (from digestion with H_2O_2), and tan is the inorganic (presumed mineral) contribution from the INPs remaining after H_2O_2 digestion.

2.3.2 Seasonal cycle of bioaerosols

A year in the central Arctic revealed a complex picture of the air microbiome (Fig. 2.4), with limited consistent trends among dominant bacterial taxa. Among the top 20, probable marine taxa are seen between May and November, while probable terrestrial taxa are seen between September and May, suggesting shifts in the bacterial origin. The majority of the months have top taxa that are from ambiguous origins. December was an anomaly in that the top 20 genera only explain 16 percent of the relative abundance.

For comparison to previous work, the top phyla observed were Proteobacteria, Bacteroidota, Actinobacteriota, and Firmicutes. This agrees well with previous Arctic bioaerosol

studies (Cuthbertson et al., 2017; Harding et al., 2011; Jensen et al., 2022; Šantl-Temkiv et al., 2018). Proteobacteria were found in greatest relative abundance in February (93%) and April (76%), Bacteroidota in August (77%), Actinobacteriota in July (74%), and Firmicutes in May (18%). Firmicutes were found in the aerosol in every month, in relatively equal proportions (3-18%); given they are known to produce endospores (Galperin, 2015), they appear to be a stable part of the yearly Arctic microbial composition able to survive the harsh environment, as well as able to travel long distances.

At the genus level, previous measurements from Station Nord, Greenland, found the highest relative abundance contributions from *Sphingomonas*, *Hymenobacter*, and *Methylobacterium* in air between March and June (Tignat-Perrier et al., 2019). These three genera were detected in the MOSAiC top 20, with *Sphingomonas* found in January, April, May, June, September, and December; *Hymenobacter* in April, November, and December; and *Methylobacterium* in November. The soil-inhabiting order, Frankiales, were detected in April, May, and November, with the largest contribution in November (11% relative abundance). Previously, this taxon was found in the Arctic aerosol at Villum Research Station (Jensen et al., 2022), in larger relative abundance in the summer. The psychrophile, *Polaribacter*, was the most abundant genus overall, detected in May, July, August, September, and November. This taxon has been found in high abundance in seawater samples after spring phytoplankton blooms in the North Sea (Teeling et al., 2016), and in the summer in air samples over the Southern Ocean (Uetake et al., 2020). Highest relative abundance was also found in summer during MOSAiC.

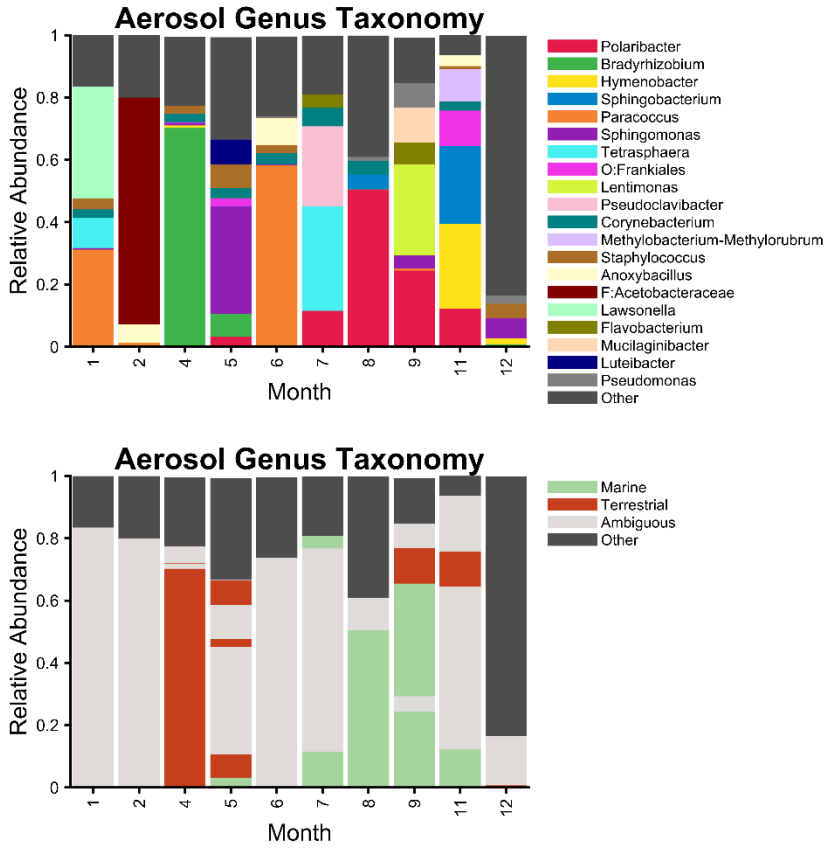

Figure 2.4: Pooled monthly aerosol bacterial taxonomy plot, colored by the top 20 genera (top) and by probable source (bottom). Any taxa contributing less than 0.1% relative abundance were excluded from the analysis.

Source tracking analysis from local sequenced sources confirmed that the Arctic air is comprised of a wide range of bioaerosol sources, with the majority (73%) of the samples showing unknown contribution (Fig. 2.5). Sequenced local sources could be identified only intermittently as contributors to the aerosol. Of the known contributions, snow was by far the most common, appearing 9 times (22% of samples). A notable event includes the November storm that took place between November 16 and 20 with two cyclones (Rinke et al., 2021), in which 47% of the aerosol was explained by the sequenced snow. Other snow contributions can also be explained by midlatitude cyclones, with cyclone start dates of December 16, January 12, May 25, May 28, July 3, July 7, August 9, September 24, overlapping with the aerosol filters

sequenced (Rinke et al., 2021). The blowing snow event on January 13-14 also can explain the January snow contribution (Gong et al., 2023). Summer filters show occasional influence explained by the Ice and MP category, which is consistent with melt ponds occurring during the summer (Creamean et al., 2022). Surprisingly, only one sample had substantial seawater influence (33%), on May 31, even though open leads were present throughout the campaign (Creamean et al., 2022).

The genus level taxonomy for the potential sources shows large contributions of *Flavobacterium* in the ice and melt pond samples, while the seawater samples (represented by 100 m CTD, FT, and lead water categories) have consistent contributions from *Clade-1a* and *Clade-II* within the order SAR11 (Fig. A.1.6). The summer transition to dominance of genera such as *Nitrincolaceae* and *Planktomarina* in FT samples has been seen in Arctic waters (Thiele et al., 2023) during phytoplankton blooms in water samples taken in July and August. The snow samples were not explained by any of the top 10 common genera; they were instead explained by a mixture of marine and terrestrial taxa such as the soil organisms *Ramlibacter* and *Bradyrhizhobium*, and the marine organisms *Octadecabacter*, *Algoriphagus*, and *Polaribacter*. In general, source tracking revealed that the air has its own unique microbiome that is often distinct from the defined communities present in the potential sources local to the ship, namely ice and seawater in the immediate surrounding environment. Sequencing of additional source samples to cover more times and a broader geographical area may have increased the explained contribution in the aerosol samples, especially in the snow samples that were more variable and not explained by the top 10 genera overall (Fig. A.1.6). However, the consistency in the CTD, FT, Ice, and MP relative abundances indicate that these communities were largely covered.

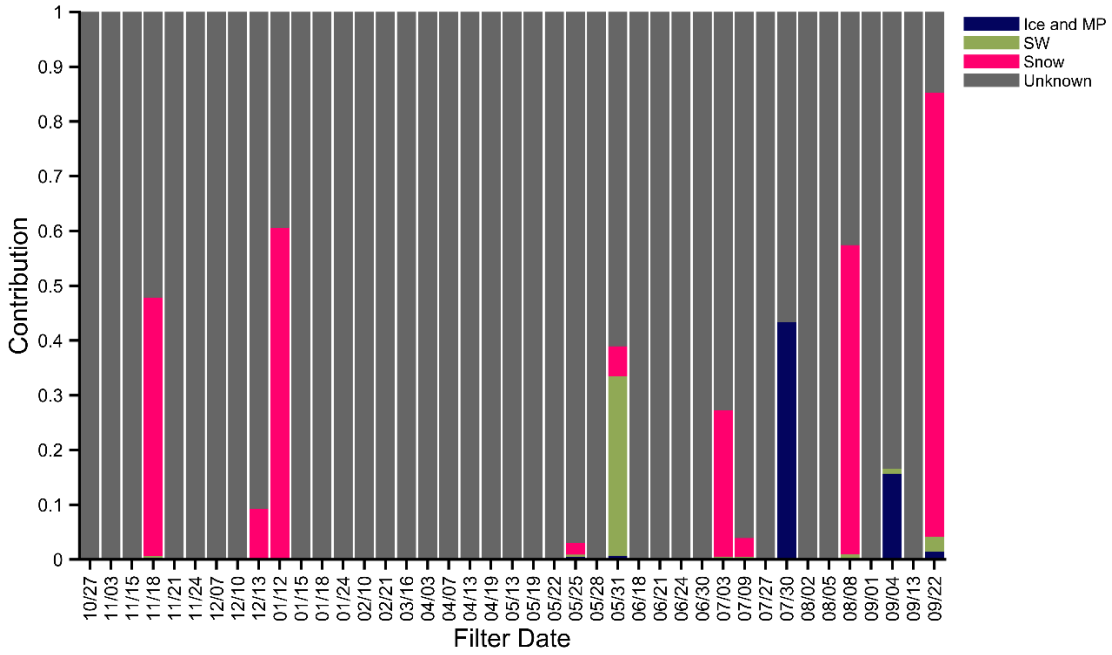

Figure 2.5: Source tracking analysis for 41 aerosol samples, organized by month of the campaign (October 2019-September 2020). The listed dates refer to the start date of the filter. 76 sources were included and composited into three categories: Ice and Melt Pond (MP: Dark Blue); Seawater (SW: Green); and Snow (Pink).

The seasonal trends of Arctic airborne eukaryotes were analyzed with ITS and 18S rRNA sequencing (Fig. 2.6). Starting with ITS, the genus *Cryolevonia* was found in samples from May to August, comprising 98% of the relative abundance in the aerosol filter that started on June 30. At the species level, all of the *Cryolevonia* reads were from *C. schafbergensis*, which has been isolated from permafrost in the Alps and sea ice in Baffin, Canada (Pontes et al., 2020). Additionally, this genus has been isolated from ice in Patagonia and Antarctica, but classified as a different species (De Garcia et al., 2020). The ubiquitous genus *Penicillium* was found in the most samples (7) throughout the year, while the class *Sodariomycetes* was only detected in December and January. There are limited previous Arctic airborne measurements of fungi, but the genera *Penicillium* and *Sordaria* were among several detected in July and August from Ft. Churchill, Manitoba, (Pady & Kapica, 1953) and the maximum of detected fungal spores was found in late July and August (Johansen, 1991; Johansen & Hafsten, 1988). More recent studies

detected high levels of the genus *Cladosporium* from Longyearbyen, Svalbard, Norway, in May, which they attributed to organic matter accumulation under snow (Pusz & Urbaniak, 2021), and high relative abundance of the genus *Alternaria* between March and June at Station Nord, Greenland (Tignat-Perrier et al., 2019). We did not detect *Alternaria* during MOSAiC, which could be attributed to periodic nature of the detected fungi, the distance from land, or different meteorological conditions like airmass origin. *Cladosporium* was not detected in any ITS sample but was detected in 5 18S samples.

The 18S rRNA results (Fig. 2.6), excluding fungi, that the genus *Bacillariophyceae* (4: diatoms) were detected in multiple samples, presence between May and September. This shows that local marine eukaryotes were present during this time period. *Mollusca* (mollusks) were detected in two samples in May. Including fungi, most samples had relative abundances dominated by the phyla Basidiomycota and Ascomycota. Previously, continental work showed that normalized species richness of Basidiomycota is higher in the summer and fall, while Ascomycota is higher in the winter and spring (Fröhlich-Nowoisky et al., 2009). During MOSAiC, the higher Ascomycota relative abundances were predominantly observed between the end of October and December, though smaller influences of Ascomycota exist at all times of the year. Under global sampling, greater relative proportions of Ascomycota were observed in marine and coastal air, whereas continental air had higher proportions of Basidiomycota (Fröhlich-Nowoisky et al., 2012). This was thought to be related to the size of the spores, as Basidiomycota spores are larger than Ascomycota, and have shorter atmospheric residence times. Therefore, the generally increased relative abundances of Ascomycetes at MOSAiC that occur during fall and early winter support longer-range transport [such as during the November

storm (Rinke et al., 2021)]. Similarly, the high proportions of Basidiomycetes in May-July support more local terrestrial airmasses.

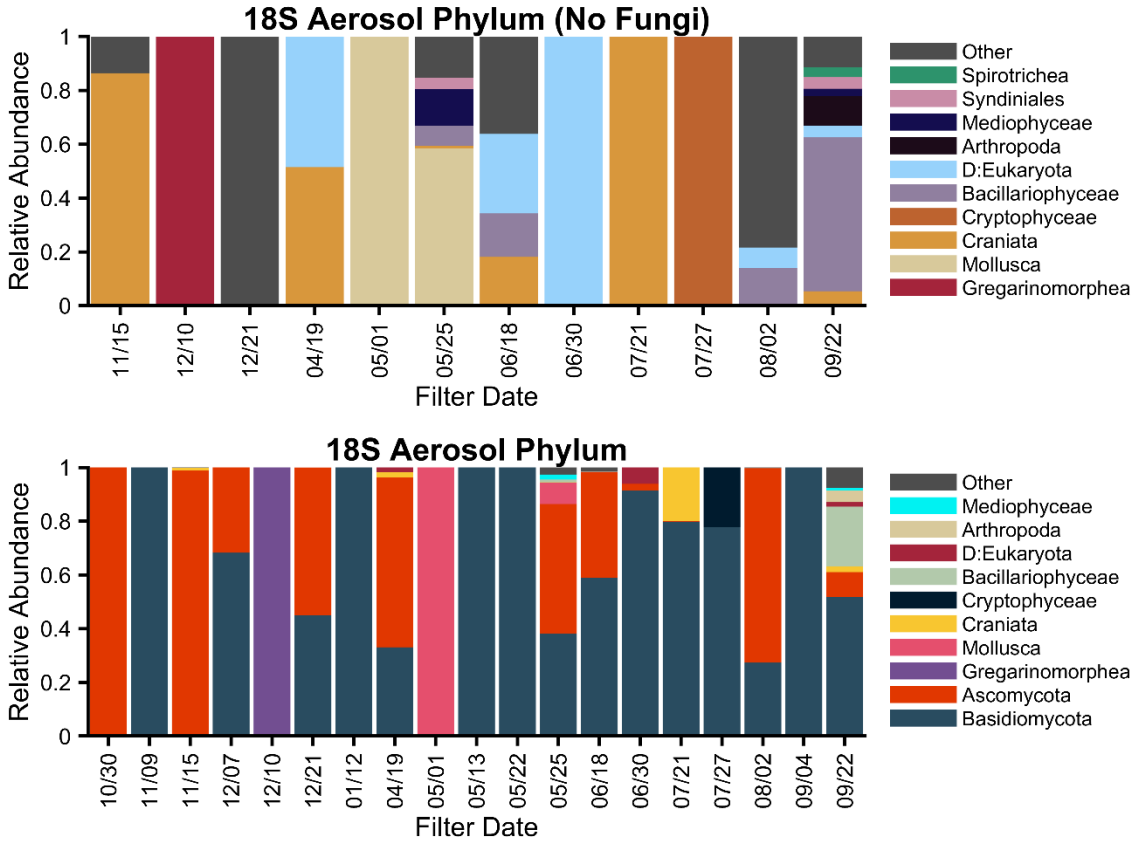

Figure 2.6: Relative abundance taxonomy for the MOSAiC aerosol for 18S at the phylum level, excluding fungi (top), and with fungi (Ascomycota and Basidiomycota, bottom). The filter starting date is given on the x-axis, and samples are colored by the top 10 abundant taxa, with domain (D) given if not resolved at the phylum level.

2.3.3 Investigating potential INP origins through bioaerosol linkage

As almost every sample had heat labile INPs, suggestive of biological influences on the INP populations, we explore the use of bacterial and fungal DNA as a proxy for air mass origin and as a tracer for INPs; we cannot further identify the composition of heat labile INPs on the basis of DNA sequencing. IN fungi typically release copious extracellular IN proteins, so a DNA signature is not assured (e.g. Schwidetzky et al., 2023). We first present the top 20 abundant

genera (for samples with corresponding INP concentrations) separated by the days with lower (Group 1) and higher (Group 2) INP concentrations at -15 °C (Fig. 2.7). Taxa that were more frequently associated with higher INP concentrations in Group 2 included the likely marine *NS9-marine-group*, *Formosa*, the diverse origin family Intrasporangiaceae, and genera *Tetrasphaera* and *Paracoccus*. For taxa associated with lower INPs with greater frequency in Group 1, the likely terrestrial genera *Bradyrhizobium, Mucilaginibacter, Luteibacter*, terrestrial order Frankiales, marine genera *Lentimonas*, and ambiguous origin genera *Sphingomonas, Sphingobacterium, Methylobacterium-Methylorubrum*, *Amnibacterium*, and *Pseudomonas* were found. The marine *Polaribacter*, and ambiguous origin *Corynebacterium, Flavobacterium*, and *Staphylococcus* were detected relatively evenly among INP groups. This analysis shows unexpectedly that the airmasses with lower (< 0.01 L^{-1} at -15 °C) INP concentrations are typically associated with more abundant probable terrestrial taxa, whereas airmasses with higher INPs are typically associated with more abundant probable marine taxa. As a whole, the airmasses with different INP concentration levels are compositionally quite different from each other. However, we note that the selection of 0.01 L^{-1} as a threshold concentration has effectively separated the dataset by season (Figure 2.2), likely accounting for at least some of the observed differences.

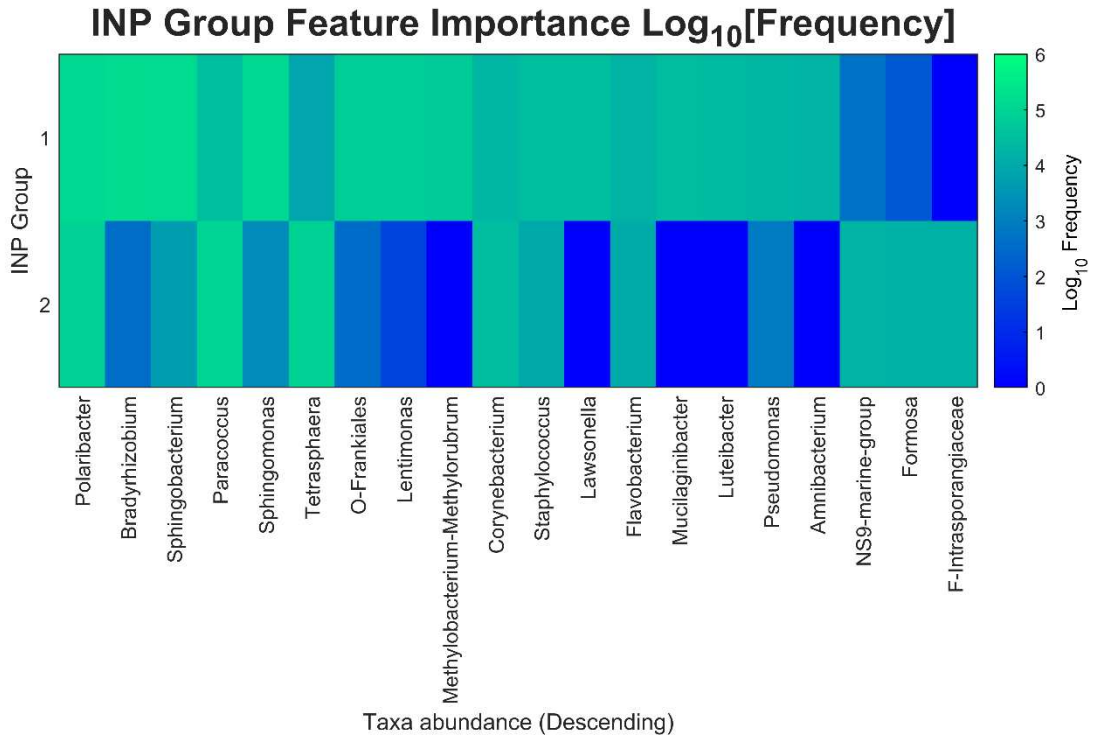

Figure 2.7: Heatmap showing the top 20 Genus level taxa as a function of INP group, colored by the log10 of the frequency. The taxa abundance is ordered from highest to lowest. Group 1 represents INP concentrations at -15 °C that were less than 0.01 L^{-1}, and Group 2 is INP concentrations greater than 0.01 L^{-1}.

To further investigate possible airmass origins during specific events, all INP measurements at -15 °C and three biological tracers were plotted along with 5-day HYSPLIT back trajectory airmass percentages (Fig. 2.8). The methodology is described in Creamean et al. (2022) for 5-day back trajectories using only trajectory points ≤ 500 m above mean sea level, and describes the percentage of time spent over a certain region. Ice is greater than 85% coverage, marginal ice zone (MIZ) is between 15 and 85% coverage, open ocean is less than 15% coverage, and a land category was included. *Cryolevonia*, due to being isolated from cold regions (Pontes et al., 2020), are a likely tracer for a local terrestrial airmass, *Mycena*, saprotrophic fungi, are a likely tracer for a longer-range terrestrial airmass, and *Polaribacter*, cold-dwelling ocean bacteria, are a tracer for a marine airmass. *Mycena* and *Polaribacter* were

both detected during the November 16-20 storm that advected warm air from the North Atlantic (Rinke et al., 2021), so this likely indicates that the air during this time was a mixture of local and longer-range sources. The 5-day back trajectories during this time indicate a shift from air predominantly over the ice-free ocean on the 16th and 17th, to predominantly over the ice on the 18th-20th. *Mycena* were detected on the filter that started on the 15th, while *Polaribacter* were not detected, and *Polaribacter* were detected on the filter that started on the 18th (not sequenced for ITS), so the airmass change could be responsible for the different populations detected. Between those two filter time periods, the INPs at -15 °C went up by an order of magnitude from 1.7×10^{-4} to 1.8×10^{-3} L^{-1}. After November 18th, *Polaribacter* were not detected again until May 2020, as the ship continued to move north, and the ice coverage expanded.

INPs were elevated (0.12 L^{-1} at -15 °C) and *Mycena* were detected on the filter starting on April 19th. This filter was collected within the time period of southerly warm air advection between April 15-21 (Rinke et al., 2021). The airmasses were quite variable during this time period, with maximums of 100% ice, 64% ice-free ocean, 33% land, and 8% MIZ over the daily 5-day back trajectories. April 15th and 16th were the dates of a warm air mass intrusion event with air from Eastern Europe that substantially changed the aerosol composition and size distribution (Dada et al., 2022). There was an increase between the INP filters collected from April 13-16 and that from April 16-19 (from 1.5×10^{-3} to 5.6×10^{-3} L^{-1} at -15 °C), but this approximate 4-fold increase was much smaller than the subsequent 20-fold increase seen in the INP filter collected from April 19-22. Overall, during this April warm air advection event, there was a clear INP increase, with indication of some terrestrial and marine influences.

In the summer, when the highest INP concentrations were observed, *Polaribacter* was commonly detected, which suggests that the air during this time had local or regional marine

influence. However, there were contributions from all tracers. In particular, analysis of the May 25-28 filter detected *Mycena*, *Cryolevonia*, and *Polaribacter*, and subsequently had maximums of 83% ocean, 77% ice, and 5% land. On June 18-21, *Mycena* and *Cryolevonia* were detected and maximums of 100% ice, 53% land, and 23% ocean were observed. This is when *Polarstern* had to leave the pack ice to travel to/from Svalbard for exchange of personnel and provision resupply (Shupe et al., 2022). On August 2-5, only *Cryolevonia* was detected during a local minimum of INP concentration (7.6×10^{-3} at -15 °C. The airmasses during this collection period were still variable, with maximums of 100% ice, 85% ocean, and 13% land. In summary, while INPs followed a clear seasonal trend, their concentrations were also affected by periodic events such as the November storm and April warm air mass intrusion. Even during stable INP compositional periods during the summer (Fig. 2.3), the airmasses generally show the influence of multiple source regions that can include both likely terrestrial (local and longer range) and marine emissions.

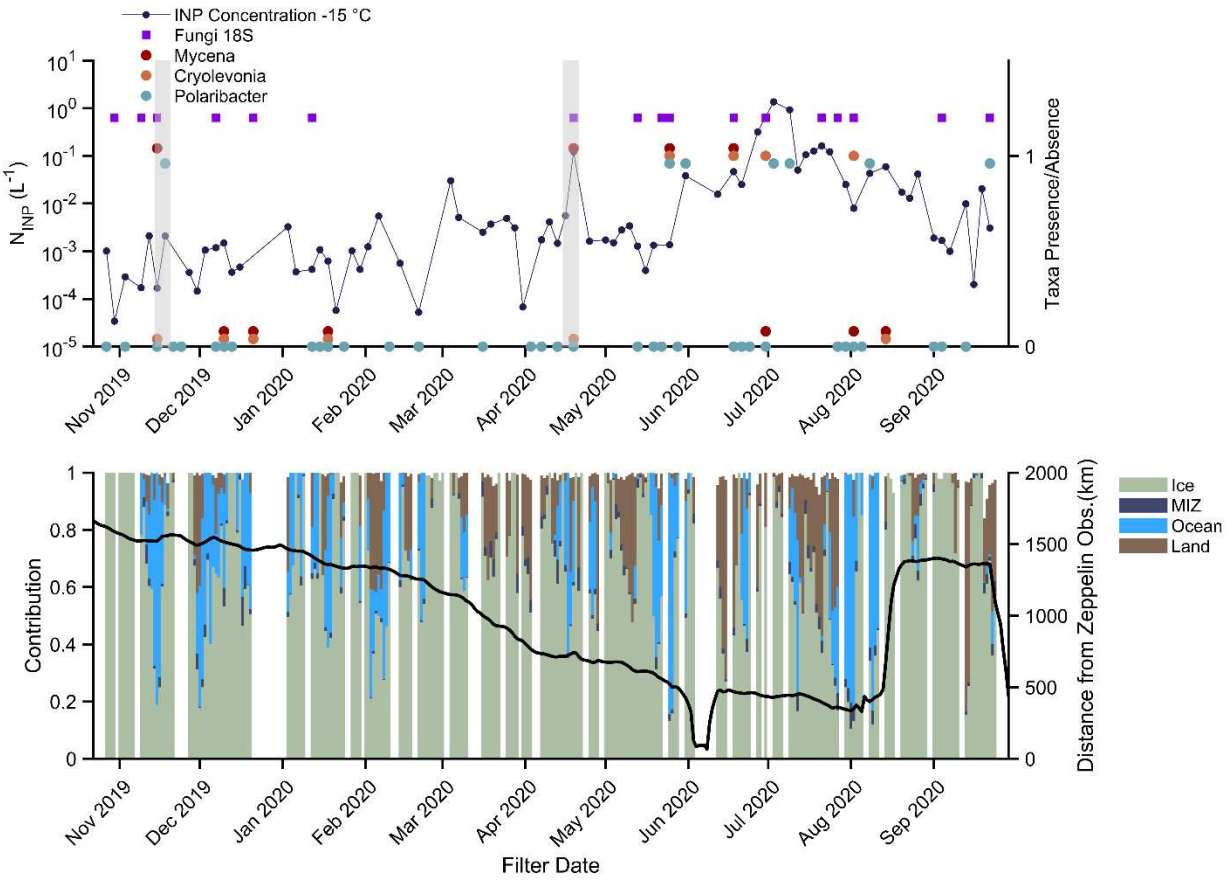

Figure 2.8: (Top) INP concentration at -15 °C and corresponding presence (plotted around 1)/absence (plotted around 0) of two fungal taxa (*Mycena*: red and *Cryolevonia*: orange) and one bacterial taxon (*Polaribacter*: blue). The presence of fungi is also given with purple squares (from the 18S data). (Bottom) Percent contribution to 5 day <500 m back-trajectory and corresponding latitude. Ice (green) refers to greater than 85% sea ice concentration (SIC), MIZ (dark blue) is the marginal ice zone and refers to 15-85% SIC, Ocean (blue) refers to the ice-free ocean <15% SIC, and Land (brown). Latitude data is from GPS monitoring onboard the *Polarstern*. Gray boxes indicate the November storm (11/16-20/2019) and the April warm air mass intrusion (4/15-21/2020).

2.4 Conclusions

Measurements of INPs from the Arctic continue to be important as the region warms disproportionately to the rest of the globe and potential INP sources change, and to improve representation of INPs in climate models for better simulations of cloud properties. Therefore, we sought to improve understanding of the INPs in the central Arctic by reporting a seasonal

cycle of aerosol INP concentrations and composition, and relating this cycle to the seasonality of bacteria and fungi at coincident locations as indicators of air mass influences. What was uncovered is both complicated and promising for future understanding. First, the airmasses sampled tended to be a mixture of marine and terrestrial origin, with most samples involving time spent over ice, open ocean, and land. The annual cycle of bacteria was comprised of many taxa that varied in relative abundance, and few consistent taxa-specific seasonal trends could be detected outside of *Polaribacter*. Basidiomycetes, even though they possess larger spores with faster settling rates, were detected in greater abundance than Ascomycetes mainly in the spring and summer. This implies that there is more local transport in these seasons, but Ascomycetes in large proportions were also detected at all times of the year. Source tracking analysis indicated that the sampled airmasses could rarely be explained by local sequenced sources, except for periodic influence mainly from snow that coincided with cyclones. This result was surprising, in that it implies that even in summer, the bioaerosols and potentially some of the INPs were primarily influenced at times by regional or long-range transport, and not just local emissions. This finding is not something that could be uncovered from the INP data alone, which had its most compositionally stable time from May-August with nearly all of the INPs indicating a heat-labile nature (likely proteinaceous). Heat-labile INPs were detected in high abundances at all times of the year, with some mineral influence possible outside of the summertime period. Comparison of the INPs with bacterial and fungal tracers and airmass trajectories reiterated that terrestrial airmasses can occur at any time of the year, and that bioaerosols and INP concentrations were sensitive to larger scale airmass changes (such as occurred with the November storm and April warm airmass intrusion). This is consistent with the finding that proximate sources did not dominate during MOSAiC in the central Arctic, and general

comparability with coincident long-term measurements at Zeppelin Observatory (Pereira Freitas et al., 2023). Therefore, it is promising for future modeling parameterizations that the measurements in the central Arctic are similar to those made in the wider Arctic, and that even though the air composition for biological aerosols and INPs is complex, the complexity appears to extend Arctic-wide.

3. Permafrost as a source of INPs: persistence during transport

3.1. Introduction

Recent estimates place the Northern Hemisphere permafrost land coverage at approximately 22% of exposed land area (Obu et al., 2019). However, permafrost—earth material like bedrock, soils, and peat that remains at or below 0 °C for two or more years—is thawing across the Arctic, because mean annual ground temperatures have been increasing over the past several decades. For example, Burn and Kokelj (2009) found increases of 1.5 °C in the Mackenzie Delta, Canada, between the 1970s and 2007, and globally, permafrost temperature has increased by 0.29 °C from 2007-2016 (Biskaborn et al., 2019). Thermokarst lakes (TKLs), land depressions resulting from the thawing of ice-rich permafrost, are forecast to increase in a warmer climate (Luo et al., 2015), exacerbated by an increase in wildfires accelerating thaw (Y. Chen et al., 2021). Within permafrost regions, TKLs cover up to 50% of land (Kokelj & Jorgenson, 2013). However, TKLs are inherently dynamic due to being susceptible to drainage, and a projected increase of drained area will further alter the Arctic landscape by, for example, promoting a rapid accumulation of peat (Jones et al., 2022). Additionally, an increased likelihood of coastal erosion from thawing permafrost bluffs poses innumerable economic and environmental challenges, such as damaged infrastructure and ecosystem shifts (Irrgang et al., 2022).

TKLs are vessels for undecomposed carbon from deep permafrost, altering the surface microbial community as well as leading to greenhouse gas production (methane and carbon dioxide) emitted into the atmosphere through ebullition (in ’t Zandt et al., 2020; Jones et al., 2022; Walter et al., 2006). Permafrost harbors a wide diversity of both anerobic and aerobic bacteria, (Ottoni et al., 2022) and contrasts with communities both within and near TKLs, which

have been found to be distinct and complex. For example, Ren et al. (2022) found a higher bacterial alpha diversity in thermokarst water than sediment, and Zhou et al. (2020) found higher sample richness and evenness in thermokarst pit and headstream samples than in rivers.

Thawed permafrost material entering TKLs and the ocean through coastal erosion or riverine transport can become aerosolized through wave breaking and bubble bursting, forming lake and sea spray aerosols. For example, freshwater whitecaps were found in Lake Michigan at wind speeds greater than a modest 3.5 meters per second (Slade et al., 2010) and a quadratic relationship was found between droplet production and wind speed in a simulated freshwater experiment (Pietsch et al., 2018). These lake and sea spray aerosols could be a significant source of ice nucleating particles (INPs), particles that affect cloud glaciation. INPs are necessary to initiate cloud ice formation at temperatures warmer than the level of homogeneous freezing (-38 °C) and by doing so, alter cloud microphysics, radiative properties, and lifetime (DeMott et al., 2010; Kanji et al., 2017). Despite a diverse range of sources (Hill et al., 2018; Šantl-Temkiv et al., 2020), and ice-containing clouds being the dominant source of global precipitation (Mülmenstädt et al., 2015), INPs are atmospherically rare. In the Arctic, land-based INP measurements highlighted a seasonally-dependent contribution of terrestrial sources (soil dust, vegetation) (Creamean et al., 2018; Šantl-Temkiv et al., 2019; Si et al., 2018; Wex et al., 2019). Previously, Alaskan permafrost was collected and tested (Creamean et al., 2020), and INP concentrations were found to be similar to midlatitude soil (Hill et al., 2016) and glacial dust (Tobo et al., 2019). The permafrost INPs were predominantly organic with some biological (inferred from heat sensitivity) influence.

An important concern is the potential for INPs from thawed permafrost to affect Arctic mixed-phase clouds (AMPCs), as AMPC persistence and ubiquity across all seasons exerts

extensive influence on the surface energy budget (Intrieri, 2002; Morrison et al., 2012; Shupe et al., 2006). AMPC cloud temperatures are commonly between -25 and -5 °C (Shupe et al., 2006), which is within the range of activity of many INP sources: mineral dust is efficient below about -15 °C (Murray et al., 2012), biological material (e.g. bacteria, fungi, plant tissue) initiates freezing up to, and at times warmer than, -5 °C (Hill et al., 2018; Huang et al., 2021), and heat-stable organics (e.g. fractions of soil organic matter) dominate across the temperature spectrum (Hill et al., 2016; Kanji et al., 2017; Testa et al., 2021; Tobo et al., 2014). Currently, climate models vary in their representation of Arctic cloud coverage over an annual cycle, likely due to their cloud ice parameterizations (Taylor et al., 2019). INPs are generally poorly represented in models (Murray et al., 2021), but are fundamental to better constrain Arctic amplification, the enhanced high-latitude surface warming (Tan et al., 2022). Given the potential of thawed permafrost to serve as a reservoir of Arctic INPs, this potential feedback to climate warming must be considered for inclusion in future models. Aerosolization of permafrost material from TKLs during fluvial and estuarine transport, and following discharge into the Arctic Ocean, provides pathways for injection of INPs to the atmosphere. In this study, we build off previous work showing the potential of permafrost to be a notable INP source (Creamean et al., 2020) by using tank experiments to simulate the hypothesized transport and aerosolization processes to gain insight into the potential for thawed permafrost to influence AMPCs.

3.2. Materials and Methods

3.2.1 Tank and experimental design

Two separate experiments on permafrost cores were conducted between February and April 2021. Permafrost samples were collected at the Cold Regions Research Laboratory's Permafrost Research Tunnel in Fox, Alaska, and analyzed for their intrinsic INP properties

(Creamean et al., 2020). The Tunnel provides access to ice cemented silt representing high carbon content "Yedoma" permafrost that is largely comprised of windblown loess (Douglas & Mellon, 2019; Kanevskiy et al., 2022). From regional studies, the climate is estimated to have been 5 to 9 °C colder during the period between 15,000 and 40,000 years when the Tunnel soils were syngenetically frozen (Barber & Finney, 1999; Edwards et al., 2001; Kurek et al., 2009; Lachniet et al., 2012). A Snow, Ice and Permafrost Research Establishment (SIPRE) auger was used to collect a range of permafrost core ages and likely variable compositions. A 30,000-year-old core was acquired 83 m into the Tunnel (OT83L), and above the Tunnel, a sample of 500-1,000-year-old permafrost [based upon a loess deposition rate of 1 mm per year (Douglas et al., 2021)] was collected at the top of the permafrost table, 69 cm below the surface (S69CM) (Creamean et al., 2020). Samples were transported frozen in sterile Whirlpak® bags to Colorado State University (CSU), where they remained frozen at -20 °C until analysis. These cores were used in the first and second experiments, respectively, and were chosen to span the largest age range from previous work (Creamean et al., 2020) for simulation of permafrost transport and aerosolization. Ten grams of each permafrost core (with material gathered from multiple core locations) were placed into a 9.5 L tank with 4 L of 0.2 µm-filtered artificial freshwater (AFW), with the recipe based on the Arctic tundra lakes sampled in Pienitz et al. (1997) (Table A.1.1). The tank was based on a design by May et al. (2016) used to generate lake spray aerosol (Fig. 3.1). To isolate the tank from laboratory air, it was fitted with inlets for HEPA- and carbon-filtered air that continuously entered the tank at 4 L min^{-1} to flush the headspace. Two plunging jets (2.55 mm diameter) driven by a peristaltic pump (Cole-Parmer) periodically generated aerosols through bubble bursting. A magnetic stir bar in the tank ran continuously on a low

setting for gentle mixing throughout the course of the experiment, but material was still able to settle (Fig. 3.1).

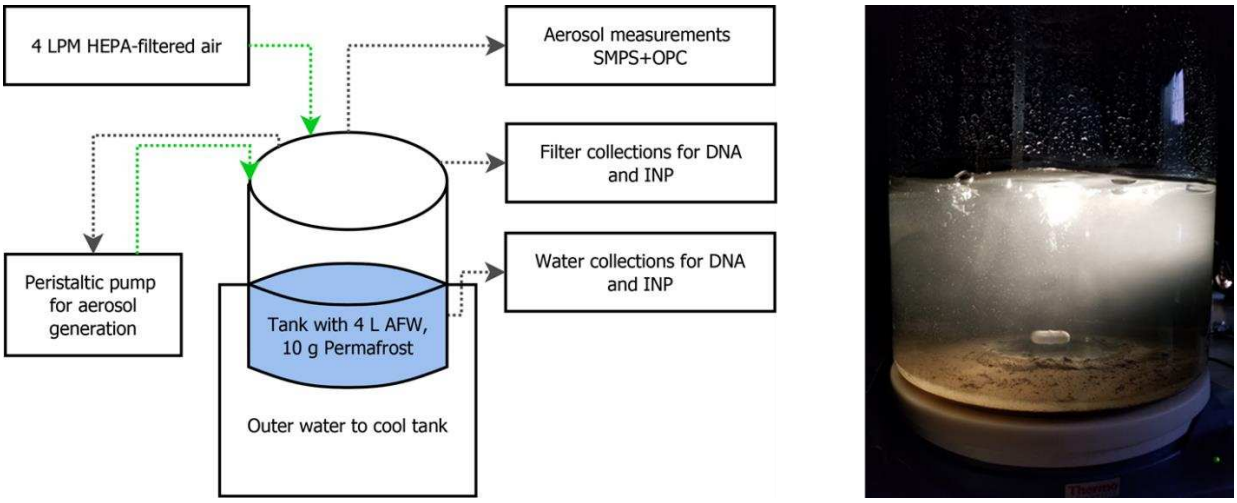

Figure 3.1. (Left) A diagram showing inputs (green) and outputs (gray) into/from the tank. (Right) Image of the tank running at Day 2 with 20,000-year-old permafrost (experimental pre-test). The tank body is glass, the lid is stainless steel, and the tank is sealed with a silicone gasket.

Each experiment ran for 3-4 weeks (Fig. 3.2), with the second experiment (S69CM) extended to 28 days to hand-stir and resuspend all sediment and re-test the water for INPs since it was found visually to contain coarser material. The temperature of the water was controlled with an outer basin connected to a chiller. Tank temperatures and salinities were selected based on previous water temperature and salinity measurements in Arctic tundra lakes, Admiralty Bay, Alaska and the proximate Beaufort and Chukchi Seas (Goñi et al., 2019; Philo et al., 1993; Pienitz et al., 1997; Hartwell et al., 2018). Salinity was increased (with Brightwell Aquatics NeoMarine Salt) and water temperature simultaneously decreased in three steps (Fig. 3.2), mimicking changes during the transport of thawed permafrost material from a TKL into the Arctic Ocean through estuaries in late summer. Microbes released through the dissolution of the

permafrost samples were allowed to remain in solution and evolve over the course of the experiments. The only additions to the tank were weekly 0.2 µm-filtered AFW (~200 mL) to compensate for initial evaporative and sample collection losses (during AFW conditions only), and sea salts dissolved in 0.2 µm-filtered deionized (DI) water to compensate for later evaporative and collection losses.

Days 1-13	Day 14	Days 15-16	Days 17-25
Artificial Freshwater Temperature= 15 °C	Salinity=5.5 g/L Temperature= 9 °C	Salinity=17.5 g/L Temperature= 9 °C	Salinity=30 g/L Temperature= 4 °C

Figure 3.2. Approximate experimental schedule showing tank water salinity and temperature over time. Conditions were selected to mimic thermokarst lakes (Days 1-13), estuaries (Days 14-16), and the Arctic Ocean (Days 17-25). The color scale used here and in subsequent plots represents the phases of the experiments, defined by increasing salinity and decreasing temperature.

3.2.2 Aerosol measurement and collection

Outlets directly off the tank fed headspace air through pre-cleaned polycarbonate filters held in aluminum in-line filter holders (Pall), which collected aerosol for INP and DNA analyses (Whatman Nuclepore Track-Etched membranes, 47 mm diameter with 0.05 and 0.2 µm pore size, respectively). All filters had a 10 µm pre-cleaned backing filter underneath to prevent contamination from the filter holder support mesh. Filters for INP analyses were pre-cleaned with brief ultrasonication in methanol (two 10 s pulses) (Barry et al., 2021b), those used for DNA analyses were soaked in 10% hydrogen peroxide (H_2O_2) for 10 min (Uetake et al., 2020), and each followed by rinses with 0.1 µm-filtered DI water. Aerosols were dried with silica gel diffusion driers <30% RH and then measured with a Scanning Mobility Particle Sizer (3080 SMPS, TSI) that sized particles from approximately 10-500 nm and an Optical Particle Counter

(OPC, Alphasense OPC-N2) to measure number concentrations of particles with diameters from 0.38 to 17 µm.

Aerosol filters and water samples for INP and DNA analyses were collected at several times throughout the experiments. Aerosol size distributions measured with the SMPS and OPC ran in parallel during INP filter collection periods. During filter collections, the peristaltic pump was turned on (280 mL min^{-1} per jet) to simulate wave breaking and bubble bursting or heavy rain. Filters for INP analyses were sampled for 2-3 hours at a flow rate of about 1.75 standard Liters (sL) min^{-1} (0 °C and 101.325 kPa) to collect approximately 250 sL per filter. DNA filters ran overnight for about 12 hours to obtain a greater sample volume for downstream analyses. Both INP and DNA filter samples were stored in sterile Petri dishes (Pall). At the end of each INP filter period, water samples for both INP and DNA analyses were collected into sterile 50 mL centrifuge tubes (Corning) by briefly disconnecting the peristaltic pump tubing (but leaving the tank sealed). For INPs, approximately 20 mL of water was collected. For DNA, 150 mL was passed through a Sterivex (Millipore) 0.22-µm pore filtering unit. All samples were either stored at -20 °C until processing to avoid degradation of DNA and INPs, or time-permitting, some INP samples were tested fresh (no difference in concentration was found: Fig. A.1.1). In periods of non-disturbance, the peristaltic pump ran continuously at the lowest setting to avoid an anaerobic environment forming in the tubing.

3.2.3 Processing INP samples

INP concentrations on filters and in water samples were measured with the CSU Ice Spectrometer (IS). The current setup is most recently described in Barry et al. (2021a) and DeMott et al. (2018). Briefly, aerosol filters were resuspended in either 10 or 12 mL of 0.1 µm-filtered DI water. Both the aerosol and water samples were dispensed, along with 20-fold

dilutions (250 µL sample and 4750 µL 0.1 µm-filtered DI water), in groups of 32-50-µL droplets into 96-well PCR trays (Optimum Ultra, Life Science Products). The trays were placed into aluminum blocks in the IS, cooled at 0.33 °C min^{-1}, and corrected with a corresponding 0.1 µm-filtered DI water negative control. Frozen fractions were converted to cumulative INP concentrations (sL^{-1} air or mL^{-1} water) (Vali, 1971), the former by considering the total volume of air passed through each filter. Undiluted estuarine and seawater samples were corrected for approximate freezing point depressions of 0.4, 1.2 and 2 °C, at respective tank salinities of 5.5, 17.5, and 30 g L^{-1}. All samples were further corrected with a tank blank experiment with samples collected under the same conditions without permafrost. During this tank blank, aerosol and water samples were collected at three time points: artificial freshwater, artificial seawater, and one-week settled artificial seawater. Exponential regressions, with interpolations as needed, were fit to the blank samples to correct corresponding INP concentrations as a function of time and salinity (typically <10% of the original value). Ninety-five percent confidence intervals were calculated based on Agresti and Coull (1998).

Treatments on the aerosol and water samples give general INP composition (McCluskey et al., 2018; Suski et al., 2018). Selected sample suspensions were heated at 95 °C for 20 min to destroy proteinaceous (heat labile) INPs and digested in 10% H_2O_2 under UV-B light and 95 °C heat for 20 min to remove all organic (both heat labile and -stable) INPs. The INPs remaining after peroxide digestion comprise the inorganic fraction and were presumed to be of mineral origin. Samples from the blank experiment were also put through treatments to produce corrections for the treatment data. Additionally, Day 1 water samples for each experiment were passed through 10, 1, and 0.2 µm pore size filters, using 13 mm diameter polycarbonate filters

(Whatman Nuclepore Track-Etched membranes) for size-fractionation of the initial permafrost INPs after their suspension in the tank.

3.2.4 Processing of DNA samples

Aerosol samples for DNA analyses were concentrated and extracted following the methods in Uetake et al. (2020). For water samples, the Sterivex unit was cracked open with a PVC pipe cutter (Cruaud et al., 2017) before the filter resuspension was concentrated, and DNA extracted identically to the aerosol samples. The V4-V5 region of the 16S ribosomal RNA gene was targeted with 515yF/926pfR primers (Parada et al., 2016) with Illumina adapters and temperature cycling conditions identical to Uetake et al. (2020). One point of difference is the use of UCP Multiplex PCR master mix (Qiagen), after tests, indicated enhanced amplification. After amplification, samples were purified with AMPure XP (Beckman Coulter), barcoded with IDT for Illumina Nextera DNA UD Indexes, and sequenced at the Colorado State University Next Generation Sequencing Core with the Illumina MiSeq Reagent Kit v3 (600-cycle). Reads were demultiplexed in the Illumina BaseSpace Sequence Hub platform and imported into QIIME2 Version 2021.11 (Bolyen et al., 2019) for subsequent analyses. Files were denoised with DADA2 to generate an amplicon sequence variant table (Callahan et al., 2016). Next, pre-formatted SILVA 138 reference sequence and taxonomy files were used (Quast et al., 2012; Robeson et al., 2020), and taxonomy assigned using the QIIME2 feature-classifier plugin (Bokulich et al., 2018; Pedregosa et al., 2011). Any mitochondrial, chloroplast, and archaeal reads were removed. Samples were corrected for the tank (2 aerosol and 1 water), 1 concentration and extraction blank, and 2 PCR negative controls with the decontam package (Davis et al., 2018) prevalence and frequency methods. Lastly, samples were rarefied at approximately 17000 reads for calculation of diversity metrics.

3.3. Results and Discussion

3.3.1 Temporal variability of INP concentrations

Over the course of the experiments, the INPs in the 30,000-year-old (OT83L) and 1,000-year-old (S69CM) permafrost had intrinsic differences (Fig. 3.3). The older permafrost had 2-3 orders of magnitude higher INP concentrations compared with the younger permafrost in both the aerosol and water, across all temperatures and salinities. Complete INP-temperature spectra are shown in Figures A.2.2. The INP concentrations from the 30,000-year-old permafrost were relatively constant with time. Notably, there was effectively no change in the aerosol and water INP concentrations for 2 weeks after addition to freshwater. Later, there was a steady but modest decrease when incubated in full seawater. Percent decreases between Day 1 and 25 were 40% in the aerosol and 72% in the water at -18 °C. However, INP levels in the water were still elevated, with 400,000 mL^{-1} at -18 °C on Day 25. Therefore, this type of permafrost material entering TKLs is likely to contribute emissions of INPs for several weeks.

The 1,000-year-old permafrost had larger INP decreases overall between Day 1 and 25, with 95 and 85% reductions at -18 and -26 °C, respectively, in the aerosol. In the water, decreases between Day 1 and 25 were >99% at -10, -18, and -26 °C. In contrast to the older permafrost, salinity had an immediate effect on the younger permafrost, as concentrations dropped shortly after the salt was increased. For example, INPs in the water went from 200,000 mL^{-1} to 5,000 mL^{-1} at -26 °C, a 97.5% decrease in 2 days (Days 14-16 when salt was increased to 17.5 g L^{-1}). However, this change was somewhat temperature (i.e., INP activation) dependent, with a decrease of 68% at -10 °C within the same period. The lower INP concentrations, compared to the 30,000-year-old permafrost, combined with a large effect of salinity, suggests a reduced influence of this type of permafrost material on atmospheric INP concentrations.

To test if the rapid decrease of INPs with increasing salinity in the 1,000-year-old permafrost was caused by their deactivation or by settling, the tank was hand-stirred on Day 28 to resuspend all sediment and re-tested immediately (Figs. 3.3 and A.2.3). INPs increased in both the aerosol and water across the entire temperature spectrum, rebounding to the original levels measured in artificial freshwater. Thus, the majority of the INP decrease is attributed to sedimentation (of larger INPs: Section 3.3.2), although flocculation and other unknown mechanisms cannot be ruled out (with some unexpected variability in the aerosol under full salt conditions). Overall, the INP concentrations from the 30,000-year-old permafrost were much more constant with time and salinity than those from the 1,000-year-old permafrost, as evidenced by a lower slope of the INP concentration with time in both the aerosol and water (Fig. A.1.4).

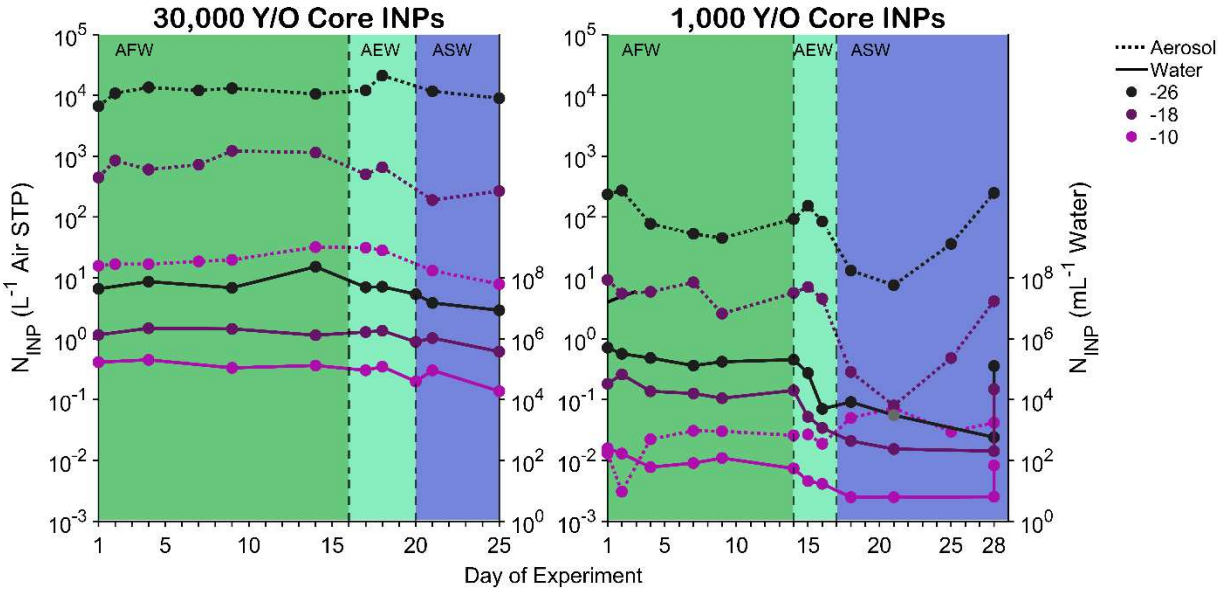

Figure 3.3. Measured ice nucleating particle (INP) concentrations for the aerosol (dotted lines: left axes) and water (solid lines: right axes) as a function of experiment day for temperatures of -26 (black), -18 (purple), and -10 °C (magenta). The 30,000-year-old (OT83L) permafrost core experiment is plotted on the left and the 1,000-year-old (S69CM) permafrost core experiment on the right. Background shading denotes salinity transitions (AFW=Artificial Freshwater; AEW=Artificial Estuary Water; ASW=Artificial Seawater). Filled gray marker for S69CM Day

21 water at T=-26 °C is given the value before background correction as the corrected value went below the limit of detection.

3.3.2 Permafrost INP composition

To investigate reasons for INP concentration differences between the experiments, we next examine their size and composition. The 1,000-year-old permafrost contained coarser material and the water in the tank was visually clearer throughout the experiment compared with the 30,000-year-old permafrost. Size-filtration of the Day 1 water indicated INPs larger than 10 µm accounted for 60% of the total down to -15 °C of the 1,000 year-old core experiment (Fig. A.2.5). The younger permafrost also had a bimodal INP population in the water at colder temperatures, with the majority larger than 1 µm or smaller than 0.2 µm (e.g., combined 89% at -25 °C), whereas the INPs in the older permafrost were predominantly between 0.2 and 10 µm (e.g., 89% at -25 °C; 97% at -15 °C). Heat and peroxide treatments on the starting and ending aerosol and water samples for the two experiments revealed that nearly all the INPs were organic compounds (Figs. 3.4, A.2.6, A.2.7). Mineral INPs were only detected at the coldest temperatures (i.e., ~3% mineral in the Day 1 30,000-year-old permafrost aerosol and 10% mineral in the Day 1 and 28 1,000-year-old permafrost water at -26 °C). The largest percentage of heat-labile organics was at the warmer temperatures, consistent with the results in Creamean et al. (2020); however, they contrastingly always predominated to -20 °C and sometimes colder than -25 °C. The fraction of heat-labile and heat-stable organics changed with time and between experiments but was also temperature dependent. For example, in the 1,000-year-old permafrost Day 1 water, about 50% of the INPs at -26 °C were heat-labile, while there were no detectable heat-labile INPs at the same temperature by Day 28. At the same time, heat labile INP fractions at -18 and -10 °C increased with time. In the 30,000-year-old permafrost, the compositional

changes were more gradual, with a general trend of increased heat-labile INP fractions over time in both the air and water. This may help to explain the greater variability of INP concentrations with time in the younger core (Figs 3.3 and A.2.4). In both permafrost samples, organic INPs dominated in both aerosol and water across the temperature spectrum for the range relevant to AMPCs [-25 to -5°C (Shupe et al., 2006)].

To confirm if the decreases in INPs in the 1,000-year-old permafrost were predominately due to sedimentation, treatments were done on the post-stir Day 28 water to investigate compositional changes pre- and post-stirring (Fig. A.2.8). In the warmer temperatures bins (-18 and -10 °C), the post-stirring fractions were almost identical to the Day 1 water. However, for the coldest bin (-26 °C) the fractional contributions were more similar to the Day 28 pre-stir sample than to Day 1. This indicates that in addition to INP sedimentation, there were compositional changes over time at colder temperatures, with a permanent loss of a heat-labile population. However, this compositional change did not seem to influence the overall INP concentrations (Fig. 3.3), which suggests a diverse range of INP sources derived from thawed permafrost.

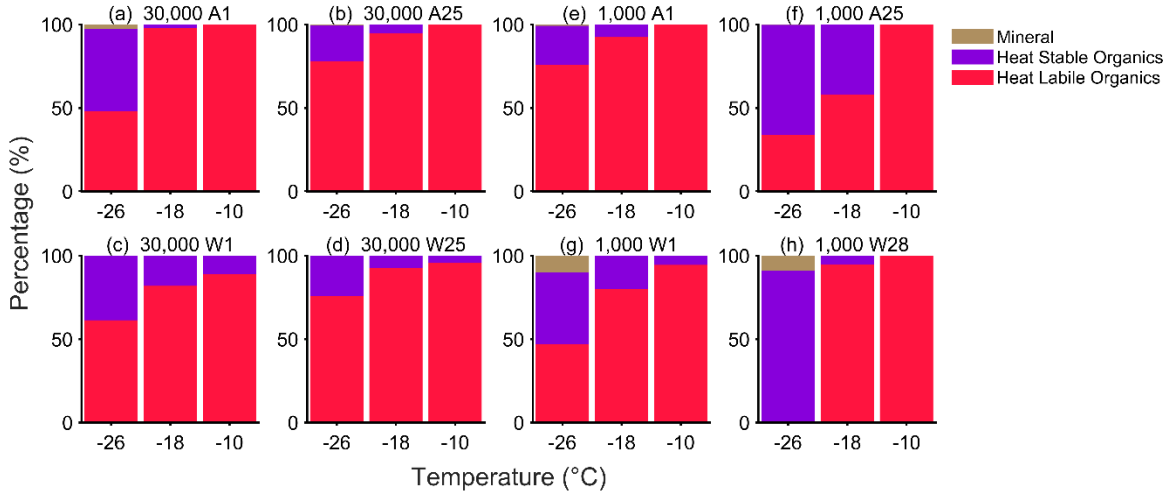

Figure 3.4. Ice nucleating particle (INP) compositional histograms for the 30,000-year-old (OT83L: a-d) and 1,000-year-old (S69CM: e-h) permafrost core experiments from the treatment

analyses. Sample type [aerosol (A) or water (W)] and day of experiment are denoted in each plot title. Heat labile organics (INPs destroyed after 95 °C heating) are in red, heat stable organics (INPs additionally destroyed after hydrogen peroxide digestion) are in purple, and the remainder (presumed mineral INPs) are shown in tan.

3.3.3 Compositional and temporal variability of the bacterial community

With both permafrost core experiments exhibiting differences in INP concentration and composition, and a large fraction of INPs in all experiments identified as heat-labile and therefore likely of biological origin, we next explore the bacterial community composition. The aerosol and water genus-level relative abundance heat maps (Fig. 3.5) show the bacterial community varied in time and between experiments. The initial compositions were similar to previous permafrost profiles at the phylum level (Jansson & Taş, 2014), with the 30,000-year-old permafrost containing a majority of Firmicutes (89%), while the 1,000-year-old permafrost contained a mixture of Firmicutes, Chloroflexi, Acidobacteriota, Actinobacteriota, and Proteobacteria.

As the experiments progressed, the 30,000-year-old permafrost was rapidly dominated by fewer taxa, and after the salt was added on Day 16, the water and aerosol contained virtually only *Pseudomonas*. The 1,000-year-old permafrost also contained a high relative percentage of *Pseudomonas* that increased with time; however, a greater number of taxa co-dominated compared with the older core, even after the salt was added, and there was more temporal variability. *Pseudomonas* was likely present in low levels in the original permafrost samples, as only 6 of the 209 *Pseudomonas* amplicon sequence variants (ASVs) were detected in the tank water control (0 detected in the tank aerosol, extraction, and PCR controls); these 6 may have been carried over since the tank blank experiment was performed last. Additionally, the dominant *Pseudomonas* ASVs varied between experiments.

The trends in the heatmaps are consistent with the aerosol and water alpha diversities (Fig. A.2.9), with a lower Shannon Index in the older versus younger core throughout the entire period (Shannon, 1948), consistent with previous studies [e.g., Mackelprang et al. (2017)]. A Kruskal-Wallis test confirmed the alpha diversities of the two experiments were significantly different between the aerosol ($p=0.02$) and water ($p=0.04$) samples. Within experiments, a p value of 0.03 was found between the aerosol and water in the 1,000-year-old permafrost, but no significance was found between the aerosol and water in the 30,000-year-old permafrost ($p=0.57$). A higher alpha diversity in the aerosol than the water in the younger core (Fig. A.2.9) shows the taxa came out of the water in different relative proportions under the disturbance of simulated wave breaking. However, this same trend was not found in the older permafrost, which may be a property of its lower alpha diversity.

In both experiments, the alpha diversity changed rapidly over the first few days and then stabilized, which was expected as a consequence of placing diverse communities specialized for cold environments into a warm and homogeneous aerobic environment. A comparable attenuation was seen by Zhou et al. (2020), who found significantly lower sample richness and evenness in river versus thermokarst pit and headstream samples. However, the relative stabilization in diversity over several weeks was maintained under changing salinity, despite a changing community composition (most pronounced in the younger permafrost). The higher alpha diversity in the younger permafrost along with greater temporal fluctuations in bacterial community composition are consistent with its larger INP variability, in both number and composition, compared with the older permafrost (Figs. 3.3, 3.4, and A.2.4), although this method can only serve as a proxy for trends in ice nucleating bacteria.

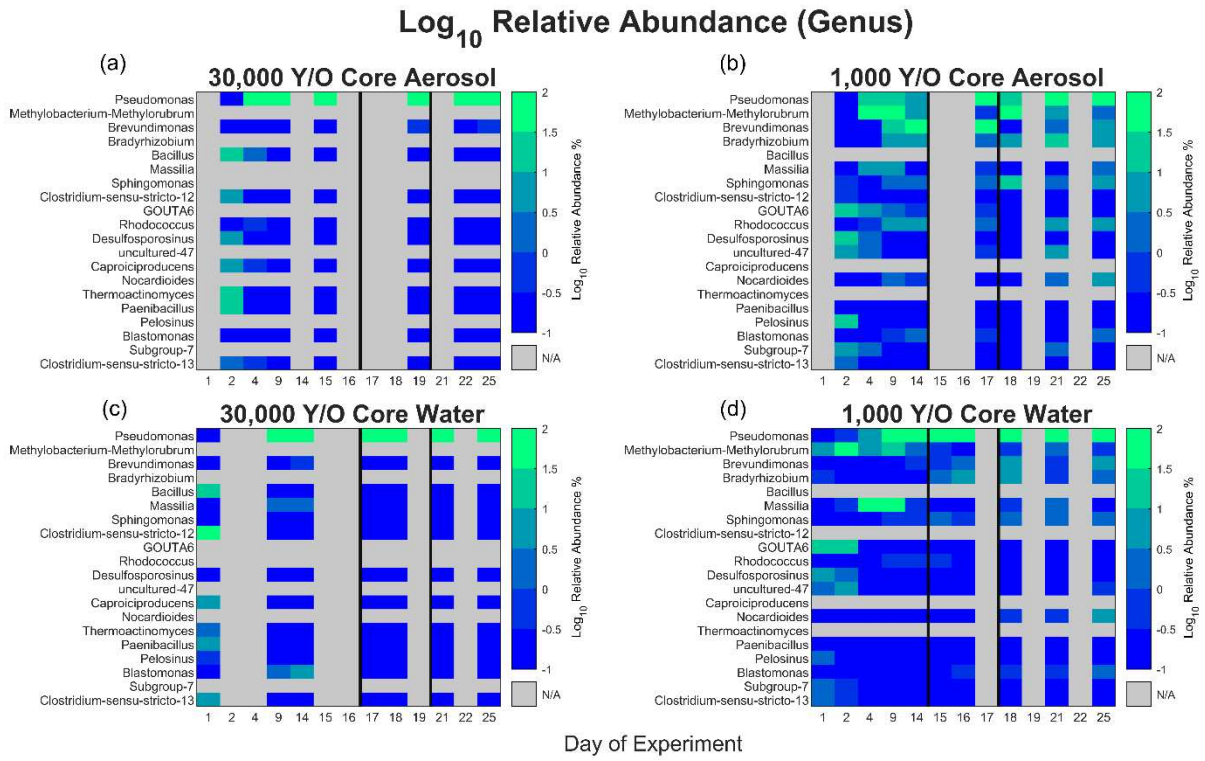

Figure 3.5. Genus-level relative abundance heatmaps for the aerosol (a-b) and water (c-d) bacterial community for the 30,000-year-old (OT83L; a,c) and 1,000-year-old (S69CM; b,d) permafrost core experiments. The top 20 abundant taxa for the combined dataset are given from top to bottom on the y-axis, with the color bar referring to units of log base 10 of the relative abundance percentage. Gray indicates taxa comprising less than 0.1% relative abundance (y-axis) or samples not collected on a particular day (x-axis). Black lines indicate tank transitions to estuarine (first) or full salt (second) conditions.

3.3.4 Broader atmospheric implications

Both experiments showed variability in the INPs and bacterial community in time and between permafrost cores, but to compare these findings to other known INP sources, a normalization basis is needed, such as the surface active site density parameter (n_s) (DeMott, 1995; Niemand et al., 2012). This parameter normalizes aerosol INP concentrations by the total aerosol surface area and has been commonly used to describe local and global INP sources such as mineral dust (DeMott et al., 2015), clean marine air (McCluskey et al., 2018), and wildfire smoke (Barry et al., 2021a). Here, we assume all aerosolized particles and INPs are solely from

permafrost material exiting a water body and use the measured aerosol size distributions and an assumption of particle sphericity to compute particle surface areas. Figure 3.6 reveals a wide variability of the n_s parameter spanning over 5 orders of magnitude, with the 30,000-year-old permafrost having larger n_s values overall (significant at 95% confidence across entire temperature spectrum). For reference, previous parameterizations from laboratory-generated desert dust (Ullrich et al., 2017) and clean marine air (McCluskey et al., 2018) are plotted. This large range is attributed to a decrease of INPs with time for both cores combined with increased emissions of total aerosol (Figs. A.2.10 and A.2.11) with salinity (for example, in the 30,000-year-old permafrost, the total surface area increased from 150 μm^2 to 2500 μm^2 between Days 1 and 25). The elevated aerosol concentrations with salinity are consistent with May et al. (2016) who found a positive relationship between aerosol concentration, bubble number, and ion solution concentration among freshwater and seawater and Zinke et al. (2022) who found increased particle surface area with salinity. Decreased tank temperature could have also contributed to increased aerosol with time during periods with temperatures below 10 °C (when the salts were added) (Salter et al., 2014; Zinke et al., 2022). The n_s values from the 30,000-year-old permafrost indicate activity near to or exceeding the desert dust parameterization, which is considered a dominant source of INPs below approximately -15 °C (Murray et al., 2012). Overall, the 30,000-year-old permafrost contained more INPs per surface area of emitted material than the 1,000-year-old permafrost. The 1,000-year-old permafrost also had more variable n_s values that coincide with its fluctuating INP concentrations and bacterial community composition. Nonetheless, most values for the younger core (including under oceanic salinity) and all values for the older core were higher than the clean marine airmass parameterization across all temperatures. This suggests that thawed permafrost material could enhance INP

emissions in estuarine and sea spray aerosol, despite reductions from INP sedimentation and dilution due to greater aerosol concentrations generated by seawater (than freshwater). However, investigation of the true atmospheric emission rates and potential impacts require considerable future field, lab, and modeling efforts.

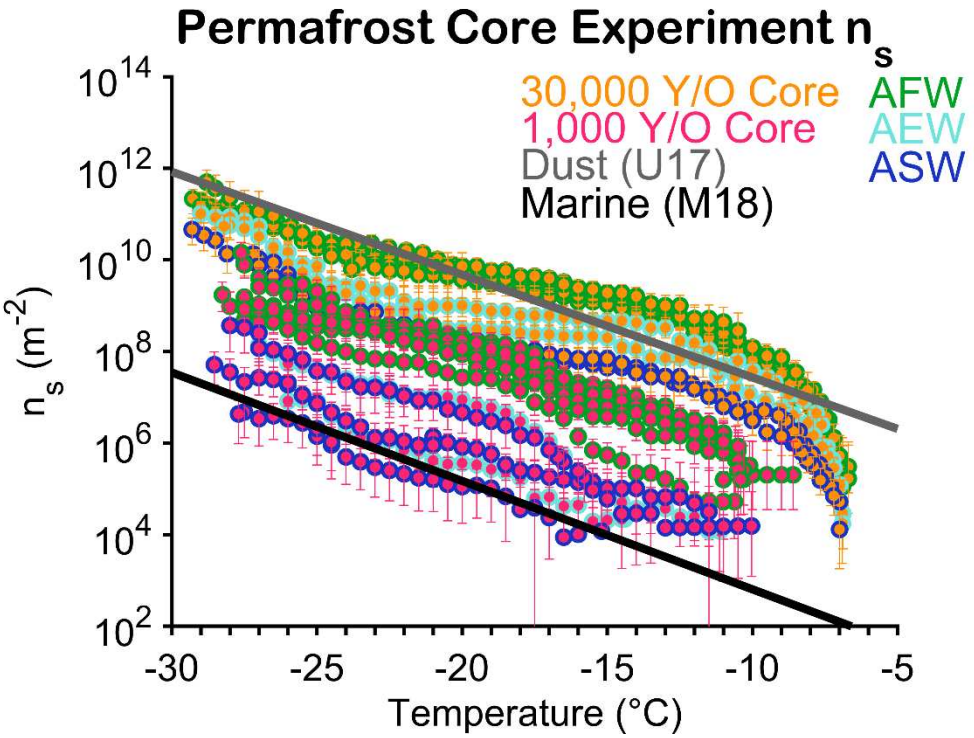

Figure 3.6. Ice nucleating particle (INP) surface active site density (n_s) spectra for all aerosol samples from the 30,000-year-old (OT83L: orange) and 1,000-year-old (S69CM: pink) permafrost core experiments. Green outlined markers indicate emissions from artificial freshwater (AFW), light blue outlined markers indicate emissions from artificial estuary water (AEW), and dark blue outlined markers indicate emissions from artificial seawater (ASW). Previous parameterizations for desert dust (Ullrich et al., 2017) and clean marine air (McCluskey et al., 2018) are given in gray and black, respectively.

Given their high n_s values, aerosolized INPs from thawed permafrost material entering thermokarst lakes, rivers, and oceans have the potential to be a source of atmospheric INPs, but their importance is dependent upon release into and from water bodies through wave breaking and bubble bursting. Potential release mechanisms include top-down permafrost thaw, slope

failure (e.g., retrogressive thaw slumping, active layer detachment slides), and coastal and riverbank erosion. Top-down permafrost thaw is increasing as global permafrost temperatures rise (Biskaborn et al., 2019) and from the conversion between bedfast and floating lakes (those which do not freeze all the way down). Climate warming is leading to the formation of taliks that consist of a year-round thawed zone (in ’t Zandt et al., 2020). Retrogressive thaw slumping is a prodigious source of particulate organic matter that can enter water bodies (Shakil et al., 2020) and is projected to increase with an increase in rainfall (Kokelj et al., 2015). Active layer detachment slides, through which the top layer of the soil becomes detached from the underlying permafrost, can exacerbate permafrost thaw and be an additional source of organic matter to water bodies (Bowden, 2010). Permafrost coastal erosion and riverbank retreat are also likely to increase in the future (Irrgang et al., 2022; Nielsen et al., 2022), especially with ice-rich Yedoma permafrost similar to our core samples, with a higher ice content being more prone to erosion. For example, Kanevskiy et al. (2016) found an average retreat of a riverbank in northern Alaska of 11 m per year over 15 years of monitoring. All of these pathways could be sources of INP-rich organic material into water bodies, which may be subsequently emitted into the atmosphere through disturbances. Thawed permafrost material that does not enter water bodies may be an episodic source of INPs to the atmosphere with wind exposure, but we hypothesize the primary mechanism is through wave breaking and bubble bursting.

Previous work showed the tested permafrost cores had ice nucleation abilities comparable to glacial soil dust (Tobo et al., 2019) and midlatitude soil (Hill et al., 2016), which means a large potential reservoir of INPs that could be released under a warming climate (Creamean et al., 2020). If the INPs did not become aerosolized, the INP source to the atmosphere would be negligible. For example, the ice nucleation ability of Arizona Test Dust degrades rapidly with

only 2 days of aging in deionized water (Perkins et al., 2020). However, in this small-scale laboratory study, we were able to confirm the ability of thawed permafrost INPs to both persist in suspension and enter the atmosphere. When portions of a 30,000-year-old and 1,000-year-old permafrost core were placed into a tank with artificial freshwater and subjected to a simulated disturbance, the aerosol INP concentrations were elevated, with those of the older core approaching levels of pure desert dust on a surface area basis.

Even though both permafrost cores showed a potential source of atmospheric INPs, they had fundamentally different properties. Compared with the ancient permafrost, the 1,000-year-old permafrost had lower and more variable INP concentrations, coarser material with many INPs greater than 10 μm in the water (susceptible to sedimentation), and a higher bacterial community alpha diversity. The INPs that sediment out may, however, be periodically re-suspended by storms [average of 12-22 stormy days per year in the Arctic Ocean near Alaska (Yang, 2004)], which can additionally incorporate sediment in sea ice (Molnia, 1983). For example, Inoue et al. (2021) found an order of magnitude increase in INPs in the Chukchi Sea under stormy conditions with high turbidity. Compositionally, both permafrost samples had INPs that were nearly all organic across the temperature spectrum, but the younger core was more variable in the heat-labile versus heat-stable fractions over time. The temporal bacterial community composition shifts confirm that thawed permafrost is a dynamic substrate, though the INP populations, especially of the older permafrost, were more resistant to change. More data are needed for model parameterizations, which will not only depend on the type of permafrost, but also the water type and likelihood of mixing. Since thawed permafrost INPs have the potential to alter the regional Arctic INP budget and longevity of Arctic mixed-phase clouds, further investigation is of utmost importance under a warmer climate. Overall, the atmospheric

implications could extend far beyond the thermokarst lake or coastline from which the thawed material enters the water.

4. Active thermokarst regions contain rich sources of ice nucleating particles

4.1. Introduction

The Arctic landscape is sensitive, dynamic, and changing, with many of the shifts connected to the permafrost. Permafrost, earth material like soil, ice, rocks, and organic matter that remains frozen for more than two years, underlies approximately 22% of the Northern Hemisphere landmass (Obu et al., 2019), and is rapidly thawing from Interior Alaska to the Arctic (Douglas et al., 2021; Farquharson et al., 2022; Streletskiy et al., 2015; Streletskiy et al., 2017). Melting of ice-rich permafrost leads to development of "thermokarst", which includes the formation of water bodies called thermokarst lakes (TKLs). The formation and drainage of TKLs strongly impact surrounding ecosystems, and additionally TKLs are sources of methane and carbon dioxide to the atmosphere (Jorgenson, 2013; Walter et al., 2006). Other thermokarst landforms include retrogressive thaw slumps, slope failures often triggered by the flow of material from the top seasonally frozen and thawed active layer, and thermokarst troughs and pits, low-lying areas created when ice-rich permafrost or massive ice features like ice wedges degrade. It was estimated in a study in Prudhoe Bay, Alaska, that 23% of the surface ice wedges degraded between 1949 and 2012, leading to major impacts on the composition of the vegetation (Jorgenson et al., 2015). Permafrost coasts across the Arctic are increasingly sensitive to erosion, the loss of which has environmental and economic impacts (Irrgang et al., 2022).

In addition to landforms created, thawing permafrost has broad atmospheric impacts, as it can potentially alter clouds by serving as a source of ice nucleating particles (INPs) (Barry et al., 2023a; Creamean et al., 2020). INPs are particles that trigger ice formation in clouds, and are necessary to initiate ice formation warmer than -38 °C (level of homogeneous freezing). They can alter the surface energy budget by impacting the cloud phase and optical thickness, as Arctic

liquid clouds strongly contribute to a positive cloud forcing (Shupe & Intrieri, 2004). Replacement of ice with liquid in clouds has been shown to strengthen Arctic amplification, which is the enhanced regional warming due to phenomena such as the ice-albedo feedback (Tan & Storelvmo, 2019). Sources of INPs include: biological material such as proteins from certain species of bacteria and fungi active at temperatures up to and warmer than -5 °C; mineral dust that is efficient below about -15 °C; and complex organics that are effective over the entire temperature range (e.g. Hill et al., 2018; Murray et al., 2012; Testa et al., 2021; Tobo et al., 2014). Thawed permafrost material was shown to have comparable ice nucleation activity to midlatitude and glacial soil dust (Creamean et al., 2020). If the material enters TKLs, its persistence in the water and release in lake spray aerosol could persist for weeks, with ice nucleation activity on a surface area basis up to and exceeding that of mineral dust (Barry et al., 2023a). Moreover, the majority of the INPs were inferred to be of biological and organic origin and highly active at relatively warm temperatures (Creamean et al., 2020), and therefore could impact the lifetime of long-lasting Arctic mixed-phase clouds that commonly exist between -25 and -5 °C (Morrison et al., 2012). Although permafrost is a massive reservoir of INPs, it is not represented as a source in global or regional climate models. Models struggle to accurately represent Arctic clouds, with current ice microphysical parameterizations thought to be a large contributor to biases (Taylor et al., 2019), underscoring the value of Arctic INP measurements.

Previous Arctic INP measurements have largely focused on collecting air samples from ships, aircraft, or fixed ground-based sites (e.g., Bigg, 1996; Hartmann et al., 2021; Mason et al., 2016; Prenni et al., 2007; Wex et al., 2019). Recent studies have noted evidence of increased INP concentrations in terrestrial airmasses (Conen et al., 2016; Creamean et al., 2018; Irish et al., 2019; Šantl-Temkiv et al., 2019). Most recently, a year-long observation of INPs in the central

Arctic revealed a seasonal dependence with the highest concentrations found in summer (Creamean et al., 2022a), similar to trends observed in other Arctic work (e.g., Creamean et al., 2018; Wex et al., 2019). Despite several Arctic studies, a comprehensive source-based analysis has not been done. In the ARCtic Study of Permafrost Ice Nucleation (ARCSPIN) of September 2021, we surveyed several previously-uncharacterized potential sources of airborne terrestrial-based Arctic INPs in a region underlain by continuous permafrost. Permafrost and ice wedge cores, active layer, vegetation, sediment, and water samples were collected at peak thaw in late summer to profile their INP contents and relate this to coincident air measurements.

4.2 Methods

4.2.1 Measurement overview

The ARCSPIN sampling campaign was conducted from September 1-17, 2021, within and near Utqiaġvik, Alaska. Its surficial geology is categorized as marine silt and sand, where permafrost temperatures have increased by 0.85 °C (-8.532 to -7.678 °C) at 20 m between 2009 and 2021 (Romanovsky, 2021). The lowland landscape is dominated by patterned ground comprised of ice wedge polygons that are actively undergoing thermokarst processes (Farquharson et al., 2016). Common vegetation in this region includes sedge, grass, moss, rush, dwarf-shrub, and forb (Raynolds et al., 2006).

The overview of all sampling days is detailed in Table 4.1 and Figure 4.1. Half (6) of the days focused on downwind TKL (both fresh and brackish) measurements, where, if feasible, upwind measurements were included (3 of 6 days). Upwind and downwind locations were determined by the wave movement and wind direction. All wind data came from the Wiley Post–Will Rogers Memorial Airport weather station (PABR). Other periods focused on sampling in the saline lagoon with a small boat (3 days) and coastal estuarine and oceanic sampling (3 days).

Sites were chosen based on accessibility with all-terrain vehicles (ATVs) as well as to maximize areal coverage and diversity of terrain and weather conditions (e.g., targeting onshore versus offshore winds). Additionally, pre-campaign water measurements were made at one location in the Chukchi Sea (71.32921429 °N, 156.678083 °W), approximately 2 meters from the coast, on August 22-24 to sample conditions during (22^{nd}) and post (23^{rd} and 24^{th}) stormy weather. The storm had minimal precipitation, and was instead marked by strong winds and waves, with average sustained winds of 7.6 (gust>13), 3.1, and 1.8 m s^{-1}, respectively, on the 3 days.

At each measurement site, coastal and lake-shore aerosol filters, TKL or ocean water, sediment, permafrost, ice wedge, active layer, and vegetation samples were collected. Aerosol for INP analyses was collected onto 0.2 µm Nuclepore track-etched membranes (Whatman) in disposable filter units (Nalgene) with a battery-powered pump (Gilian 12). The filters were precleaned before loading by brief ultrasonication (2 ×10 s) in methanol followed by two 0.1 µm filtered deionized (DI) water rinses (Barry et al., 2021b). The sampling height was approximately 1.5 m, and filters were collected after sampling 2 to 4 hours, depending on site. Typical flow rates were 7 standard L (sL: 0 °C, 1013.25 mb) min^{-1}, and the average total volume of air filtered per sample was 1350 sL. The filter setup in the field locations is shown in Figure 4.2. Additionally, filters were collected at the U.S. Department of Energy Atmospheric Research Measurment North Slope of Alaska (DOE ARM NSA; herewithin: DOE) facility (Fig. 4.1). Five samples were collected between 2 and 22 hours, with sample length determined by the consistency of the wind direction. The wind directions covered were out of the S, SE, E, NE, and NW. The average flow rate was 22 sL min^{-1}, which resulted in an average volume of air filtered of 17400 sL at a sampling height of approximately 10 m. Additional aerosol samples were collected for DNA analyses, but are not presented in this work.

Water samples were collected into a prerinsed (with sample) 500 mL bottle (Nalgene), before placed into sterile 15 or 50 mL tubes (Corning). Water was collected at the surface and near the bottom of the TKLs (depth 0.6-2 m) and coastal ocean (depth ~1.5 m) with a kayak and horizontal water sampler (Pentair), up to 70 m from the shoreline. TKL and oceanic sediment samples were collected with a Universal Corer (Aquatic Research Instruments) approximately 5-10 cm below the floor from the same location as the water sample, and subsamples were placed into 1-oz Whirl-Pak bags. Permafrost and ice wedge cores in proximity to the water were taken with an 8 cm diameter Snow, Ice, and Permafrost Research Establishment (SIPRE) auger, and 2-4 subsamples were taken at various depths along the core (based on visual differences in composition) and packed into Whirlpak bags. The average core length was 84 cm. A corresponding active layer sample was taken directly above each permafrost core and placed into 1-oz Whirl-Pak bags. Representative vegetation clippings were collected into plastic slider bags, weighed, 250 mL of DI water added, shaken, and poured into a sterile 15 mL tube (Corning). All samples were stored in a cooler at the measurement site, and then in a -20 °C freezer in Utqiaġvik at the Naval Arctic Research Laboratory for the duration of the campaign. They were subsequently transported frozen in coolers back to Colorado State University (CSU) and stored at -20 °C until analysis.

4.2.2 Sample analysis

Samples were analyzed for INP concentrations, each as a function of temperature, with the CSU Ice Spectrometer [IS; (Creamean et al., 2022; DeMott et al., 2018)]. Sediment, active layer, ice wedge, and permafrost samples were thawed, stirred, and a suspension made by weighing approximately 2 g of material and combining it with 20 mL of DI water. Filters were resuspended in 7-8 mL of 0.1 µm filtered DI water. Due to the abundance of INPs, dilution series

were made with suspensions and water samples in 0.1-µm-filtered DI water: 11-fold dilutions for the aerosol (400 µL sample and 4000 µL 0.1-µm-filtered DI water) and 20-fold dilutions (250 µL sample and 4750 µL 0.1-µm-filtered DI water) for all other samples. Suspensions and their corresponding dilutions were dispensed in blocks of 32-50 µL aliquots in single-use 96-well PCR trays (Optimum Ultra), along with a 32-well negative control of 0.1-µm-filtered DI water. The trays were placed into the aluminum blocks of the IS, cooled at a rate of 0.33 °C min^{-1}, freezing detected optically with a CCD camera, and 1-s data recorded. Next, the frozen fractions were converted to cumulative INP concentrations per mL of water, per L of air (considering the volume of air filtered and resuspension volume), or per g of material (considering the weight of material and resuspension volume) (Vali, 1971). 95% confidence intervals were computed following Agresti and Coull (1998). In total, 20 aerosol, 47 water, 20 permafrost, 8 sediment, 11 ice wedge, 6 active layer, and 5 vegetation washing samples were processed.

Aerosol INP concentrations were corrected from the average of two blanks that were prepared, transported, and processed identically, except that no airflow was sent through them, by subtraction of the average INPs per filter as a function of temperature before conversion to concentration. These corrections were minor since, for example, there were only an average of 73 INPs per blank filter at -28 °C where there were typically around 5000 INPs at -28 °C even in many of the lower volume tundra air samples. Undiluted estuarine and seawater samples were corrected for freezing point depression (FPD), based upon measured conductivity in the field (Extech EC400) and at CSU for the saltier samples (Extech EC150). Samples were normalized to the average measured conductivity of seawater samples of 51383 µS cm^{-1} corresponding to a 1.8 °C FPD, resulting in a lagoon correction of 1.2 °C and brackish TKL correction of 1.1 °C. The dilutions were not adjusted since they were prepared with 0.1-µm-filtered DI water. Thermal

treatments were done on select samples for insight into sample composition. 2.4 mL of selected samples were heated at 95 °C for 20 min and retested on the IS to determine the heat labile fraction of INPs. This treatment has been used extensively in the past on samples from diverse environments (e.g. Kanji et al., 2017; McCluskey et al., 2018; Suski et al., 2018), to estimate contributions of INPs that are inferred to be of proteinaceous origin.

Total organic carbon (TOC) concentrations were measured in a subset of representative water samples (28 of 47 total) by injecting 3 mL of sample into a TOC-VCSH (Shimadzu). Total carbon was first determined through combustion at 680 °C, creating CO_2, and inorganic carbon was determined through sample acidification followed by sparging to additionally liberate CO_2. The CO_2 was detected and compared to calibration curves. TOC was calculated by subtracting the inorganic carbon from the total carbon. The background TOC was subtracted by injecting 3 mL of DI water in sample tubes 3 times and taking the average.

Principal component analysis (PCA) was performed on all INP-temperature spectra over the temperature interval from -6 to -20 °C. This range was chosen because the majority of data had measurements and definable characteristics over this interval (as many spectra are similarly log-linear, at colder temperatures). Samples that did not have complete measurements in this range were either interpolated or extrapolated. To build the matrix for analysis, the slope in 2 degree temperature intervals was calculated (change in $\log_{10}$[INP concentration]/change in temperature). Another potential defining variable, $\log_{10}$ of the ratio of the average INP concentration in each 2 degree temperature interval and the average INP concentration at -12 °C, was also calculated. In total, there were 121 samples included, each with 14 variables. Next, the sampling dimension mean was removed, all variables were standardized, and the temporal covariance matrix calculated before performing eigenanalysis.

Table 4.1. Name, latitude, longitude, environmental location, and list of processed sample types for the main sample collections. Lagoon locations on September 7, 9, and 15 refer to an average latitude and longitude of the collected samples, and the locations of TKLs with both upwind and downwind collections refer to the downwind measurement site. "DOE" refers to the location of the fixed Department of Energy site. For "Samples analyzed", DA=Downwind Aerosol, UA=Upwind Aerosol, A=Aerosol, AL=Active Layer, P=Permafrost, I=Ice Wedge, S=Sediment, LW=Lagoon Water, SW=Seawater, TW=Thermokarst Lake Water, V=Vegetation.

Date (2021)	***Name***	***Latitude (°)***	***Longitude (°)***	***Environment/ Collection type***	***Samples analyzed***
1-Sep	Emaiksoun Lake	71.25057	-156.77317	Thermokarst lake (TKL)	DA, P, S, TW
2-Sep	Untitled Lake 1	71.23529	-156.30406	TKL: upwind and downwind	DA, UA, AL, P, I, S, TW, V
4-Sep	DOE	71.32272	-156.61506	Fixed	A
5-Sep	Point Barrow	71.38535	-156.46100	Ocean and lagoon	A, LW, SW
6-Sep	Nunavak Bay	71.25240	-156.87332	TKL (brackish)	DA, AL, P, I, S, TW, V
7-Sep	Elson Lagoon	71.29581	-156.26890	Lagoon	A, LW
8-Sep	Will Rogers/ Wiley Post Monument	71.15311	-157.06609	Ocean: onshore	A, AL, P, S, TW, V
9-Sep	Elson Lagoon DOE	71.25556 71.32272	-156.01580 -156.61506	Lagoon Fixed	A, LW, SW A
11-Sep	Untitled Lake 2	71.23806	-156.60472	TKL: upwind and downwind	DA, UA, AL, P, S, TW, V
12-Sep	DOE	71.32272	-156.61506	Fixed	A
13-Sep	Mayoeak River	71.25915	-156.44528	TKL (brackish)	DA, P, I, S, TW, V
14-Sep	Will Rogers/ Wiley Post Monument	71.15312	-157.06609	Ocean: offshore	A, AL, P, I, S
15-Sep	Elson Lagoon DOE	71.31522 71.32272	-156.29845 -156.61506	Lagoon Fixed	A, LW, SW A
17-Sep	Emaiksoun Lake	71.23097	-156.77237	TKL: upwind and downwind	DA, UA, AL, P, I, S, TW, V
18-Sep	DOE	71.32272	-156.61506	Fixed	A

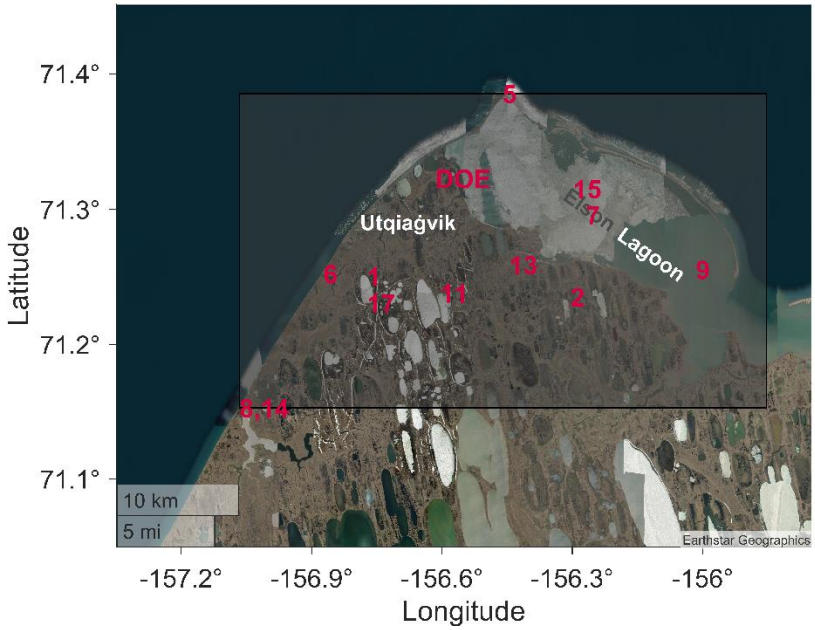

Figure 4.1. Area map showing the bounding box of all samples obtained in black, and the location of the specific sampling days (in September 2021) from Table A1 in red. “DOE” refers to the location of the fixed site. The locations of TKLs with both upwind and downwind collections refer to the downwind measurement site.

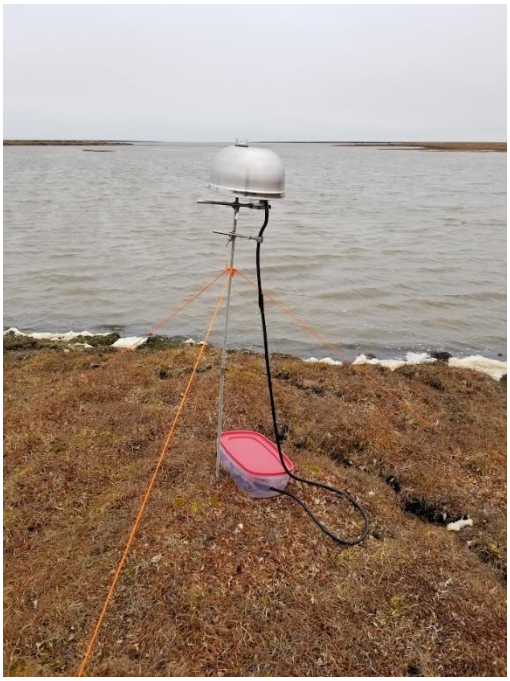

Figure 4.2. Sampling setup for measuring ice nucleating particles (INPs) in the aerosol near a thermokarst lake.

4.3 Results and Discussion

4.3.1 Overview of Arctic INP measurements

INP concentrations active at -15 °C measured in the ambient aerosol during ARCSPIN ranged from 0.0009 to 0.4 L^{-1} (average 0.04 L^{-1}) (Fig. 4.3; spectra in Fig. A.3.1). -15 °C is focused upon for comparison to previous Arctic INP measurements and due to its relevance for Arctic mixed-phase clouds (Morrison et al., 2012). The highest values were found downwind of TKLs, near the coast, and over Elson Lagoon (Figs. 4.3-4.4). Among aerosol filter sample types (TKL, ocean, lagoon, and DOE), the DOE had the lowest variability (SD: 0.0076 L^{-1}) while the lagoon had the highest variability (SD: 0.23 L^{-1}), attributed to sampling diverse sources from a moving boat.

To test the contribution of water bodies to atmospheric INPs, a pairwise t-test indicated increased INP concentrations downwind of TKLs at 95% confidence in all three cases at -18 to -23 °C and at the coldest temperatures (-23 to -28 °C) for September 17th only (Fig. A.3.2). Wind speeds were variable, with the averages on the 2nd, 11th, and 17th, of 9.3, 2.9, and 6.2 m s^{-1} respectively, near and above the 3.5 m s^{-1} threshold found by Slade et al. (2010) for freshwater aerosol enhancement. There was no obvious correlation between INP concentrations and wind speed, which agrees with recent relative insensitivity found between freshwater aerosol mass flux and wind speed (Harb & Foroutan, 2022). We conclude that TKLs can generate INPs, but their impact on ice nucleation activity may be freezing temperature-dependent. For the potential of coastal INP enhancement, a comparison between wind directions at one location was made on September 8th and 14th (Table 4.1 and Fig. 4.1; values in Fig. 4.3). INP concentrations were higher across all measured temperatures at 95% confidence when the wind was onshore (average

direction on the 8th of 246°) from the Chukchi Sea compared with offshore (average on the 14th of 115°). This is despite slightly greater average wind speeds on the 14th (5.1 vs. 4.3 m s^{-1}). This analysis provides evidence for water bodies as potential vessels for transporting INPs to the air under wind stress or alternative mechanisms such as methane bubbling up through TKLs, called ebullition (Walter et al., 2006). Primary marine aerosol has been found to have a power law relationship with wind speed over the Southern Ocean (Moore et al., 2022; Sanchez et al., 2021) and North Atlantic (Saliba et al., 2019), and an exponential relationship was found between particle concentration and wind speed over the Arctic Ocean (Leck et al., 2002). Enhancement in aerosol does not necessarily translate to enhancement of INPs. Further, the wind speeds experienced during ARCSPIN were typically less than 10 m s^{-1}, with an average of 6 m s^{-1} for the month of September. At the DOE, which was removed from local direct inputs, there was consistency in INP concentrations regardless of wind direction (captured from terrestrial and marine sources) and average wind speed (ranging from 3.9-7.2 m s^{-1}), suggesting a background level of INPs in the air coexisting with periodic coastal and TKL enhancement.

The aerosol INPs measured during ARCSPIN varied in comparability to other terrestrial-based Arctic campaigns, partially attributed to seasonality. The concentrations were higher than Creamean et al. (2018), who measured an average INP concentration of 0.005 L^{-1} at -15 °C between March and May at Oliktok Point, and Mason et al. (2016), who also found an average INP concentration of 0.005 L^{-1} at -15 °C at Alert between March and July. The INPs were more similar to those reported by Šantl-Temkiv et al., (2019), who measured an average INP concentration of 0.07 L^{-1} at -15 °C in August at Villum Research Station. Wex et al. (2019), who measured INPs at Utqiaġvik for a year, found concentrations up to 0.01 L^{-1} at -10 °C during September, which is within the range and time period of ARCSPIN (Fig. A.3.1).

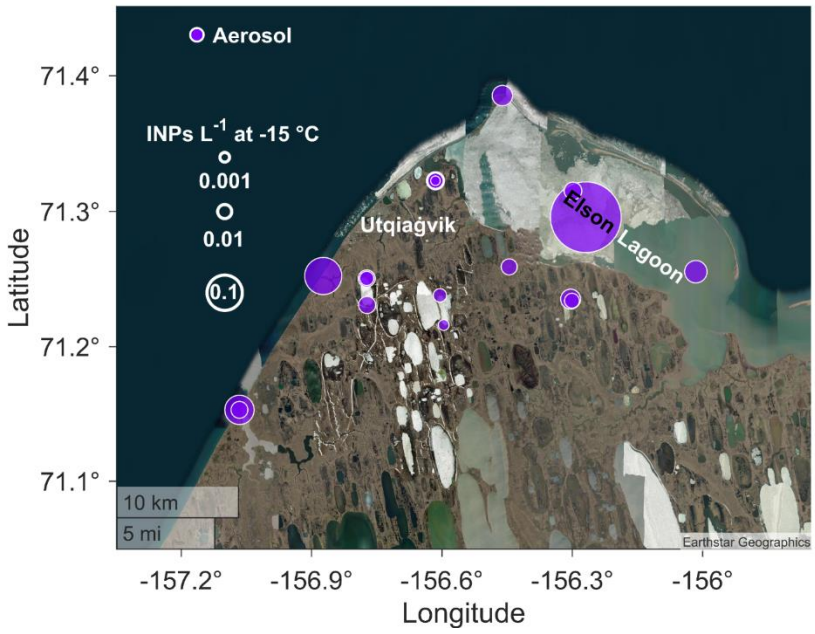

Figure 4.3. INP concentration per L air at -15 °C for aerosol samples (purple). The size of the markers corresponds to the INP concentration. Lower left coastal samples were sampled on September 8th and September 14th.

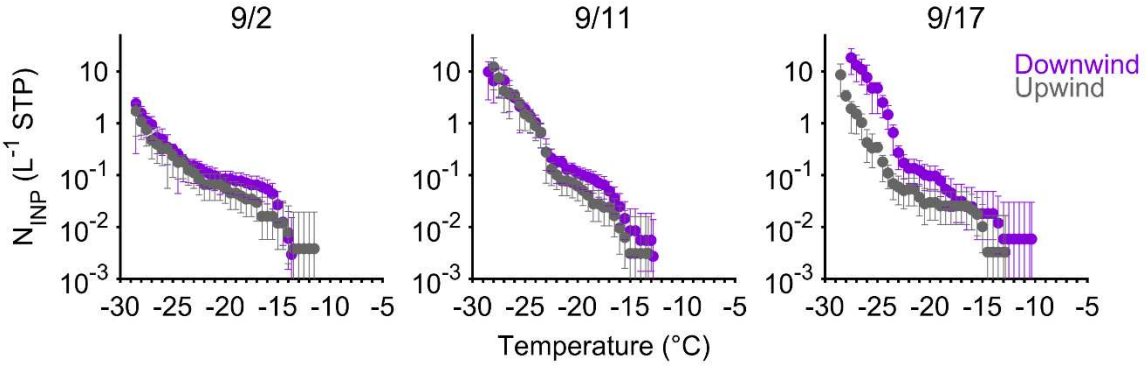

Figure 4.4. Cumulative INP-temperature spectra for the three cases that sampled aerosol upwind (gray) and downwind (purple) of a thermokarst lake. 95% confidence intervals are plotted (any confidence intervals overlapping with 0 are not shown).

In addition to TKLs serving as sources for aerosolized INPs, INP concentrations in water samples were highest (but most variable) in the TKLs, followed by the lagoon and seawater, respectively (Fig. 4.5; spectra in Fig. A.3.3). At -15 °C, the average TKL INP concentration was

120,000 mL^{-1} (SD=178,000 mL^{-1}) compared with 31,000 mL^{-1} (SD=17,000 mL^{-1}) in the lagoon and 17,000 mL^{-1} (SD=19,000 mL^{-1}) in seawater. However, stormy conditions increased INPs in seawater from 1,300 mL^{-1} to 63,000 mL^{-1} at -15 °C. Previous measurements from the Bering Strait and Chukchi Sea (Creamean et al., 2019) measured INP concentrations of 100-3000 mL^{-1} at -15 °C, much lower than ARCSPIN. Other ship-based Arctic measurements farther from land (Hartmann et al., 2021; Wilson et al., 2015) reported INP concentrations less than 100 mL^{-1} at -15 °C in bulk seawater during summer. Therefore, the weather conditions, type of water body, and proximity to the coast are all important for determining water INP concentrations.

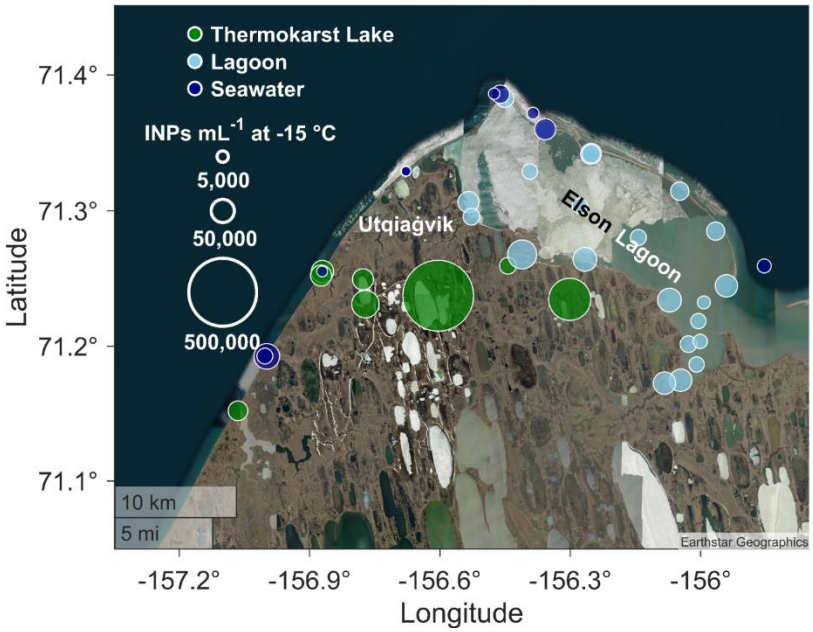

Figure 4.5. INP concentration per mL water at -15 °C for thermokarst lake (TKL) (green), lagoon water (light blue), and seawater (dark blue) samples. The size of the markers corresponds to the INP concentration.

Next, we measured many of the terrestrial-based sources in a thermokarst region that may contribute to the Arctic INP budget. Soil and vegetation samples were rich sources of INPs (Fig. 4.6; spectra in Fig. A.3.4), with permafrost having up to $5x10^8$ INPs g^{-1} at -15 °C (average of

$1.1x10^8$ g^{-1}, SD=$1.4x10^8$ g^{-1}). The highest permafrost values were found near the coast, suggesting a prodigious reservoir of INPs that could be released into water bodies undergoing coastal erosion or thermokarst degradation. Permafrost sampled at different core depths showed similar INP concentrations (Fig. A.3.5) and, therefore, only the sample closest to the surface is presented. The permafrost INP spectra largely agree in concentration with permafrost samples from Fairbanks, Alaska, in Creamean et al. (2020) and with glacial outwash sediments from Svalbard, Norway (Tobo et al., 2019), with values between 10^8 and 10^9 g^{-1} at -15 °C. The comparability to ARCSPIN, despite differences in collection depths and locations, is promising for modelling of permafrost sources.

Lake and ocean sediment contained up to 10^8 INPs g^{-1} (average of $3.2x10^7$ g^{-1}, SD=$3.5x10^7$ g^{-1}) at -15 °C, with the highest values in sediment found inland within freshwater TKLs and lower values found near and from the Chukchi Sea. Despite the ocean sediment being a lower source of INPs, its suspension would have contributed to the 50-fold INP increase observed in Chukchi Sea water during the stormy period. Vegetation washings contained lower levels of INPs overall (average of $2x10^6$ g^{-1}, SD=$1.7x10^6$ g^{-1} at -15 °C), but were the source of the warmest temperature INPs (Fig. A.3.4), with a detected freezing onset as warm as -4 °C, likely indicative of populations of ice nucleation-active bacteria (e.g., Hill et al., 2014; Huang et al., 2021). Active layer samples (Figs. A.3.6 and A.3.7) had similar ice nucleation activities to permafrost, with an average concentration of $3.6x10^8$ g^{-1} at -15 °C. Ice wedges (Figs. A.3.6 and A.3.7) had values comparable to TKLs (assuming a density of 1 g mL^{-1}), with an average of $1.7x10^5$ g^{-1} (SD=$1.7x10^5$ g^{-1}) at -15 °C. The similarity between ice wedges and TKLs is ascribed to snow melt being the dominant source of ice wedge ice and contributing to a majority of TKL

water. Thermokarst landscapes are therefore comprised of several potent (and deep) INP reservoirs that are comparable with midlatitude soils and could influence Arctic clouds.

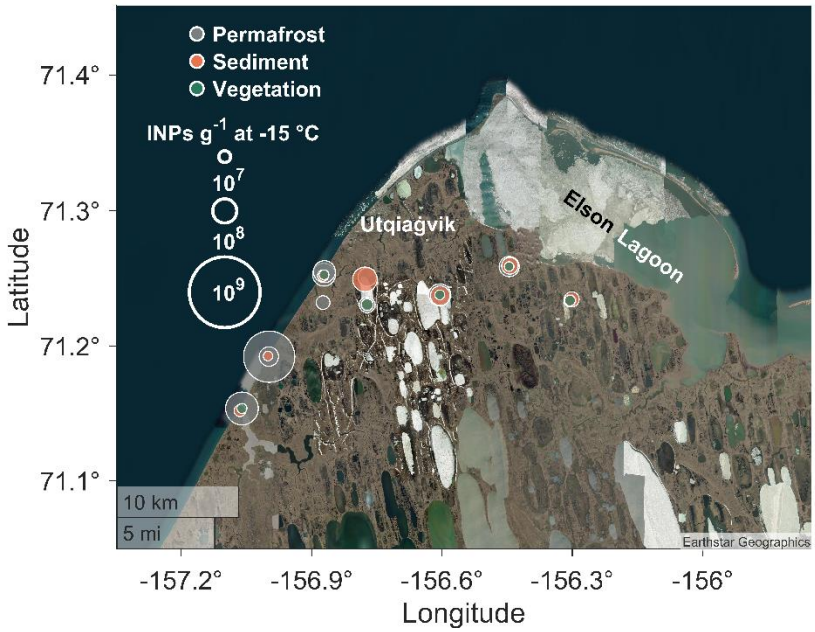

Figure 4.6. INP concentration per g at -15 °C for permafrost (gray), lake and ocean sediment (salmon), and vegetation (dark green) samples. The size of the markers corresponds to the INP concentration.

4.3.2 Source separation and characterization

To better understand similarities and differences among thermokarst landscape sources and aerosol samples, we next present PCA and heat treatment results. PCA was applied to visualize how samples' spectral profiles clustered within and between categories to relate INPs from sources to the aerosol. Figure 4.7 shows all source and aerosol samples colored by sample type. PC1 explains 47% of the variance while PC2 explains an additional 23% of the variance. Among sources, PC1 and PC2 separate water and vegetation (negative PC1 values) from permafrost and sediment samples (positive PC1 and negative PC2 values). The aerosol spans the range of collected samples along PC1, but is separated on PC2.

Samples can be further analyzed for characteristic INP differences through response to heating. In Figure 4.8, suspensions of all samples for September 2nd and 17th were heated to 95 °C to divide the INPs into heat labile and stable fractions. The heat labile fraction identifies putative biological INPs through protein denaturation, and the heat stable fraction may be organic or mineral. Among sources, the TKL water, ice wedge, and vegetation had the highest fractions of heat labile INPs, with above 95% at -10 °C, and above 90% at -15 °C except for the ice wedge on the 2nd (Fig. 4.8). The permafrost, active layer, and TKL sediment samples had high fractions of heat labile INPs at -10 °C (>70%: except for the sediment on the 2nd), while only the active layers and sediment sample from the 17th had greater than 50% heat labile INPs at both -15 and -20 °C.

The PCA revealed that while most sources, especially water and vegetation washings, cluster together within their groups, indicating relative homogeneity across location and time, there was substantial variability among permafrost. This suggests permafrost INP composition may be more heterogeneous, despite concentration comparibility to previous work presented in section 3.1. Both methods reveal differences between the permafrost and active layer, which were similar in INP concentrations (Table S1) but have relative separation in PCA (Fig. 4.7) and heat sensitivity (Fig. 4.8), suggesting dissimilar INP populations. TKL sediments may also harbor distinct INP populations from other samples, with some uniqueness in heat labile fractions (Fig. 4.8), but similar values to permafrost on the PCA (Fig. 4.7). TKL sediments are comprised of former permafrost, but undergo loss of organic carbon, nitrogen, and phosphorous during the transition (Ren et al., 2022), which could have contributed to both measured similarities and differences to permafrost seen with the PCA and heat treatment. These tools

should be seen as complimentary in providing pieces of evidence, as PCA utilizes the spectral shape of the original sample, while the heat treatment compares proportions in the two spectra. All aerosol samples contained abundant heat labile INPs, with fractions of nearly 100% at all temperatures (Fig. 4.8). With PCA, the aerosol spans the range of collected samples along PC1, suggesting diverse source types contributing to the collected airborne INPs (Fig. 4.7). As many source samples contained abundant heat labile INPs, with the most prominent being the TKL water, ice wedge, and vegetation, this analysis agrees with the PCA that multiple sources could have contributed. However, the PCA also uncovers that the aerosol are separated from most other samples along PC2, implying the aerosol additionally contained unsurveyed sources (e.g. other local or long range transport).

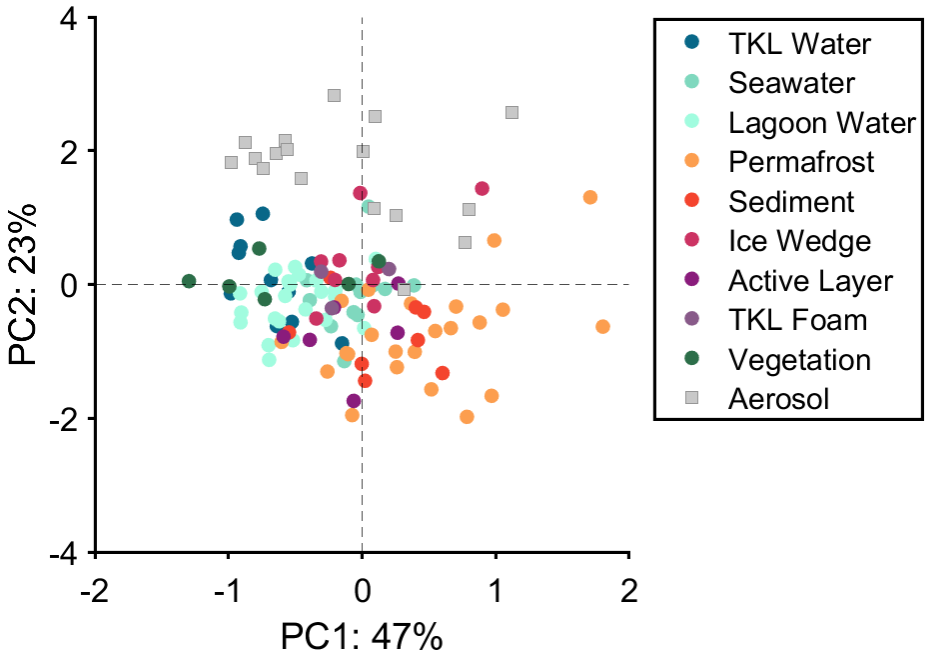

Figure 4.7. Principal component analysis for all processed samples, broken down by sample type, based upon sample slope and a midpoint concentration ratio between -6 and -20 °C. Percent variance explained is given on each respective axis. The axes limits are scaled by the variance explained.

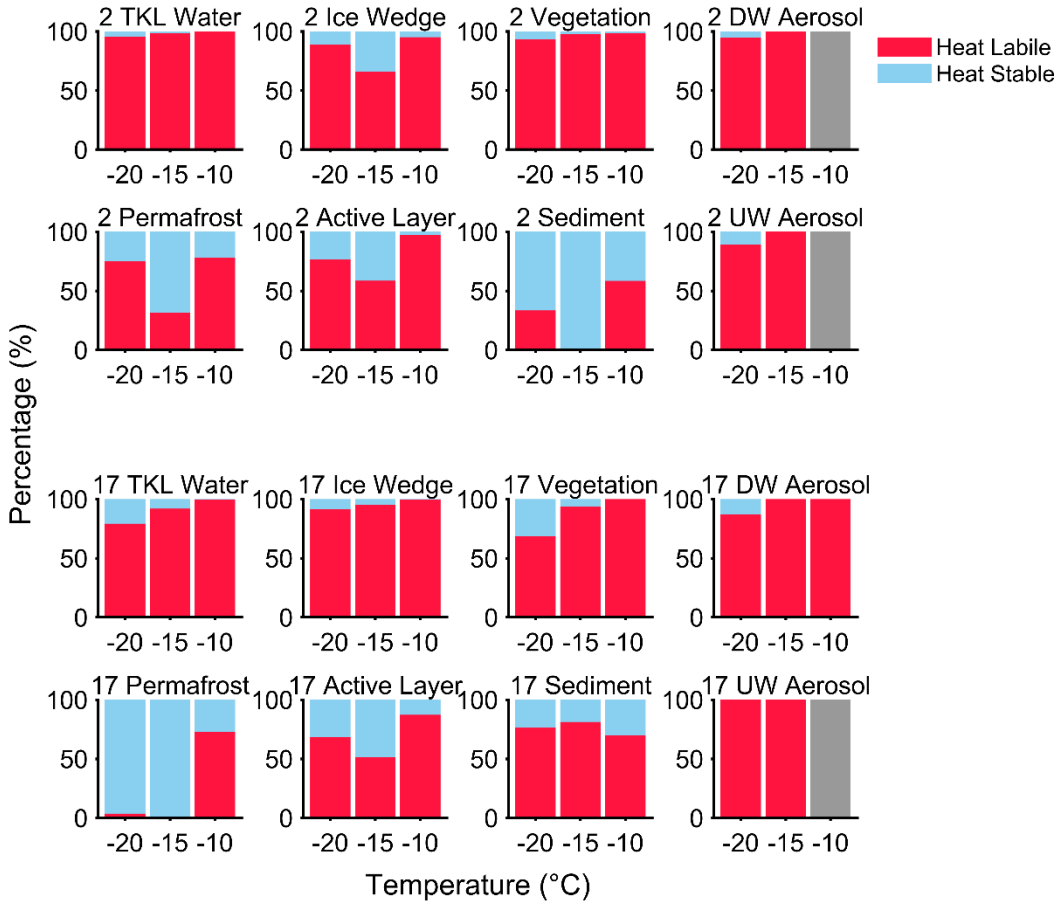

Figure 4.8. Histograms for samples collected on September 2nd (top) and September 17th (bottom), 2021, showing the percentage of INPs that are heat labile (sensitive to 95 °C heating: red) and heat stable (other: blue). Gray indicates INPs in the aerosol that were below the detection limit of the IS.

4.3.3 Covariance of INPs with organic carbon in water

Since water bodies can serve as a reservoir and source of atmospheric INPs, tracking their concentrations is important to better understand the Arctic INP budget. Water TOC concentrations have been used previously to normalize and derive relationships with INP concentrations in Arctic and North Atlantic Ocean sea surface microlayer samples (Wilson et al., 2015) and were found to overpredict corresponding North Atlantic INP aerosol concentrations (McCluskey et al., 2018). Based on heating to 95 °C (Fig. 4.8), the INPs in the water were

predominantly heat labile (presumably organic), and therefore might correlate with TOC. Figure 4.9 confirms this hypothesis, with higher levels of TOC generally associated with increased INP concentrations. Taken together, there is a strong correlation (R^2=0.85). However, when water types are treated separately, the correlations are weaker for the lagoon (R^2=0.12) and ocean (R^2=0.45), likely due to increased homogeneity. Therefore, we consider the complete landscape to cover the most variability, although TKLs on their own have the same coefficient of determination (R^2=0.85). As wave breaking and bubble bursting are hypothesized to be the main mechanisms of release of INPs from thawing permafrost into the atmosphere (Barry et al., 2023a), this relationship suggests a potential means of representing not only thawing permafrost, but other mixed thermokarst sources of Arctic INPs using TOC as a proxy variable.

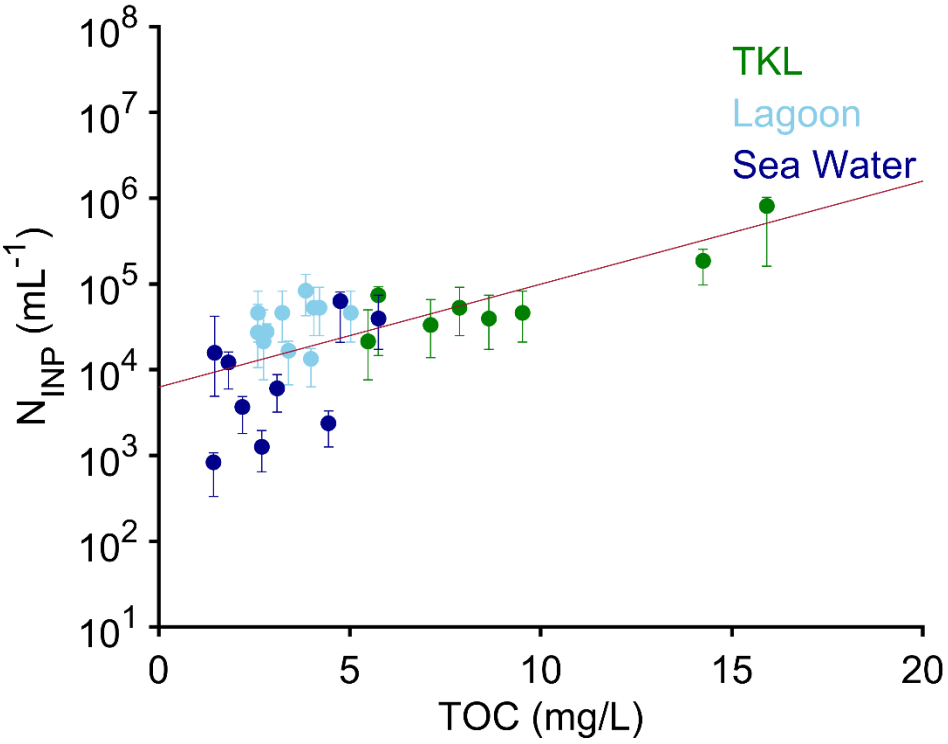

Figure 4.9. Water INP concentrations active at -15 °C (thermokarst lake water: green; lagoon: light blue; seawater: dark blue) versus total organic carbon (TOC). The red line gives an exponential best fit (R^2=0.85). 95% confidence intervals for the INP concentrations are given.

4.4 Conclusions

The Arctic is important to study sources of INPs due to limited previous observations in areas that have exhibited or are actively exhibiting thermokarst development and the sensitivity of mixed-phased clouds to INP concentrations. During ARCSPIN, we comprehensively surveyed likely sources in an environment dominated by thermokarst processes, representing the first Arctic terrestrial-based source survey of INPs. Permafrost was found to be a large reservoir of INPs, with maximum concentrations of $5x10^8$ g^{-1} at -15 °C, and furthermore, the highest concentrations were found closer to the coast, which could release more INPs with erosion. This analysis revealed many rich potential sources of INPs that are unaccounted for in current climate predictions. Water bodies have the potential to transfer INPs from these sources to the atmosphere, since they were enhanced in the aerosol downwind of TKLs in all three cases measured, as well as the case with onshore winds off the ocean. However, a background level of INPs seem to exist given the relative insensitivity of the DOE INP concentrations to measured average wind direction and speed, and so the enhancement from TKLs and the ocean may be better viewed as periodic or a combined effect of passing over multiple TKLs.

This study represents the first attempt at INP source apportionment through PCA. Most source samples clustered together within their groups and were separated on PC1 with overlap between the permafrost, sediment, and active layer, and additionally between water groups and vegetation. The permafrost had the most group variability, which may complicate future representation. Most of the aerosol INPs likely originated from a mixture of sources from separation on PC2 but spanning the range of source samples on PC1. The aerosol INPs were also found to be heat labile. These biogenic INPs could affect glaciation of Arctic clouds through their warm temperature activity. Heat tests on the potential source samples indicated high heat

labile populations from TKL water, vegetation, and ice wedge samples, but inconsistency and some temperature dependent insensitivity in the permafrost, sediment, and active layer samples. Differences between seemingly similar samples, such as permafrost and the active layer, were also discovered through response to heat. The positive relationship found between INPs and TOC in the water suggests a potential approach to estimate INP concentration in models, similar to the approach suggested by McCluskey et al. (2018), since water can play a role for emission of INPs into the atmosphere. This connection may be the most practical way to track current Arctic terrestrial INPs given the complexity of the landscape. To fully understand atmospheric Arctic INPs both now and in the future, knowing the permafrost coverage is critical due to it not only being a large reservoir of INPs, but also because it dictates the thermokarst landscape itself.

5. Best practices for sampling INPs cleanly

5.1 Introduction: Importance of working cleanly

Ice nucleating particles (INPs) are necessary for initiation of ice formation in clouds above the level of homogeneous freezing (-38 °C); mixed-phase and glaciated clouds serve as the primary source of precipitation outside of the tropical oceans (Mülmenstädt et al., 2015). Despite their importance in influencing precipitation, as well as cloud reflectivity and lifetime, INPs are rare in the atmosphere (DeMott et al., 2010; Kanji et al., 2017) and have a diverse range of sources (Šantl-Temkiv et al., 2019).

Filters and impingers are commonly used to sample air for offline immersion freezing measurements of INPs, and their validity is supported by recent intercomparisons with other methods for sampling ambient INPs (DeMott et al., 2017, 2018). Aerial samples and samples from remote marine regions can be especially challenging to analyze because few INPs are captured. For example, a filter sample of 20 m^3 of air from above the Southern Ocean will typically collect only around 20 INPs active at -20 °C (McCluskey et al., 2018). By contrast, the dust that covers every laboratory surface harbors millions of warm-temperature INPs that can easily taint such clean samples during preparation. Contamination will also limit the temperature to which a test can be taken, by raising the background INP level in the dilutions and negative controls.

Surprisingly, there are very few systematic assessments of the sources of INP contamination from substrates and water (e.g., Creamean et al., 2018; Polen et al., 2018). Since contamination may entail multiple inputs from numerous sources, the entire processing train needs to be scrutinized to quantify all identifiable potential sources so that preventative protocols can be designed. In this work, we measured the number of INPs present on tools, containers, and

surfaces used for offline analysis of INPs. Since consumables designed primarily for molecular biology are increasingly used as receptacles for holding aliquots of suspensions in a range of immersion freezing instruments (Beall et al., 2017; J. Chen et al., 2018; David et al., 2019; Garcia et al., 2012; Gute & Abbatt, 2020; Harrison et al., 2018; Kunert et al., 2018; Miller et al., 2020; Moffett, 2016; Schiebel, 2017; Stopelli et al., 2014; Zaragotas et al., 2016), we also evaluated several brands of 96-well polymerase chain reaction (PCR) trays for intrinsic contamination. Using this comprehensive survey, we provide a pragmatic general handling and sampling protocol for measurement of INPs via immersion freezing. Since Nuclepore™ polycarbonate filters are a commonly used medium for aerosol filtering, we applied the protocol to develop an improved method for their cleaning.

5.2 Methods

All tests were performed using the CSU Ice Spectrometer (IS), which analyzes liquid suspensions for INPs active via immersion freezing. The IS is constructed using two aluminum blocks, designed for incubating PCR plates, encased by cold plates that contain copper coils through which coolant is circulated. The IS produces spectra spanning a wide dynamic range of temperatures and INP concentrations and is supported with well-established experimental protocols applied in diverse scenarios (Beall et al., 2017; DeMott et al., 2017; Hill et al., 2016; Hiranuma et al., 2015).

Prior to measurement of INPs in the IS, filters are placed into sterile 50 mL polypropylene centrifuge tubes, with 7-10 mL of 0.1 µm-filtered deionized (DI) water added and particles re-suspended by tumbling end-over-end. Next, 50 µL aliquots of suspensions are dispensed into sterile, 96-well PCR trays in a laminar flow hood and covered with clean lids and wrapped in foil before transport to the IS. The trays are then placed into the blocks, the device

covered, and the headspace purged with high efficiency particulate air (HEPA)-filtered N_2 (750 mL min^{-1}). The IS is cooled at 0.33°C min^{-1} using a recirculating low temperature bath, and the freezing of wells is recorded through an interface with a charge-coupled device camera system. The limit of measurement is between –27 and –30 °C, depending on the number of INPs in the DI water background. Immersion freezing temperature spectra are obtained by converting the number of frozen wells at each temperature to the number of INPs mL^{-1} suspension using equation 13 in Vali (1971). Ninety-five percent confidence intervals for binomial sampling are obtained from equation 2 in Agresti and Coull (1998). All tests presented here were corrected for INPs in the 0.1 µm-filtered DI sample blank, unless otherwise noted.

5.2.1 Water

DI water is used for cleaning, for collection of INPs in impingers, and to re-suspend and dilute INPs caught on filters. Its INPs content will limit the temperature to which immersion freezing tests can be made. For all tests, we used deionized water from a centralized supply (Evoqua), "polished" using 0.1 µm-pore-diameter syringe filters (Whatman® Puradisc 25 TF) or 0.02 µm-pore-diameter Anotop® syringe filters (Whatman®).

5.2.2 Minimizing INP contamination during sample handling for analysis

As a preamble to this section, we suggest using a laminar flow hood, if available, for all preparatory steps to avoid contamination of filters and tools with ambient aerosol particles. We use a standard Table Top Work Station (Envirco), which comes fitted with a HEPA filter, and produces an ISO Class 5 environment. The particle number concentration inside the laminar flow hood, measured using an ultrafine condensation particle counter with a detection limit of 2.5 nm (TSI, model 3776), was 0 cm^{-3} (i.e., undetectable). By contrast, the laboratory air contained >1,000 particles cm^{-3}.

Various means can be used to clean laboratory utensils, such as soaking in dilute hydrochloric acid (HCl), followed by methanol/ethanol and DI rinses, or 10% hydrogen peroxide (H_2O_2) followed by DI rinses. Immersion in an ultrasonic bath (in a plastic bag) efficiently dislodges attached particles. For glassware, all organics can be removed by baking to 550 °C for 2-3 h. To clean most laboratory items, we use Windex®, followed by DI rinses, because it is designed to remove surface particles and organics without leaving a residue.

5.2.2.1 Minimizing INP contamination during filter manipulation

Forceps should be used to handle filters. We use acetyl plastic forceps (Fine Science Tools®, Cat. 11700-00), because they are precisely manufactured and inert. To test them for contamination, the tips of 10 pairs of cleaned forceps were swirled in a reservoir of 5 mL of DI water. This was compared with a replicate 5 mL of DI water.

Since filters may need to be cut into pieces, we tested scalpel blades (Swann-Morton, No. 10) for cleanliness. The tips of 32 scalpel blades, taken from individual foil packs, were dipped, one per well, into 50 µL aliquots of deionized water in a PCR tray. This array was compared with an adjacent control array of 32-50 µL aliquots of DI water.

5.2.2.2 Reducing potential INP contamination from plasticware

Many types of plasticware are used during the collection, storage and analysis of filters, and in the preparation of DI water. Specifically, these include:

- Plastic slider bags, which are used for cleaning and storage of laboratory items. We tested them by adding 20 mL of 0.1 µm-filtered DI water and shaking vigorously for approximately 1 min. Hefty® Quart Freezer Storage Slider Bags were used for analysis. We also assessed the usefulness of washing bags by initially spraying the interior with Windex® followed by several DI rinses, before testing.

- Petri dishes are used for rinsing filters in DI water during cleaning, and for storage of filters after sampling. They were tested by adding 4 mL of 0.1 µm-filtered DI water to the upturned lid, swirling, and then transferring the liquid to the base and swirling again. These results were not corrected for INPs in the negative control since the values were comparable. The Petri dishes analyzed were Pall® Laboratory 50 × 9 mm sterile (Cat. 7232), and Life Science Products 60 × 15 mm sterile (Cat. LS-6706).
- Pipette tips dispense aliquots of filter suspensions and make the dilutions. They were examined by opening a new box and aspirating 1 mL of water from 10 mL of 0.1 µm-filtered DI water in a pre-rinsed centrifuge tube, and then dispensing it back into the reservoir. This was repeated with 15 tips using the same reservoir. Eppendorf™ ep Dualfilter T.I.P.S.® (50-1250 µL, Cat. 0030078594) were tested.
- Corning® 50 mL polypropylene centrifuge tubes (Cat. 89093-190) serve as the receptacle for the filter suspensions and dilutions, as well as for the reservoir of the 0.1 µm-filtered DI water. To test whether they are a potential source of INP contamination, an unrinsed tube was compared with a pre-rinsed tube. For the unrinsed tube, 10 mL of 0.1 µm-filtered DI water was added and hand-shaken to re-suspend residual INPs in the tube. For the pre-rinsed tube, 5 mL of 0.1 µm-filtered DI water was initially added, hand-shaken for approximately 20 s, and discarded. This step was repeated before 10 mL of 0.1 µm-filtered DI water was added and shaken as for the unrinsed tube. These results were not corrected for INPs in the negative control since these tubes, pre-rinsed, serve as the reservoir for such.

5.2.3 INP mitigation with exterior surfaces

We use compressed air dusters to blow off dust that accumulates on surfaces, such as on pipettes, the plexiglass lids of the IS, and the aluminum blocks into which the PCR trays are placed. To check for potential INPs in their propellant, 20 mL of 0.1 µm-filtered DI water was added to a plastic slider bag, and the duster was sprayed into the bag in three 2 s pulses. The bag was then closed and shaken to re-suspend the particles in the liquid. We tested GUST® Dusters, Stoner® - 94203, 340 g, Difluoroethane (Cat. 89065-918) which contain 0.2 µm-filtered propellant.

5.2.3.1 Personal coverings

Clothing, and especially sleeves, or bare skin, may be large sources of readily dislodged ice nucleation-active particles. Given the inherent variability of clothing we did not test it, but advise always using a dedicated and regularly washed lab coat (stored in a bag), disposable cleanroom sleeves (e.g. Kimberly-Clark Professional™ KIMTECH™, Cat. 49815), and cleaned gloves to minimize shedding of INPs from the operator.

Gloves must be used at all points in making INP measurements, from the field to the laboratory analyses, to avoid contamination from numerous INPs on hands. We screened a variety of different materials (latex, nitrile, copolymer, vinyl, and polyethylene) and brands to find those with the lowest number of INPs adhering to their surface. Glove tests were performed by first adding 20 mL of 0.1 µm-filtered DI water to a fresh plastic slider bag. A new pack of gloves was opened, and a glove from the middle of the pack was carefully fitted onto the hand without touching the exterior. Next, the gloved hand was immersed and enclosed tightly in the plastic slider bag and vigorously shaken back and forth for approximately 1 min. Using a pipette, the liquid was dispensed into a pre-rinsed centrifuge tube for analysis. Washed gloves were first sprayed with Windex® and rinsed thoroughly under DI water before immersion in the plastic

slider bag. For comparison, we also tested an unwashed and washed (with Windex®) hand following the same method.

The gloves surveyed included:

- Ansell™ FoodMates™ Disposable Polyethylene Gloves
- Ansell™ Microflex® Derma Free® Vinyl Gloves
- Ansell™ Microflex® Latex Gloves
- Ansell™ Microflex® MidKnight™ Powder-Free Nitrile Examination Gloves
- Fisher Scientific™ Safety Choice™ Economical Vinyl Exam Gloves
- Great Value™ Disposable Vinyl Gloves
- Great Value™ Disposable Poly Gloves
- Kimberly-Clark Professional™ KIMTECH™ Pure® G5 Co-Polymer Gloves
- PIP™ CleanTeam™ Vinyl Cleanroom Gloves (Cat No. 191201452B for medium)
- VWR® Soft Nitrile Examination Gloves

5.2.3.2 Working on surfaces

Clean surfaces, both in the laboratory and field, are essential for making accurate INP measures. To quantify differences between lab surfaces as sources of contaminating INPs, 0.05 or 0.1 m^2 of laboratory floor, uncleaned bench top (2 weeks since last clean), cleaned bench top (wiped with Windex® followed by a DI rinse), and the inner (intrinsically cleaner) surface of aluminum foil (Reynolds Wrap® Heavy Duty) were tested. Between 7.5 and 30 mL of DI water was swirled on each surface, and a proportion retrieved with a pipette and dispensed into a pre-rinsed centrifuge tubes for analysis.

5.2.4 Screening for contamination in PCR trays

Sterile, 96-well polypropylene PCR trays hold the aliquots of suspension for testing with the IS. They are typically certified to be free of DNA and RNA. However, this does not equate to them being particle free. PCR tray tests were performed by pipetting 50 µL aliquots of 0.1 µm-filtered DI water into three 32-well sectors per tray (left, center and right), and analyzing with the IS. The tray tests were not corrected for INPs in the DI water.

Brands used were:

- BIO-RAD Multiplate™, 96-well PCR Plates (Cat no.: MLP9601)
- Fisherbrand™, 96-well PCR Plates (Cat. No. 14-230-232)
- Lifeline™ PCR Plates Life Science Products (Cat. No. PCR-9620-01, from Life Science Products)
- OPTIMUM® ULTRA Brand, PCR Plates (Cat. No. LS-9796, from Life Science Products, Frederick, CO)
- Thermo Scientific™ ABgene™, 96-well PCR Plates (Cat. No.: AB0600)

5.2.5 Filter preparation protocol

An improved technique for cleaning Nuclepore™ polycarbonate membrane filters was developed to remove INPs introduced during manufacture and packaging. This method is especially ideal for sampling in low INP environments.

1) Fill a clean 500 mL polypropylene bottle completely with methanol (or ethanol). We used Fisher Scientific™ (Certified ACS) 99.9% methanol
2) Immerse filters (up to about 30) completely in the methanol
3) Cap the bottle, hold upright in an ultrasonic bath, and ultrasonicate for two 10 s pulses
4) Discard half of the methanol, fill with DI water, and gently mix
5) Discard half of the solution, fill with DI water, and repeat gentle mixing

6) Discard most solution, fill with DI water, and repeat gentle mixing
7) Discard most water and then tip filters in the residual water into a large Petri dish (Life Science Products, 150 × 15 mm, sterile, Cat. LS-6725). Drain out the DI water
8) Fill Petri dish with 100 mL of 0.1 µm-filtered DI water
9) Separate filters individually with clean plastic forceps to ensure efficient rinsing
10) Drain and repeat the filtered DI rinse
11) Drain water and lay filters to dry on new foil in a laminar flow hood
12) Wrap filters in individual aluminum foil pockets to be stored and transported for use in the field

5.3. Results and Discussion

5.3.1 Water

Standard laboratory water deionizers should produce water usable to -20 °C or colder, depending on droplet size. The temperature limit to which measures can be taken can be extended by "polishing" the DI water by using, for example, 0.1 µm-pore-diameter syringe filters (Whatman® Puradisc 25 TF) as used in this study. Our polished deionized water contained ~1 INP mL^{-1} at -25 °C. Harrison et al. (2018) noted that filtering of Milli-Q water through Sartorius Minisart filters (0.2 µm, product code 17597-K) lowered the temperature at which pure water droplets froze by 2–3 °C, while O'Sullivan et al. (2015) found up to a 5 °C reduction by using a 100 kDa filter (Millipore, Amicon Ultra, UFC910008). By contrast, Polen et al. (2018), who performed a comprehensive water analysis, found erratic results when repeatedly testing Milli-Q water, even after 0.02 µm-filtration; they suggested bottled HPLC grade water instead, for consistency. Additionally, regularly changing syringe filters is recommended, as Polen et al.

(2018) found an increase in INPs active colder than about -25 °C when using the same 0.02 µm filter for several weeks. If deionizers are not well maintained, they will release INPs, irrespective of whether the system outlet filter (generally 0.2 µm) is working, since those INPs active at cold temperatures tend to be small (O′Sullivan et al., 2015). In a system overdue for servicing, we found that 0.02 µm-filtering performed better than 0.1 µm-filtering.

5.3.2 Minimizing INP contamination during sample handling

5.3.2.1 Minimizing INP contamination during filter manipulation

The cleaned acetyl plastic forceps did not shed any INPs (the spectrum was not significantly higher than the control), but the steel scalpel blades did release INPs active below –22 °C. This may be caused by microscopic metal shards or INP contamination introduced during packaging; there are many seemingly innocuous sources of INP contamination. We therefore recommend using a small ceramic blade knife, since the blade is smooth, unreactive, and easily cleaned with Windex® or H_2O_2.

5.3.2.2 Minimizing INP contamination from plasticware

- Freshly opened (unwashed) plastic slider bags were found to contain less than 100 INPs per quart-sized bag active at -27 °C (Fig. 5.1a). Washing the plastic bags before use may slightly reduce the number, but in practice, this benefit may be offset by the additional handling introducing contamination. Cleaning items, such as plastic forceps, in plastic bags is advisable since most of the pre-existing INPs in the bags will also be removed during the wash step. Change bags used for cleaning or storage often in the field.
- Rinsing centrifuge tubes (Fig. 5.1b) with 0.1 µm-filtered DI water reduced the number of INPs introduced during manufacture by approximately 4-fold at -25 °C, although there

was no difference by -28 °C. There was also a 2 degree colder onset temperature with the rinsed centrifuge tube.

- Both brands of newly-opened packs of Petri dishes possessed few if any INPs, with none at all detectable until around -25 °C.
- The pipette tips released no detectable INPs (no difference with the 0.1-µm DI water blank). Pipette tips with filters should always be used, since the interior of the pipette can be a major source of contamination. We also advise wiping down their exteriors with DI water before each use. Disassembling the lower part, rinsing the components in DI water, and using a compressed air duster to blow them dry should be done once a month.

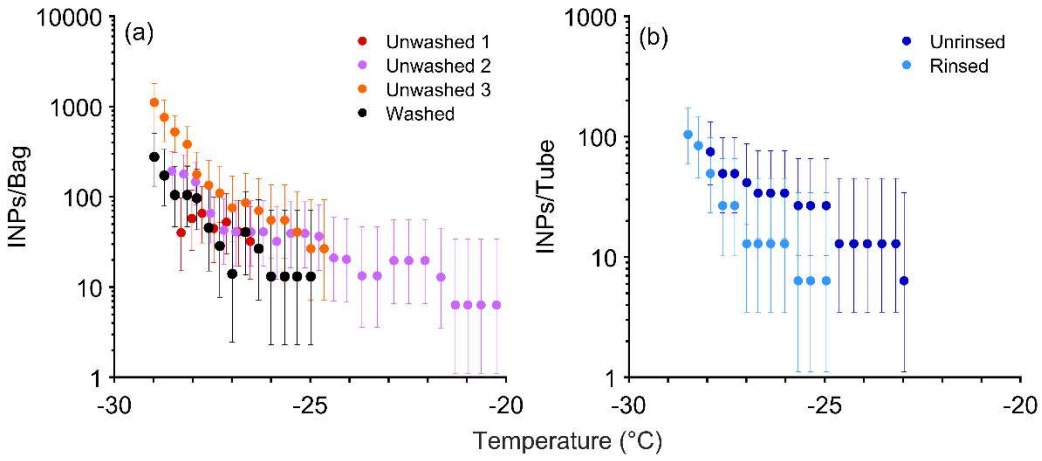

Figure 5.1. Cumulative INP spectra from (a) unwashed and washed quart plastic slider bags (with background DI water INPs removed), and (b) an unrinsed and rinsed Corning 50 mL polypropylene centrifuge tube.

5.3.3 Limiting INPs on exterior surfaces

Compressed air dusters emitted no detectable INPs in their gas stream once correction for the water blank and plastic bag had been made. Therefore, they can be safely used to blow dust off external surfaces. We recommend using dusters that have filtered propellant.

5.3.3.1 Gloves

Gloves should always be used, since hands are covered in INPs: A bare hand, even after washing, can release over 1,000 INPs active at -16 °C (Fig. 5.2a). Gloves, however, can also be a source of INPs. Washing gloves by spraying them with Windex® followed by rinsing under DI water will remove INPs from dust acquired during production or which has settled upon an open pack. By contrast, wiping gloves with alcohol will have little benefit other than denaturing proteinaceous INPs, which are likely a minor contributor. Avoid powdered gloves. For a consistent comparison, only washed glove results are presented in Figure 5.2a. Gloves that shed the fewest INPs are the cleanroom vinyl and polyethylene gloves. Both released around 50 INPs per glove at -25 °C. Polyethylene gloves (typical food preparation gloves) are inexpensive but hard to use as they lack a textured surface for grip. They are also harder to clean and have lower durability. Copolymer (cleanroom produced) and nitrile gloves have similar INP-temperature spectra, releasing approximately 700 INPs per glove at -25 °C, over 10-fold more than a washed cleanroom vinyl glove.

Since nitrile gloves are popular, we show a direct comparison between washed and unwashed cleanroom vinyl and nitrile gloves in Figure 5.2b. An unwashed cleanroom vinyl glove is better than a washed nitrile glove. Comparing unwashed and washed cleanroom vinyl gloves, the number of INPs at -25 °C were 360 for the unwashed compared with only 50 for the washed. As they were taken from a fresh, cleanroom-produced pack, it underscores the importance of always washing gloves and never assuming anything is INP-free. Washing nitrile gloves usefully removed warmer temperature INPs, lowering the onset from -16.5 °C to -21 °C. However, there was essentially no difference by -24 °C, suggesting there is something intrinsic to the nitrile material itself that ice nucleates at colder temperatures. This contrasts with the washed cleanroom vinyl that showed a reduction in INPs across the entire temperature spectrum.

This superior performance is consistent with the findings of Garçon et al. (2017), who showed that vinyl gloves released lower amounts of most trace elements than other gloves.

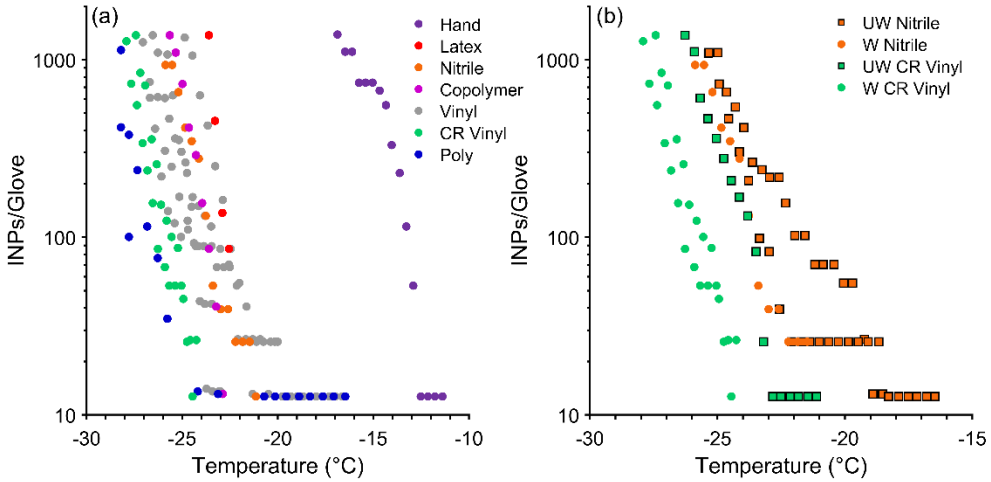

Figure 5.2. Cumulative spectra of INPs on (a) the surfaces of washed gloves compared with a washed hand, and (b) on washed (W) and unwashed (UW) nitrile and cleanroom (CR) vinyl gloves. All glove tests were corrected for background INPs in the DI water blank.

5.3.3.2 Cleanliness of work surfaces

Surfaces are major direct as well as indirect (by transferring INPs to items) sources of INP contamination. Not surprisingly, Figure 5.3 confirms that laboratory floors are an especially high source, with over 10,000 m^{-2} by -7.5 °C. Benches that are not regularly cleaned will also support many INPs, with over 10,000 m^{-2} at -12 °C. Cleaning them definitely helps, as this number is reduced to only 100 m^{-2} at the same temperature. However, with the number of INPs active at colder temperatures remaining large (i.e., >10,000 m^{-2} at -20 °C), this is still not sufficient since even terrestrial ground-based daily filter samples, which are quite heavily loaded with particles, may only collect a few thousand INPs at -20 °C. By stark contrast, aluminum foil had essentially zero detectable INPs down to the limit of testing at -28 °C. Hence, simply doing all work, both in the laboratory and field, on fresh foil will eliminate this major source of

contamination. Foil should be changed every day before commencing work, and the underlying surface pre-cleaned to minimize lofting of dust when the foil is laid down. Additionally, regularly wiping down all bench tops and storing items on foil will reduce the overall number of INPs in the general workspace.

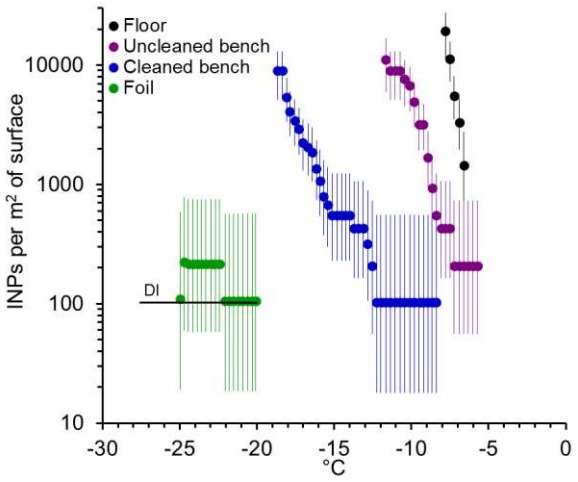

Figure 5.3. Cumulative spectra from laboratory testing of background INPs on the uncleaned floor, 2-week uncleaned benchtop, cleaned benchtop, and aluminum foil (the inner side of the roll). The "DI" line indicates INPs in the 0.1 µm-filtered DI water sample blank, which was subtracted from all surface tests.

5.3.4 PCR trays as a source of INPs

Polypropylene trays are mass produced for performing PCR reaction tests. They are, thus, a convenient platform for measuring INPs, and are used in a growing number of ice spectrometer designs (mentioned in Section 1). We compared 96-well PCR trays from five suppliers, each loaded with 0.1 µm-filtered DI water, for their low temperature performance. Unexpectedly, one brand, OPTIMUM® ULTRA, consistently performed better, by a margin of 2-3 °C, over the other well-known brands (Fig. 5.4). A consistent feature of the other brands was a habit of freezing in the center first (Fig. 5.5), which was not, or minimally, displayed by the OPTIMUM® plates. This appears to be a signature of some form of contamination introduced during

manufacture, and suggests that the lower temperature limit of immersion freezing tests using PCR plates is typically controlled by contamination in the plate itself. Low temperature limitation caused by the PCR plate brand was alluded to by Kunert et al. (2018) when comparing 96-well plates from one company with 384-well plates from another. In the former, 50% of 3 µL droplets of DI water froze by around -25.5 °C, while in the latter, this level wasn't reached until -29 °C. The lower temperature limit of the OPTIMUM® plates may also be due to the plate or to impurities in the DI water. While PCR trays are DNA/RNA-free they are clearly not particle-free, and this could partially explain, in addition to droplet volume differences, why cold plates can reach colder temperatures (e.g. Creamean et al., 2018; Tobo, 2016).

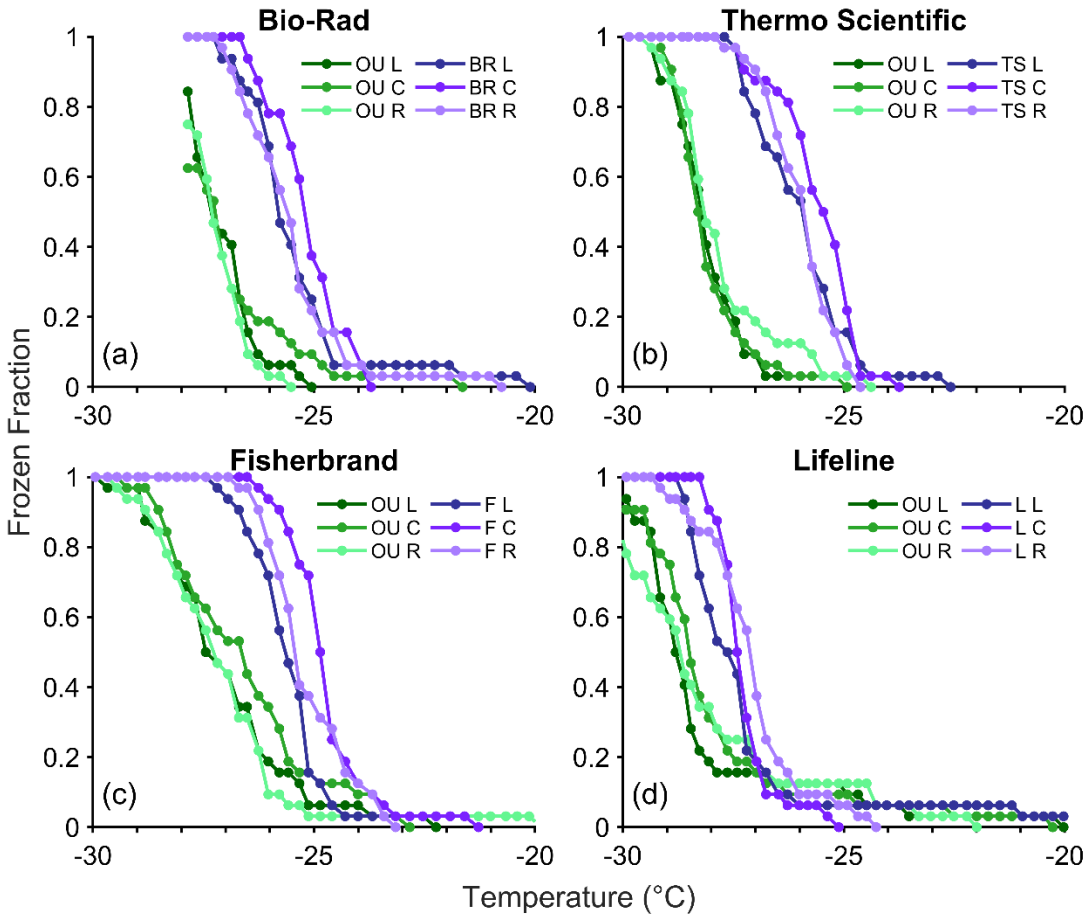

Figure 5.4. Frozen fraction comparison of (a) Bio-Rad (BR), (b) Thermo Scientific™ (TS), (c) Fisherbrand™ (F), and (d) Lifeline™ (L) with OPTIMUM® ULTRA (OU) PCR trays. Each 96-well tray was divided into three 32-well sectors designated left (L) center (C) and right (R). All wells contained 50 µL of 0.1 µm-filtered DI water.

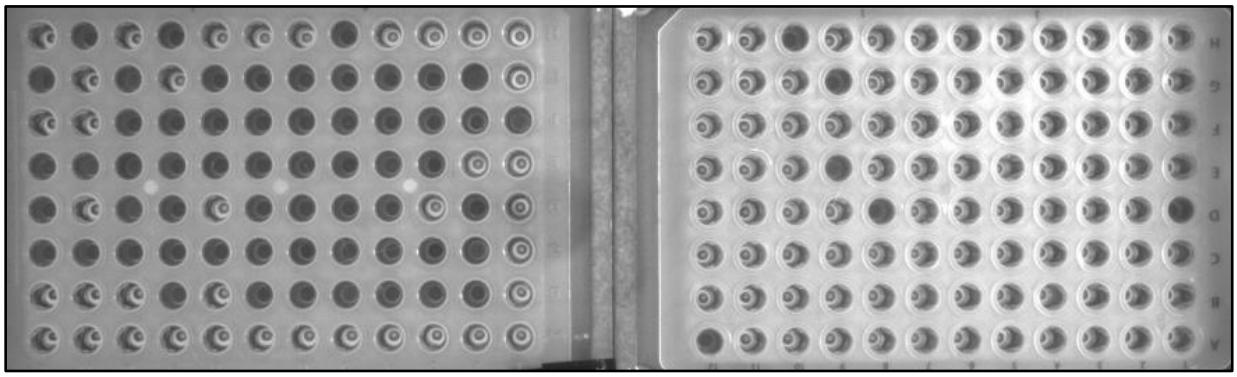

Figure 5.5. Frozen wells of 0.1 µm-filtered DI water (dark gray) in adjacent PCR trays in the Ice Spectrometer at -26 °C. The left tray was made by Thermo Scientific™ and the right-side tray by OPTIMUM® ULTRA. Note that in the left tray most frozen wells were clustered in the center.

5.3.5 Filter cleaning for sample collection

Contamination of filters with INPs during manufacture and packaging can limit the lower temperature to which they can be used. Our new method for cleaning Nuclepore™ polycarbonate filters reduces the intrinsic INPs on each filter to less than 20 at -27 °C (Fig. 5.6). This translates to an approximately three-degree improvement from the previously used method of soaking in 10% H_2O_2, and over a five-degree improvement from using unwashed filters. In the process of sampling, the filters may collect more INPs in their handling, but this method works to eliminate a major source of contamination. Although the difference in background INPs released might not be essential for terrestrial ground-based measures, this will certainly improve detection limits for aerial and marine studies. Most importantly, the two short pulses of ultrasonication did not affect the integrity of the filters; three filters were checked before and after cleaning with a mass flow

meter, and the flows and pressure drops across them were unchanged. Ultrasonication for longer periods of time (i.e., minutes) can result in tears at the edges of filters.

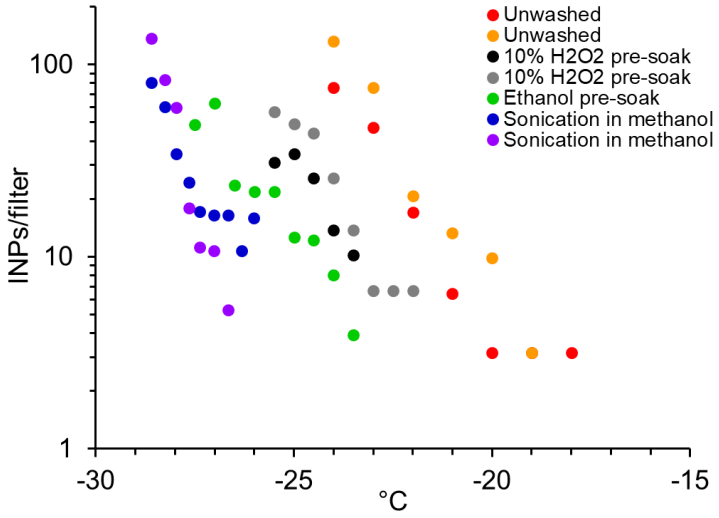

Figure 5.6. Cumulative spectra of INPs released from Nuclepore™ polycarbonate filters after different cleaning protocols. Apart from unwashed Nuclepore™ filters, which were taken directly from a new pack, all filters were rinsed three times in DI water post treatment, the last two rinses using 0.1 µm-filtered DI. All filter tests were corrected for INPs in the DI water blank.

5.4. Conclusions

This work aimed to quantify, and subsequently minimize, all potential sources of INP contamination when making immersion freezing measures with filters and using PCR trays as the measurement platform. Out of an abundance of caution, we assumed that every tool, surface, and container was a significant extraneous INP source. The resulting general handling protocol delivers improvements to the limit of detection, as well as ensuring consistently accurate and representative measures over a wide temperature range. Although this continues to be a work in progress, we can recommend many straightforward and easily-adopted practices to limit INP contamination and so improve performance:

1) Work in a laminar flow hood, if available.

2) Fresh, unwashed plastic slider bags are recommended for storage and cleaning of laboratory tools as they contain few INPs.
3) The tested pipette tips, filtered compressed air dusters, Petri dishes, and pre-rinsed polypropylene centrifuge tubes are minor sources of INPs.
4) Washed cleanroom vinyl and polyethylene gloves retain very low numbers of INPs on their surfaces. Vinyl gloves are easier to work in than polyethylene gloves, and are comparable in cost to nitrile gloves, the current standard.
5) Always work on fresh aluminum foil (inner surface) in the field, laboratory, and laminar flow hood.
6) PCR trays typically contain contaminating INPs. Of the five brands tested, the OPTIMUM® ULTRA brand was clearly superior.

Enhanced by these clean-working methods, we developed a simple but effective protocol for background INP removal from Nuclepore™ polycarbonate filters. This will be particularly beneficial for INP measures in clean environments, such as over oceans and in the free troposphere. If stringent handling protocols are followed at every step of preparation, sampling, and analysis, the number of INPs on field blanks will approach the cleanliness of the ultra-clean filters themselves.

6. Summary and future/in progress work

6.1 Summary of chapters

This work has covered the presence of INPs in the Arctic, from a general, central Arctic perspective in Chapter 2, to potential terrestrial sources in Chapters 3 and 4. In Chapter 5, I stress the importance of clean working protocols and the careful filter cleaning protocol that are needed for accurate quantification of INP concentrations, particularly for aerosol samples. Some of the sample preparation and analysis protocols that have become standard for our group, that have also been shared with the broader community, include wearing vinyl gloves (not nitrile or latex), always working on aluminum foil, storage of samples and consumables in plastic slider bags, preparing samples in a clean laminar flow hood, and pre-cleaning filters by ultrasonication in methanol.

Chapter 2 took a deep dive into the seasonal cycle of INPs to see how the INPs varied over a year in their composition and concentration in the central Arctic. The INP concentrations in the summer were significantly elevated, 2 orders of magnitude on average, compared with any other season. Concentrations of up to 1.4 L^{-1} were detected at -15 °C in early July, typical of air over continental regions. Aside from having the highest average INP concentrations, summer also had the largest variability, with the highest standard deviation at -15 °C. This variability was not expressed in summer INP composition, with nearly 100% heat labile INP fractions detected at -15 and -20 °C. Samples from other times of the year could still contain high heat labile fractions, but they also included variable fractions of heat stable and mineral INPs (especially colder than -20 °C). The other part of the research question was to understand whether the sampled INPs originated locally (in proximity to the ship) or regionally (general Arctic/longer-range transport), through using the seasonality of the microbes in the air as a tracer of influences

on the air mass composition. The airborne bacterial composition varied significantly by relative abundance, limiting seasonal trends. Source tracking analysis indicated that, aside from periodic snow influence during cyclones, the microbes likely did not come from sources in proximity to the ship for most days, based on the subset of source samples analyzed. This finding was strengthened by the detection of periodic terrestrial fungal influence and the majority of airmasses spent time over the open ocean, ice, and land. Finally, the INP concentrations and seasonal trends were similar to coincident INP measurements at Svalbard (especially in the fall, winter, and spring), a maximum latitudinal distance of 1140 km, which suggests pan Arctic sources contribute to a regionally coherent population of INPs.

In Chapters 3 and 4, I explored some of the likely most active Arctic sources of INPs, with the research questions centered around the potential atmospheric relevance of permafrost. Permafrost was the most focused-upon source for a number of reasons. It has been shown to be a large reservoir of INPs with large horizontal and vertical extent across the Arctic. Permafrost is thawing, with effects especially felt near eroding coasts, and this melting process controls landscape features such as the vegetation coverage and presence of thermokarst lakes. Although previous work (Creamean et al., 2020) showed that permafrost was a reservoir of INPs, with concentrations per gram of soil on the order of midlatitude and glacial soil dusts, many questions remained. If permafrost soils were washed into a thermokarst lake, would the INP activity persist, or would it decay rapidly, since the soils were entering an environment significantly different from that when it was frozen. These questions could start to be answered by running two, 25-day laboratory experiments that placed permafrost into a tank with artificial fresh and seawater and monitored the INPs and bacterial community in the water and in aerosol produced through bubble bursting. The older permafrost had more stability and activity (on the order of

mineral dust when normalized by aerosol surface area), that lasted over the entire period. This type of permafrost could enter water bodies especially through erosion. The younger permafrost also had high levels of aerosol and water INPs that lasted throughout the period, but was compositionally different (coarser material, more variable organic fractions). Thus, we concluded that the permafrost INP reservoir has the potential to provide a source of active INPs even after multiday transport through bodies of water, and that bubble bursting mechanisms in these waters have the potential to release INPs to the air.

Chapter 4 focused solely on the field portion of the measurements, confirming not only that permafrost represents a large reservoir of INPs (can be greater than 10^8 g^{-1} at -15 °C), but that the thermokarst landscape in general contained many active sources of INPs that are presently unaccounted for in modeling emissions of Arctic INPs. Thermokarst lakes were found to have the potential to transfer these INPs to the atmosphere, an effect that could be compounded by an airmass traveling over a landscape covered with such lakes. Since Arctic waters, including the ocean in addition to land water, likely contain an amalgamation of various active sources from the complex landscape, we investigated a method for prediction of INP concentrations that could encompass the effects of such variable sources. A positive relationship between total organic carbon (TOC) and INP concentrations in lake, lagoon, and seawater suggests that this is one way to parameterize potential INP emissions from waters in this region. One of the most important findings in this study was that the aerosol filters obtained at the fixed DOE site over longer integration periods (generally 24 hours) showed relative insensitivity to wind direction, again suggesting a well-mixed regional Arctic INP population. The MOSAiC filters taken in September 2020 had the most comparability to the ARCSPIN DOE filters (Fig. 6.1), which showed that the Arctic tundra and central Arctic can have similarity in airborne INP.

The shallow slope of most of the aerosol temperature-dependent spectra implies that the INPs are from a mixture of sources, unlike a single fungal or mineral population (Kunert et al., 2019; Murray et al., 2021).

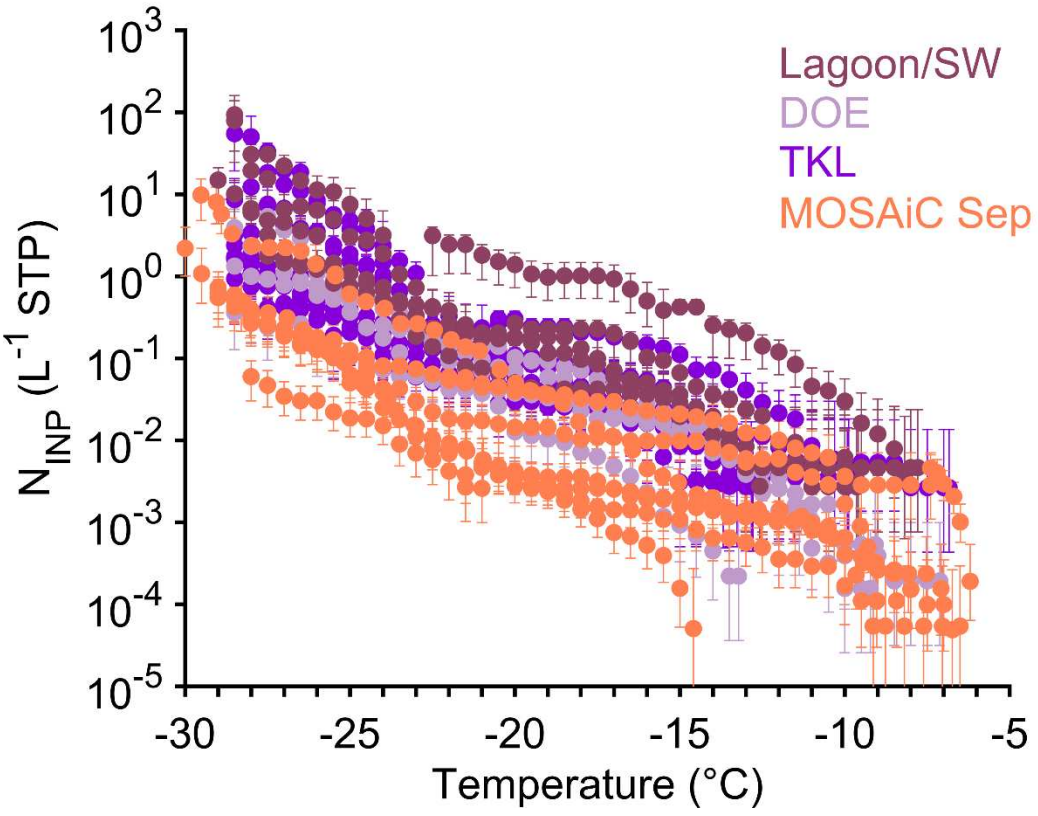

Figure 6.1. Cumulative INP-Temperature spectra from the ARCSPIN (Purple: September 2021) and MOSAiC (Orange: September 2020 only) field campaigns.

6.2 Ongoing and future work

6.2.1. ARCSPIN extended heat treatments

As INPs were enhanced downwind of all tested thermokarst lakes (Fig. 4.4), these lakes may play a role in transfer of emissions to the atmosphere, especially under periods of disturbance. Therefore, samples from these days (9/2/2021; 9/11/2021; 9/17/2021) are being investigated further to understand their INP composition. The PCA (Fig. 4.7) indicated that multiple surveyed sources likely contributed to the sampled aerosol due to the aerosol spanning

the range on PC1 (along with other, unsampled contributions). The 95 °C heat treatment indicated that most source samples, along with the aerosol itself, had high percentages of heat labile INPs (Fig. 4.8). To further test whether different behaviors could be discerned and thus linked to different or similar compositions between the aerosol and source samples, the response of the samples to other temperatures was investigated.

For the first treatment temperature, 50 °C was chosen based on several ice nucleating (IN) bacterial isolates having reduced activity after exposure to this degree of heating (lowered freezing onset: Fig. 6.2 Left). This temperature is high enough to lower the activity by breaking apart aggregates of proteins but should not denature them. This heat will also affect some IN fungi, such as *Fusarium avenaceum*, which started to lose activity above 40 °C (Hasegawa et al., 1994). 60 °C is a more commonly reported heat test in previous studies: some fungal isolates were affected by 60 °C, such as *Acremonium implicatum* and *Isaria farinose* (Pummer et al., 2015), but isolates of *Mortierella alpina* were generally not affected (Fröhlich-Nowoisky et al., 2015; Pummer et al., 2015) until they were exposed to 98 °C (we will assume comparability to 95 °C). 50 °C will also affect the IN activity of woody tissues (Gross et al., 1988), but not all plant INPs are as sensitive, such as winter rye (Brush et al., 1994).

95 °C will denature the INPs of most bacteria and fungi, since IN activity is likely derived from proteinaceous components, and has been used extensively in this dissertation. For exploring sensitivity to somewhat higher temperatures, 121 °C was chosen because of its ease of attainment in a pressure cooker, because it served as a middle point in this analysis, and because it has the potential to degrade the activity of the first known IN positive gram positive bacterium isolated from precipitation, *Lysinibacillus* (Failor et al., 2017). The molecule that is responsible for ice nucleation is likely not a protein due to its resistance to 99 °C.

The highest temperature chosen was 180 °C, based upon testing a birch pollen suspension on the ice spectrometer after heating at various temperatures (95 °C, 121 °C, 150 °C, 167 °C) without complete reduction in its activity. Virtually all activity was wiped out at 180 °C (Fig. 6.2, right panel) and so that temperature was chosen as a proxy for pollen INPs and fragmentation and breakdown of other complex organic macromolecules such as RNA/DNA. This choice is in agreement with Pummer et al. (2012) who showed reduction of activity of pine and juniper pollen between 140-170 °C dry heat and birch pollen above 170 °C dry heat.

The 50 and 95 °C heat treatments are straightforward in that a suspension is aliquoted and heated in a water bath in a centrifuge tube for 20 min before being diluted and pipetted as normal. Wet heating has not been done at the two higher temperatures before, and so they needed different vials to withstand the higher pressures experienced. For the 121 °C treatment, 2-Dram reaction vials with a pressure-relief cap were used (Chemglass). They were prerinsed with DI water before placing the sample in the vial and heated for 20 minutes after reaching 121 °C, which took about 10 minutes after insertion into the pressure cooker. The vials were placed on racks in the middle of the pressure cooker so that they could fully be exposed to the steam.

For the 180 °C treatment, a vial that could sustain a higher temperature and pressure was needed (Cole-Parmer KX Microwave Vial). Both vials were made with borosilicate glass, but the higher temperature vial had much thicker glass and had to be sealed with a crimping tool (maximum pressure of 30 bar). The cap had a thick PTFE septum with an aluminum seal, and the vials were also prerinsed with DI water. This reaction was first tried in an oven; however, the caps would pop off after about 10 minutes, which was not long enough for the treatment. Instead, a heating block with silicone oil (flash point greater than 250 °C) was used on a hot plate (Fig. 6.3) so that the sample could be fully immersed in the oil at the correct temperature, while the

cap was not subjected to the same heat and so did not fly off. This treatment was performed in a fume hood with the sash closed for safety. The treatment was run for 25 minutes, using empirical observations of the septum ballooning out and reaching an equilibrium after 5 minutes. Since all of the tests were performed under wet heat, suspensions of the original water samples and aerosol filter suspensions could be aliquoted and analyzed identically. The 180 °C heat was compared to a hydrogen peroxide (H_2O_2) digestion for Wyoming pasture soil that was originally collected in Hill et al. (2016). The 180 °C treatment yielded results similar to the H_2O_2 digestions, which means the 180 °C treatment was able to remove most of the organic INPs. Some organic polymers that would not be affected by temperatures of 180 °C and have higher decomposition temperatures include chitin, cellulose, hemicellulose, and polyhydroxybutyrate (Arora et al., 2011; Kervran et al., 2022; Yang et al., 2007).

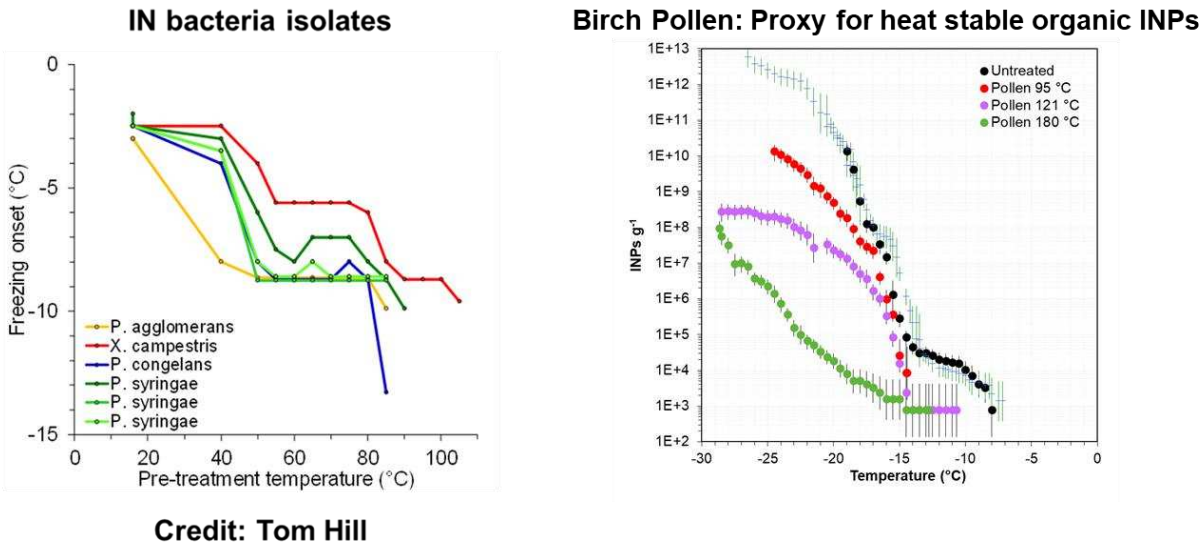

Figure 6.2. (Left) Response of 6 ice nucleation active bacterial isolates to heating (credit Tom Hill). (Right) Cumulative INP-temperature spectra for untreated birch pollen (black circles and gray lines [a replicate to extend the spectra]), after 95 °C heating (red circles), after 121 °C heating (pink circles), and after 180 °C heating (green circles).

Figure 6.3. Picture of the 180 °C treatment setup, showing the two sample vials immersed in hot silicone oil, with a thermometer constantly monitoring the temperature.

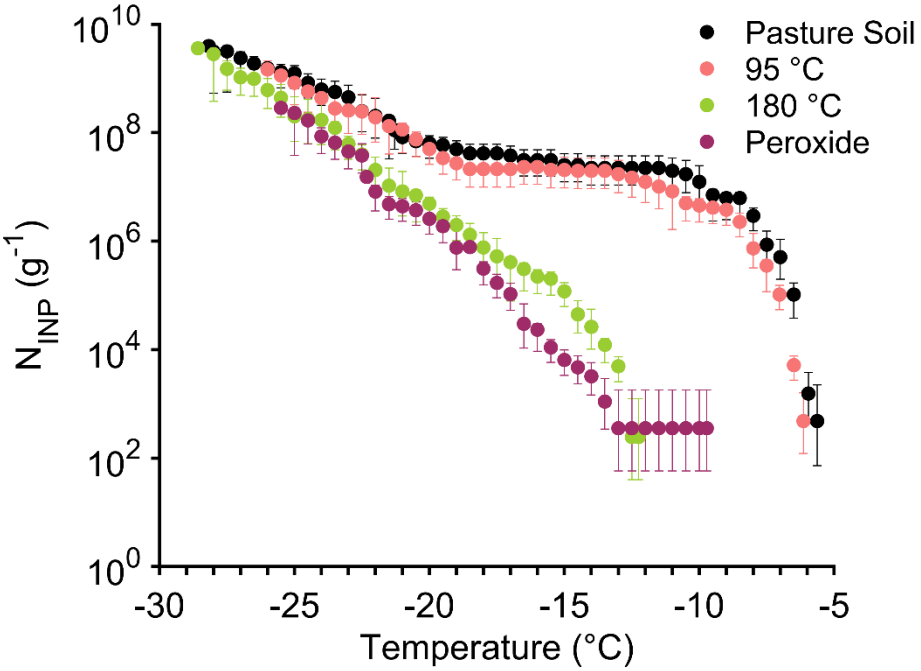

Figure 6.4. Heat tests on Wyoming pasture soil [collected in Hill et al. (2016)], with comparison to the hydrogen peroxide digestion treatment (purple) to remove all organics.

The first results of all treatments combined are presented in Figure 6.5. The 4 treatments were done on the upwind and downwind thermokarst lake aerosol samples, as well as on every potential source sample that was collected in proximity to the lake. They are presented as percent

decreases from the untreated spectra, with a colored triangle indicating a percent increased after heating, which may be from fragmentation of complex organics. They are unlikely to be from minerals, as the organics dominated the tested aerosol samples (Fig. 6.6), or pollen, due to its degradation at 180 °C (Fig. 6.4). First starting with the 50 °C treatment, the highest sensitivities across the temperature spectrum are from the ice wedge, thermokarst lake, and vegetation. The active layer, sediment, and permafrost samples showed minimal effects on contained INPs from 50 °C heating. This treatment suggests the potential presence of ice nucleating bacteria or select fungi in the water (which would be a part of the ice wedge) and vegetation. In the aerosol, 50 °C led to a large reduction at -20 °C, over 75% in both the upwind and downwind aerosol, which suggests the potential for IN bacteria in the air. The 95 °C has been shown and discussed in Section 4.3.2., but the sample with the largest contributions across the temperature spectrum was from the TKL water (e.g., 79% at -20 °C) and sediment, with large temperature dependent contributions from the ice wedge and vegetation samples (above -25 °C). Variable contributions were seen especially from the permafrost (no effect at -20 and -15 °C; 68% and 73% reduction at -25 and -10 °C, respectively). The aerosol again had large (>85% reductions) at -20 °C in both the upwind and downwind aerosol, with smaller reductions at -25 °C.

The 121 °C treatment is where samples start to diverge. Both the TKL water and sediment had large and consistent reductions in INPs for this treatment across the temperature spectrum (minimum of 94% for the TKL water and 78% for the sediment). The permafrost and active layer samples both had reductions across the temperature spectrum but were variable in the percent decrease. The vegetation and the ice wedge had nearly 100% reductions at -10 and -15 °C, but both had no reduction at -25 °C, and a significant (outside of overlapping confidence intervals) percent increase at colder temperatures. Both the upwind and downwind aerosol did

not have any reduction after 121 °C at -25 °C, with the upwind aerosol having a significant increase. These findings suggest a common INP that may have been present in the ice wedge and vegetation and the air samples, which could be fragmentation of a complex polymer that still retains its IN activity after heating, or exposure of IN active sites.

The 180 °C treatment showed large reductions with the sediment, permafrost, active layer, TKL water, and vegetation samples across the spectrum. No effect of 180 °C was detected in the ice wedge and aerosol samples at -25 °C, with a significant percent increase after heating in the upwind aerosol. There was a clear percent increase at temperatures colder than -25 °C in the ice wedge sample (not shown). The upwind aerosol had more of an increase after heating than the downwind aerosol did, which may suggest similar populations that are resistant, but a potential contribution from passing over the TKL in the downwind sample (of which the INPs were heat sensitive), leading to less of a percent increase overall.

Figure 6.5 shows that the aerosol is a complex mixture of heat-labile and heat-stable organics (minimal mineral assumed from Fig. 6.6), with potential contributions from IN bacteria or fungi at -20 °C or warmer based on the sensitivity to heating to 50 °C. These INPs could have originated from an ice wedge, TKL, or vegetation, and are unlikely to have large contributions from other sources, based on this method. At -25 °C, there appear to be different populations contributing, which could be INPs that are common to the vegetation and ice wedge sample, with potential TKL contribution in the downwind aerosol sample. Based on this analysis, the INPs from the collected active layer, sediment, and permafrost had minimal direct contributions to the aerosol.

This analysis is still preliminary and has to be expanded to other days. Slope analysis methods like the PCA used on the base samples can be used in this context as well. This analysis

would also work better on the aerosol by applying it to the fixed-site filters, as these appear to be more representative of the general Arctic (Fig. 6.1) and have collected more volume (lowering the limit of detection). In the future, these results will also be binned in temperature intervals to eliminate some uncertainty with the measurements, and more statistical testing, such as a pairwise-t test, will be implemented. Testing more source samples will also be helpful to see if, for example, a permafrost core collected along the coast has the same temperature properties to a core collected inland. Nonetheless, this analysis has the potential to eliminate major contributions of some sources to the aerosol, as some of the treatments revealed unique properties, such as lack of sensitivity at colder temperatures, that are not evident with 95 °C heating or hydrogen peroxide digestion alone.

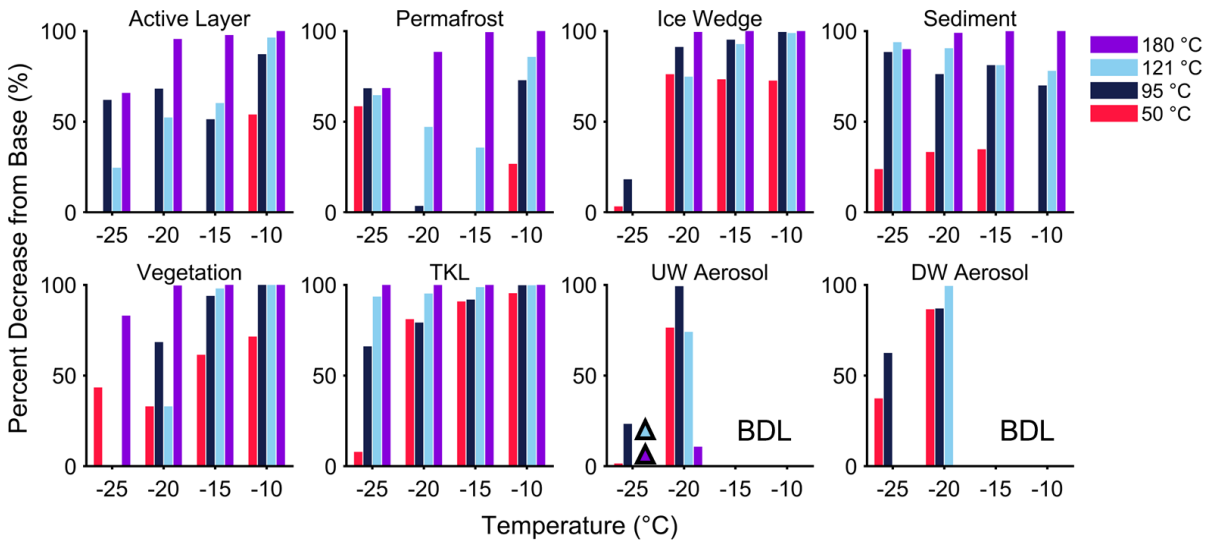

Figure 6.5. Percent decrease from untreated spectra for potential thermokarst region sources and proximal aerosol at Emaiksoun Lake, collected on 9/17/2021. Histograms are colored by the temperature of treatment and are given as a function of measurement temperature. A triangle indicates a percent increase after thermal treatment, and BDL for the aerosol at -15 and -10 °C indicates below detection limit. All treatments (4) were run for each sample.

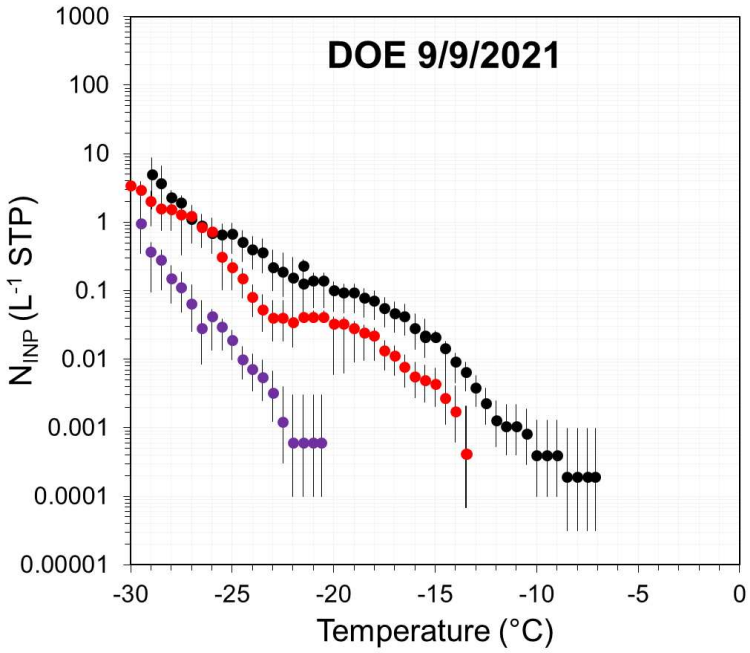

Figure 6.6. INP-temperature spectra for an aerosol sample collected at the fixed Department of Energy (DOE) site on 9/9/2021. The black indicates untreated, red is after 95 °C, and purple is after hydrogen peroxide (H_2O_2) digestion.

6.2.2. Sampler differences for bioaerosols

As the polycarbonate filters in the Arctic were used for DNA analyses in Chapters 2 and 3, an initial comparison is provided over another oceanic region that contrasts this method with a higher flow volume method. The Sea2Cloud ship campaign traveled near New Zealand in March 2020 between 41 and 47 °S, and the goal was to connect Southern Ocean properties to atmospheric fluxes and cloud formation (Sellegri et al., 2023). The polycarbonate filters used were the same ones as in MOSAiC (0.4 µm Whatman Nuclepore track-etched hydrophilic membranes). During MOSAiC, the average flow through the filters was 34.1 standard Liters (sL: 0 °C, 1013.25 mb) min^{-1} over the course of the year, and similar values were reported from Sea2Cloud. The filters in Sea2Cloud sampled for 1 or 2 days, and for comparison, a high volume liquid impingement sampler, the Coriolis [e.g. (Archer et al., 2023)], was used during some of

the time period. The benefit of this type of sampler is that it draws air at 300 L min^{-1}, and also impinges into liquid, which may be better than dry filter collection for preservation of microbes. The Coriolis typically ran for 1-3 hours, and Coriolis samples obtained within the same time period as the polycarbonate filters were pooled for analysis.

The results for taxonomy and diversity metrics are presented in Figures 6.7 and 6.8. The relative abundance plot reveals that at the class level, the samples share overlap. Many of the major groups are present in both samples, across the whole time period, with some differences in relative abundance percentages. For example, Phycisphaerae were detected consistently in the polycarbonate samples, but minimally in the Coriolis samples. Acidobacteriae were detected in the Coriolis, but minimally in the polycarbonate samples. The alpha diversities (Fig. 6.8, left panel) were very similar for the two samples, with the Coriolis sample slightly higher, which indicates the samplers are picking up similar diversities of air microbes. Figure 6.9 shows a wide diversity of taxa that were picked up in the air that were also in sequenced water samples. This is encouraging in that the polycarbonate filters, a cheaper and longer duration alternative, sampled alpha diversity levels similar to the Coriolis. For beta diversity (Fig. 6.8, right panel) there were some detected differences between sampler type, which is consistent with varying detected proportions of some taxa. The time component could be influencing the beta diversity as well, with the Coriolis samples not able to span the entire polycarbonate (either 24 or 48 hours) sampling period.

Overall, it is encouraging to see relative agreement between two methods of sample collection in an oceanic environment. Future work should include quantitative PCR to detect bacterial concentrations and track specific groups better than relative abundance, as well as explore reasons for taxa divergence between sampler types, such as abundance of Gram-positive

versus Gram-negative bacteria. Polycarbonate filters have benefits that include easier elimination of contamination potential, as the filter units are disposable and are preloaded in a clean environment, reduced costs, and a gentler flow rate that may be advantageous for sampling in stable airmasses where high variability with time is not expected (and thus not needing to be captured). Polycarbonate filters also have lower backgrounds that can be used for sampling INPs in remote regions.

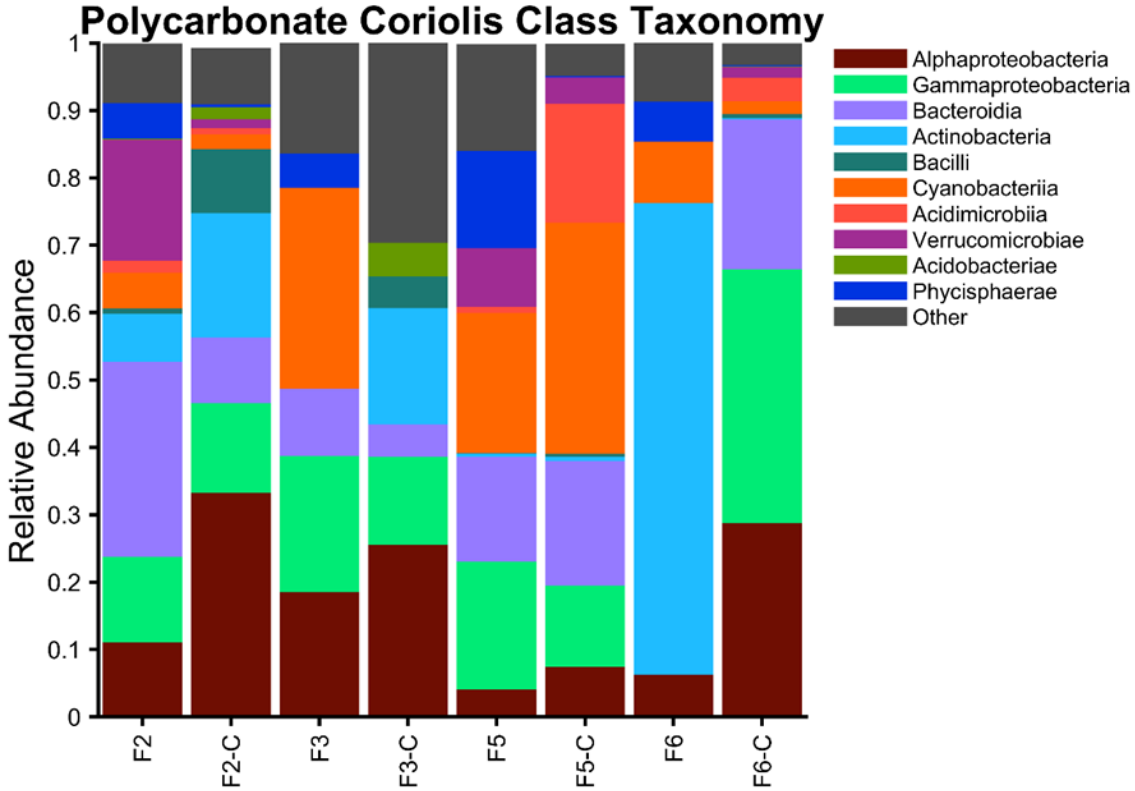

Figure 6.7. Class level taxonomic relative abundance between polycarbonate filters, denoted by "F" and pooled Coriolis samples that were taken within the same time period, denoted by "-C". Taxa that have a relative abundance of less than 0.1% are excluded.

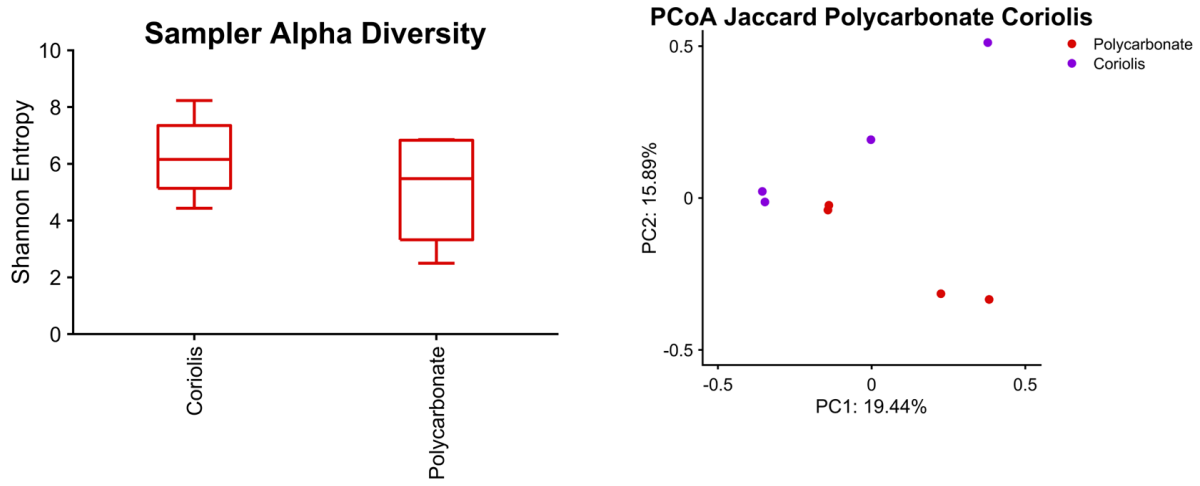

Figure 6.8. Alpha (left) and beta (right) diversity metrics between the polycarbonate and Coriolis samples.

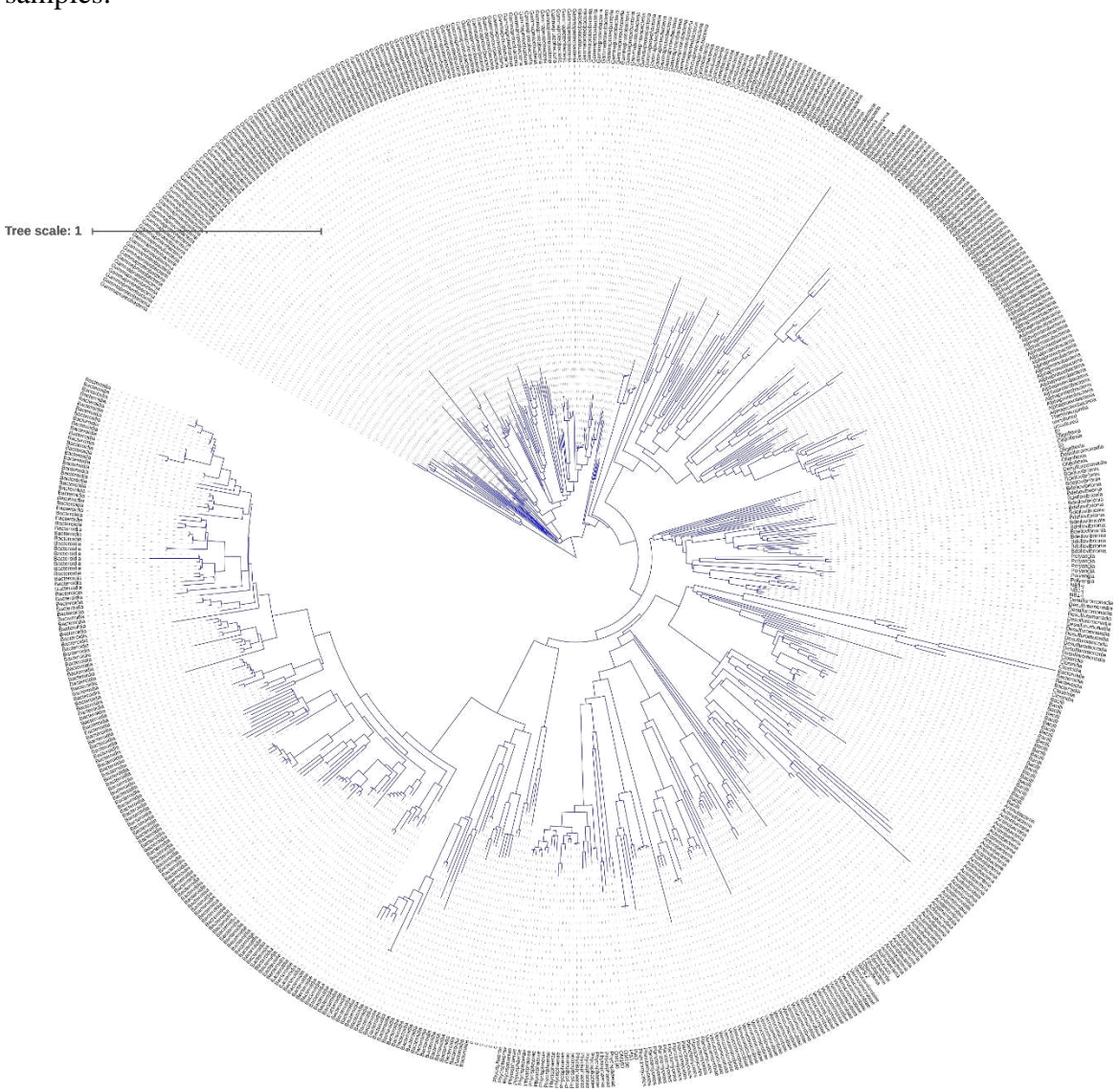

Figure 6.9. Phylogenetic tree that shows the amplicon sequence variants (ASVs: names correspond to the class level) in sequences common to both the air and the water, over the entire Sea2Cloud campaign. Names are visible with zoom but are not necessary to qualitatively see sampled diversity.

6.3 Concluding remarks

This work has focused on INPs and bioaerosols measured in the Arctic over a full year and has looked at some of the potential active sources that may contribute to the air; for the latter, using a ground up approach over an active thermokarst domain during peak thaw. In addition to its potential as an INP reservoir, permafrost is certainly critical in controlling much of the past, present, and future Arctic terrestrial landscape, and thus influences the present INP population. The MOSAiC study demonstrated the value of long-term Arctic INP measurements, which showed seasonal variations as well as the impacts of periodic cyclones. Multiyear observations, like those at Mount Zeppelin (Pereira Freitas et al., 2023), are also needed to see longer-term trends that could not be addressed in this work. The comparability of longer-term measurements taken at a variety of sites, including the Utqiaġvik DOE site, Mount Zeppelin in Svalbard, and the central Arctic MOSAiC site, points toward the benefit of continuous measures. Since the sources seem to be well mixed to create a regional INP population over the time scale of days, long term measurements may be best at fixed terrestrial sites instead of ship voyages to the central Arctic, where costs and contamination potential are easier to control. Clouds could still be affected by localized INP sources, such as melt ponds or exposed permafrost from coastline erosion, thus more localized observations might be useful for process-level models like Large Eddy Simulation.

Modeling of future changes to the Arctic aerosol and INP populations, and their impacts on clouds, requires improved representations of relevant sources, most of which contain

abundant organic INPs. Models require parameterizations for fluxes or concentrations of specialized particles such as CCN and INPs, and thus effort is needed to provide this information using new datasets. This dissertation provides the framework to be able to model emissions from a region with a high density of thermokarst lakes, as the aerosol INPs were enhanced downwind of all lakes measured, they can have a large horizontal extent, and could largely cover grid cells. The lakes encompass the variety of sources tested and measured in active thermokarst regions, as presented in Chapter 4.

Future work should further explore links to TOC, as well as refining the use of thermal treatments to characterize INP-temperature relationships that can link sources to airborne INPs. The compound heat treatment presented has the potential, depending on regional source comparability, of ruling out major contributions of INPs the Arctic aerosol (such as the permafrost, sediment, and active layer found on the September 17th samples). This method could be expanded to other Arctic sources, such as glacial soil dust (Tobo et al., 2019). If TOC of bodies of water can be predicted in models, the TOC parameterization could be the best way to track INP emissions from the sources to the atmosphere via aerosol transfer under wind stress in thermokarst lakes, estuaries, and the ocean, as this would simplify the complexity of the landscape significantly and could track future INP contributions amid landscape changes. Future measurements should additionally focus on more cloud-level sampling (such as through airborne or tethered balloon sampling campaigns) to explore yearly comparability with ground-based measures, as above -15 °C, Arctic ice-containing clouds that are coupled to the surface have been shown to be more frequent than decoupled clouds (Griesche et al., 2021). Airborne campaigns are especially valuable, as they can provide both free tropospheric and boundary layer measurements.

For bioaerosols, the largest work needed in the Arctic is increased numbers of measurements, since unlike INPs, which have had emerging fixed-term sites, MOSAiC provided the first yearly cycle of bacteria and eukaryotes in the Arctic. And additionally, unlike the INPs, which were relatively stable in terms of composition and through having a regionally mixed population, periodic influence of eukaryotes and wide diversity of aerosolized bacterial taxa show that the bioaerosol population is more complex. Since ship community contamination can easily affect bioaerosol filters, focusing on high volume samplers like the Coriolis or long-term measurements at isolated fixed sites would be the best way to see how microbes evolve in the future Arctic. Further work will additionally be done on this bioaerosol dataset, including quantitative PCR, in order to better see how the concentration of bacteria and certain subgroups varied over the year.

In summary, the best recommendation for the Arctic lies within reliable, long-term measurements to be able to track future changes as the permafrost continues to thaw and ice extent continues to decrease. All future field measurements come back to the criticality of sample cleanliness to support accurate measurement of INPs and bioaerosols in regions where numbers are low. This includes proper filter cleaning, transport, storage in the field, and analysis upon return. This is the only way to ensure reliability and comparability when comparing any seasonal and long-term trends, and to accurately quantify, parameterize, and predict INPs in the future.

References

Abarenkov, K., Zirk, A., Piirmann, T., Pöhönen, R., Ivanov, F., Nilsson, H., & Kõljalg, U. (2022). *UNITE QIIME release for Fungi* [Fungi R.T. Moore, 1980]. https://doi.org/10.15156/BIO/2483915

Agresti, A., & Coull, B. A. (1998). Approximate is better than "exact" for interval estimation of binomial proportions. *The American Statistician*, *52*, 119–126. https://doi.org/10.2307/2685469

Archer, S. D. J., Lee, K. C., Caruso, T., Alcami, A., Araya, J. G., Cary, S. C., Cowan, D. A., Etchebehere, C., Gantsetseg, B., Gomez-Silva, B., Hartery, S., Hogg, I. D., Kansour, M. K., Lawrence, T., Lee, C. K., Lee, P. K. H., Leopold, M., Leung, M. H. Y., Maki, T., … Pointing, S. B. (2023). Contribution of soil bacteria to the atmosphere across biomes. *Science of The Total Environment*, *871*, 162137. https://doi.org/10.1016/j.scitotenv.2023.162137

Arora, S., Lal, S., Kumar, S., Kumar, M., & Kumar, M. (2011). *Comparative degradation kinetic studies of three biopolymers: Chitin, chitosan and cellulose*.

Barber, V. A., & Finney, B. P. (1999). *Late quaternary paleoclimatic reconstructions for interior Alaska based on paleolake-level data and hydrologic models*.

Barry, K. R., Hill, T. C. J., Jentzsch, C., Moffett, B. F., Stratmann, F., & DeMott, P. J. (2021). Pragmatic protocols for working cleanly when measuring ice nucleating particles. *Atmospheric Research*, *250*, 105419. https://doi.org/10.1016/j.atmosres.2020.105419

Barry, K. R., Hill, T. C. J., Levin, E. J. T., Twohy, C. H., Moore, K. A., Weller, Z. D., Toohey, D. W., Reeves, M., Campos, T., Geiss, R., Schill, G. P., Fischer, E. V., Kreidenweis, S. M., & DeMott, P. J. (2021). Observations of Ice Nucleating Particles in the Free

Troposphere From Western US Wildfires. *Journal of Geophysical Research: Atmospheres*, *126*(3). https://doi.org/10.1029/2020JD033752

Barry, K. R., Hill, T. C. J., Moore, K. A., Douglas, T. A., Kreidenweis, S. M., DeMott, P. J., & Creamean, J. M. (2023). Persistence and Potential Atmospheric Ramifications of Ice-Nucleating Particles Released from Thawing Permafrost. *Environmental Science & Technology*, *57*(9), 3505–3515. https://doi.org/10.1021/acs.est.2c06530

Barry, K. R., Hill, T. C. J., Nieto-Caballero, M., Douglas, T. A., Kreidenweis, S. M., DeMott, P. J., & Creamean, J. M. (2023). *Active thermokarst regions contain rich sources of ice nucleating particles* [Preprint]. Aerosols/Field Measurements/Troposphere/Physics (physical properties and processes). https://doi.org/10.5194/egusphere-2023-1208

Beall, C. M., Stokes, M. D., Hill, T. C., DeMott, P. J., DeWald, J. T., & Prather, K. A. (2017). Automation and heat transfer characterization of immersion mode spectroscopy for analysis of ice nucleating particles. *Atmospheric Measurement Techniques*, *10*(7), 2613–2626. https://doi.org/10.5194/amt-10-2613-2017

Bigg, E. K. (1996). Ice forming nuclei in the high Arctic. *Tellus B*, *48*(2), 223–233. https://doi.org/10.1034/j.1600-0889.1996.t01-1-00007.x

Bigg, E. K., & Leck, C. (2001). Cloud-active particles over the central Arctic Ocean. *Journal of Geophysical Research: Atmospheres*, *106*(D23), 32155–32166. https://doi.org/10.1029/1999JD901152

Bintanja, R., & Andry, O. (2017). Towards a rain-dominated Arctic. *Nature Climate Change*, *7*(4), 263–267. https://doi.org/10.1038/nclimate3240

Biskaborn, B. K., Smith, S. L., Noetzli, J., Matthes, H., Vieira, G., Streletskiy, D. A., Schoeneich, P., Romanovsky, V. E., Lewkowicz, A. G., Abramov, A., Allard, M., Boike,

J., Cable, W. L., Christiansen, H. H., Delaloye, R., Diekmann, B., Drozdov, D., Etzelmüller, B., Grosse, G., … Lantuit, H. (2019). Permafrost is warming at a global scale. *Nature Communications*, *10*(1), 264. https://doi.org/10.1038/s41467-018-08240-4

Bokulich, N. A., Kaehler, B. D., Rideout, J. R., Dillon, M., Bolyen, E., Knight, R., Huttley, G. A., & Gregory Caporaso, J. (2018). Optimizing taxonomic classification of marker-gene amplicon sequences with QIIME 2's q2-feature-classifier plugin. *Microbiome*, *6*(1), 90. https://doi.org/10.1186/s40168-018-0470-z

Bolyen, E., Rideout, J. R., Dillon, M. R., Bokulich, N. A., Abnet, C. C., Al-Ghalith, G. A., Alexander, H., Alm, E. J., Arumugam, M., Asnicar, F., Bai, Y., Bisanz, J. E., Bittinger, K., Brejnrod, A., Brislawn, C. J., Brown, C. T., Callahan, B. J., Caraballo-Rodríguez, A. M., Chase, J., … Caporaso, J. G. (2019). Reproducible, interactive, scalable and extensible microbiome data science using QIIME 2. *Nature Biotechnology*, *37*(8), 852–857. https://doi.org/10.1038/s41587-019-0209-9

Bowden, W. B. (2010). Climate Change in the Arctic - Permafrost, Thermokarst, and Why They Matter to the Non-Arctic World: Climate change in the Arctic: why it matters. *Geography Compass*, *4*(10), 1553–1566. https://doi.org/10.1111/j.1749-8198.2010.00390.x

Brush, R. A., Griffith, M., & Mlynarz, A. (1994). *Characterization and Quantification of lntrinsic Ice Nucleators in Winter Rye (Secale cereale) Leaves'*. *104*.

Burn, C. R., & Kokelj, S. V. (2009). The environment and permafrost of the Mackenzie Delta area. *Permafrost and Periglacial Processes*, *20*(2), 83–105. https://doi.org/10.1002/ppp.655

Callahan, B. J., McMurdie, P. J., Rosen, M. J., Han, A. W., Johnson, A. J. A., & Holmes, S. P. (2016). DADA2: High-resolution sample inference from Illumina amplicon data. *Nature Methods*, *13*(7), 581–583. https://doi.org/10.1038/nmeth.3869

Cesana, G., & Storelvmo, T. (2017). Improving climate projections by understanding how cloud phase affects radiation. *Journal of Geophysical Research: Atmospheres*, *122*(8), 4594–4599. https://doi.org/10.1002/2017JD026927

Chen, J., Wu, Z., Augustin-Bauditz, S., Grawe, S., Hartmann, M., Pei, X., Liu, Z., Ji, D., & Wex, H. (2018). Ice-nucleating particle concentrations unaffected by urban air pollution in Beijing, China. *Atmospheric Chemistry and Physics*, *18*(5), 3523–3539. https://doi.org/10.5194/acp-18-3523-2018

Chen, Y., Lara, M. J., Jones, B. M., Frost, G. V., & Hu, F. S. (2021). Thermokarst acceleration in Arctic tundra driven by climate change and fire disturbance. *One Earth*, *4*(12), 1718–1729. https://doi.org/10.1016/j.oneear.2021.11.011

Conen, F., Stopelli, E., & Zimmermann, L. (2016). Clues that decaying leaves enrich Arctic air with ice nucleating particles. *Atmospheric Environment*, *129*, 91–94. https://doi.org/10.1016/j.atmosenv.2016.01.027

Creamean, J. M., Barry, K., Hill, T. C. J., Hume, C., DeMott, P. J., Shupe, M. D., Dahlke, S., Willmes, S., Schmale, J., Beck, I., Hoppe, C. J. M., Fong, A., Chamberlain, E., Bowman, J., Scharien, R., & Persson, O. (2022). Annual cycle observations of aerosols capable of ice formation in central Arctic clouds. *Nature Communications*, *13*(1), 3537. https://doi.org/10.1038/s41467-022-31182-x

Creamean, J. M., Cross, J. N., Pickart, R., McRaven, L., Lin, P., Pacini, A., Hanlon, R., Schmale, D. G., Ceniceros, J., Aydell, T., Colombi, N., Bolger, E., & DeMott, P. J. (2019). Ice

Nucleating Particles Carried From Below a Phytoplankton Bloom to the Arctic Atmosphere. *Geophysical Research Letters*, *46*(14), 8572–8581. https://doi.org/10.1029/2019GL083039

Creamean, J. M., Hill, T. C. J., DeMott, P. J., Uetake, J., Kreidenweis, S., & Douglas, T. A. (2020). Thawing permafrost: An overlooked source of seeds for Arctic cloud formation. *Environmental Research Letters*, *15*(8), 084022. https://doi.org/10.1088/1748-9326/ab87d3

Creamean, J. M., Hill, T., & Hume, C. (2022). *Ice Nucleation Spectrometer (INS) Instrument Handbook* (DOE/SC-ARM-TR-278, 1846263; p. DOE/SC-ARM-TR-278, 1846263). https://doi.org/10.2172/1846263

Creamean, J. M., Kirpes, R. M., Pratt, K. A., Spada, N. J., Maahn, M., de Boer, G., Schnell, R. C., & China, S. (2018). Marine and terrestrial influences on ice nucleating particles during continuous springtime measurements in an Arctic oilfield location. *Atmospheric Chemistry and Physics*, *18*(24), 18023–18042. https://doi.org/10.5194/acp-18-18023-2018

Creamean, J. M., Primm, K. M., Tolbert, M. A., Hall, E. G., Wendell, J., Jordan, A., Sheridan, P. J., Smith, J., & Schnell, R. C. (2018). HOVERCAT: A novel aerial system for evaluation of aerosol–cloud interactions. *Atmospheric Measurement Techniques*, *11*(7), 3969–3985. https://doi.org/10.5194/amt-11-3969-2018

Cruaud, P., Vigneron, A., Fradette, M.-S., Charette, S. J., Rodriguez, M. J., Dorea, C. C., & Culley, A. I. (2017). Open the Sterivex ™ casing: An easy and effective way to improve DNA extraction yields: *DNA extraction from Sterivex ™ filters . Limnology and Oceanography: Methods*, *15*(12), 1015–1020. https://doi.org/10.1002/lom3.10221

Cuthbertson, L., Amores-Arrocha, H., Malard, L., Els, N., Sattler, B., & Pearce, D. (2017). Characterisation of Arctic Bacterial Communities in the Air above Svalbard. *Biology*, *6*(4), 29. https://doi.org/10.3390/biology6020029

Dada, L., Angot, H., Beck, I., Baccarini, A., Quéléver, L. L. J., Boyer, M., Laurila, T., Brasseur, Z., Jozef, G., De Boer, G., Shupe, M. D., Henning, S., Bucci, S., Dütsch, M., Stohl, A., Petäjä, T., Daellenbach, K. R., Jokinen, T., & Schmale, J. (2022). A central arctic extreme aerosol event triggered by a warm air-mass intrusion. *Nature Communications*, *13*(1), 5290. https://doi.org/10.1038/s41467-022-32872-2

David, R. O., Cascajo-Castresana, M., Brennan, K. P., Rösch, M., Els, N., Werz, J., Weichlinger, V., Boynton, L. S., Bogler, S., Borduas-Dedekind, N., Marcolli, C., & Kanji, Z. A. (2019). Development of the DRoplet Ice Nuclei Counter Zurich (DRINCZ): Validation and application to field-collected snow samples. *Atmospheric Measurement Techniques*, *12*(12), 6865–6888. https://doi.org/10.5194/amt-12-6865-2019

Davis, N. M., Proctor, D. M., Holmes, S. P., Relman, D. A., & Callahan, B. J. (2018). Simple statistical identification and removal of contaminant sequences in marker-gene and metagenomics data. *Microbiome*, *6*(1), 226. https://doi.org/10.1186/s40168-018-0605-2

De Garcia, V., Trochine, A., Uetake, J., Bellora, N., & Libkind, D. (2020). Novel yeast taxa from the cold: Description of Cryolevonia giraudoae sp. nov. and Camptobasidium gelus sp. nov. *International Journal of Systematic and Evolutionary Microbiology*, *70*(6), 3711–3717. https://doi.org/10.1099/ijsem.0.004223

DeMott, P. J. (1995). Quantitative descriptions of ice formation mechanisms of silver iodide, type aerosols. *Atmospheric Research*, *38*, 63–99.

DeMott, P. J., Hill, T. C. J., Petters, M. D., Bertram, A. K., Tobo, Y., Mason, R. H., Suski, K. J., McCluskey, C. S., Levin, E. J. T., Schill, G. P., Boose, Y., Rauker, A. M., Miller, A. J., Zaragoza, J., Rocci, K., Rothfuss, N. E., Taylor, H. P., Hader, J. D., Chou, C., … Kreidenweis, S. M. (2017). Comparative measurements of ambient atmospheric concentrations of ice nucleating particles using multiple immersion freezing methods and a continuous flow diffusion chamber. *Atmospheric Chemistry and Physics*, *17*(18), 11227–11245. https://doi.org/10.5194/acp-17-11227-2017

DeMott, P. J., Möhler, O., Cziczo, D. J., Hiranuma, N., Petters, M. D., Petters, S. S., Belosi, F., Bingemer, H. G., Brooks, S. D., Budke, C., Burkert-Kohn, M., Collier, K. N., Danielczok, A., Eppers, O., Felgitsch, L., Garimella, S., Grothe, H., Herenz, P., Hill, T. C. J., … Zenker, J. (2018). The Fifth International Workshop on Ice Nucleation phase 2 (FIN-02): Laboratory intercomparison of ice nucleation measurements. *Atmospheric Measurement Techniques*, *11*(11), 6231–6257. https://doi.org/10.5194/amt-11-6231-2018

DeMott, P. J., Prenni, A. J., Liu, X., Kreidenweis, S. M., Petters, M. D., Twohy, C. H., Richardson, M. S., Eidhammer, T., & Rogers, D. C. (2010). Predicting global atmospheric ice nuclei distributions and their impacts on climate. *Proceedings of the National Academy of Sciences*, *107*(25), 11217–11222. https://doi.org/10.1073/pnas.0910818107

DeMott, P. J., Prenni, A. J., McMeeking, G. R., Sullivan, R. C., Petters, M. D., Tobo, Y., Niemand, M., Möhler, O., Snider, J. R., Wang, Z., & Kreidenweis, S. M. (2015). Integrating laboratory and field data to quantify the immersion freezing ice nucleation activity of mineral dust particles. *Atmospheric Chemistry and Physics*, *15*(1), 393–409. https://doi.org/10.5194/acp-15-393-2015

Douglas, T. A., Hiemstra, C. A., Anderson, J. E., Barbato, R. A., Bjella, K. L., Deeb, E. J., Gelvin, A. B., Nelsen, P. E., Newman, S. D., Saari, S. P., & Wagner, A. M. (2021). *Recent degradation of Interior Alaska permafrost mappedwith ground surveys, geophysics, deep drilling, and repeatairborne LiDAR* [Preprint]. Frozen ground/Geomorphology. https://doi.org/10.5194/tc-2021-47

Douglas, T. A., & Mellon, M. T. (2019). Sublimation of terrestrial permafrost and the implications for ice-loss processes on Mars. *Nature Communications*, *10*(1), 1716. https://doi.org/10.1038/s41467-019-09410-8

Edwards, M. E., Mock, C. J., Finney, B. P., Barber, V. A., & Bartlein, J. (2001). Potential analogues for paleoclimatic variations in eastern interior Alaska during the past 14,000 yr: Atmospheric-circulation controls of regional temperature and moisture responses☪. *Quaternary Science Reviews*.

Failor, K. C., Schmale, D. G., Vinatzer, B. A., & Monteil, C. L. (2017). Ice nucleation active bacteria in precipitation are genetically diverse and nucleate ice by employing different mechanisms. *The ISME Journal*, *11*(12), 2740–2753. https://doi.org/10.1038/ismej.2017.124

Farquharson, L. M., Mann, D. H., Grosse, G., Jones, B. M., & Romanovsky, V. E. (2016). Spatial distribution of thermokarst terrain in Arctic Alaska. *Geomorphology*, *273*, 116–133. https://doi.org/10.1016/j.geomorph.2016.08.007

Farquharson, L. M., Romanovsky, V. E., Kholodov, A., & Nicolsky, D. (2022). Sub-aerial talik formation observed across the discontinuous permafrost zone of Alaska. *Nature Geoscience*, *15*(6), 475–481. https://doi.org/10.1038/s41561-022-00952-z

Fröhlich-Nowoisky, J., Burrows, S. M., Xie, Z., Engling, G., Solomon, P. A., Fraser, M. P., Mayol-Bracero, O. L., Artaxo, P., Begerow, D., Conrad, R., Andreae, M. O., Després, V. R., & Pöschl, U. (2012). Biogeography in the air: Fungal diversity over land and oceans. *Biogeosciences*, *9*(3), 1125–1136. https://doi.org/10.5194/bg-9-1125-2012

Fröhlich-Nowoisky, J., Hill, T. C. J., Pummer, B. G., Yordanova, P., Franc, G. D., & Pöschl, U. (2015). Ice nucleation activity in the widespread soil fungus <i>Mortierella alpina</i> *Biogeosciences*, *12*(4), 1057–1071. https://doi.org/10.5194/bg-12-1057-2015

Fröhlich-Nowoisky, J., Pickersgill, D. A., Després, V. R., & Pöschl, U. (2009). High diversity of fungi in air particulate matter. *Proceedings of the National Academy of Sciences*, *106*(31), 12814–12819. https://doi.org/10.1073/pnas.0811003106

Galperin, M. Y. (2015). *Genome Diversity of Spore-Forming Firmicutes*.

Garcia, E., Hill, T. C. J., Prenni, A. J., DeMott, P. J., Franc, G. D., & Kreidenweis, S. M. (2012). Biogenic ice nuclei in boundary layer air over two U.S. High Plains agricultural regions: BIOGENIC ICE NUCLEI OVER TWO AGRICULTURAL REGIONS. *Journal of Geophysical Research: Atmospheres*, *117*(D18), n/a-n/a. https://doi.org/10.1029/2012JD018343

Garçon, M., Sauzéat, L., Carlson, R. W., Shirey, S. B., Simon, M., Balter, V., & Boyet, M. (2017). Nitrile, Latex, Neoprene and Vinyl Gloves: A Primary Source of Contamination for Trace Element and Zn Isotopic Analyses in Geological and Biological Samples. *Geostandards and Geoanalytical Research*, *41*(3), 367–380. https://doi.org/10.1111/ggr.12161

Gong, X., Zhang, J., Croft, B., Yang, X., Frey, M. M., Bergner, N., Chang, R. Y.-W., Creamean, J. M., Kuang, C., Martin, R. V., Ranjithkumar, A., Sedlacek, A. J., Uin, J., Willmes, S., Zawadowicz, M. A., Pierce, J. R., Shupe, M. D., Schmale, J., & Wang, J. (2023). Arctic warming by abundant fine sea salt aerosols from blowing snow. *Nature Geoscience*, *16*(9), 768–774. https://doi.org/10.1038/s41561-023-01254-8

Goñi, M. A., Corvi, E. R., Welch, K. A., Buktenica, M., Lebon, K., Alleau, Y., & Juranek, L. W. (2019). Particulate organic matter distributions in surface waters of the Pacific Arctic shelf during the late summer and fall season. *Marine Chemistry*, *211*, 75–93. https://doi.org/10.1016/j.marchem.2019.03.010

Griesche, H. J., Ohneiser, K., Seifert, P., Radenz, M., Engelmann, R., & Ansmann, A. (2021). Contrasting ice formation in Arctic clouds: Surface-coupled vs. surface-decoupled clouds. *Atmospheric Chemistry and Physics*, *21*(13), 10357–10374. https://doi.org/10.5194/acp-21-10357-2021

Gross, D. C., Proebsting, E. L., & Maccrindle-Zimmerman, H. (1988). Development, Distribution, and Characteristics of Intrinsic, Nonbacterial Ice Nuclei in *Prunus* Wood. *Plant Physiology*, *88*(3), 915–922. https://doi.org/10.1104/pp.88.3.915

Guillou, L., Bachar, D., Audic, S., Bass, D., Berney, C., Bittner, L., Boutte, C., Burgaud, G., De Vargas, C., Decelle, J., Del Campo, J., Dolan, J. R., Dunthorn, M., Edvardsen, B., Holzmann, M., Kooistra, W. H. C. F., Lara, E., Le Bescot, N., Logares, R., … Christen, R. (2012). The Protist Ribosomal Reference database (PR2): A catalog of unicellular eukaryote Small Sub-Unit rRNA sequences with curated taxonomy. *Nucleic Acids Research*, *41*(D1), D597–D604. https://doi.org/10.1093/nar/gks1160

Gute, E., & Abbatt, J. P. D. (2020). Ice nucleating behavior of different tree pollen in the immersion mode. *Atmospheric Environment*, *231*, 117488. https://doi.org/10.1016/j.atmosenv.2020.117488

Harb, C., & Foroutan, H. (2022). Experimental development of a lake spray source function and its model implementation for Great Lakes surface emissions. *Atmospheric Chemistry and Physics*, *22*(17), 11759–11779. https://doi.org/10.5194/acp-22-11759-2022

Harding, T., Jungblut, A. D., Lovejoy, C., & Vincent, W. F. (2011). Microbes in High Arctic Snow and Implications for the Cold Biosphere. *Applied and Environmental Microbiology*, *77*(10), 3234–3243. https://doi.org/10.1128/AEM.02611-10

Harrison, A. D., Whale, T. F., Rutledge, R., Lamb, S., Tarn, M. D., Porter, G. C. E., Adams, M. P., McQuaid, J. B., Morris, G. J., & Murray, B. J. (2018). An instrument for quantifying heterogeneous ice nucleation in multiwell plates using infrared emissions to detect freezing. *Atmospheric Measurement Techniques*, *11*(10), 5629–5641. https://doi.org/10.5194/amt-11-5629-2018

Hartmann, M., Adachi, K., Eppers, O., Haas, C., Herber, A., Holzinger, R., Hünerbein, A., Jäkel, E., Jentzsch, C., Pinxteren, M., Wex, H., Willmes, S., & Stratmann, F. (2020). Wintertime Airborne Measurements of Ice Nucleating Particles in the High Arctic: A Hint to a Marine, Biogenic Source for Ice Nucleating Particles. *Geophysical Research Letters*, *47*(13). https://doi.org/10.1029/2020GL087770

Hartmann, M., Gong, X., Kecorius, S., van Pinxteren, M., Vogl, T., Welti, A., Wex, H., Zeppenfeld, S., Herrmann, H., Wiedensohler, A., & Stratmann, F. (2021). Terrestrial or marine – indications towards the origin of ice-nucleating particles during melt season in

the European Arctic up to 83.7° N. *Atmospheric Chemistry and Physics*, *21*(15), 11613–11636. https://doi.org/10.5194/acp-21-11613-2021

Hasegawa, Y., Ishihara, Y., & Tokuyama, T. (1994). Characteristics of Ice-nucleation Activity in *Fusarium avenaceum* IFO 7158. *Bioscience, Biotechnology, and Biochemistry*, *58*(12), 2273–2274. https://doi.org/10.1271/bbb.58.2273

Hill, T. C. J., DeMott, P. J., Conen, F., & Möhler, O. (2018). Impacts of Bioaerosols on Atmospheric Ice Nucleation Processes. In A.-M. Delort & P. Amato (Eds.), *Microbiology of Aerosols* (1st ed., pp. 197–219). John Wiley & Sons.

Hill, T. C. J., DeMott, P. J., Tobo, Y., Fröhlich-Nowoisky, J., Moffett, B. F., Franc, G. D., & Kreidenweis, S. M. (2016). Sources of organic ice nucleating particles in soils. *Atmospheric Chemistry and Physics*, *16*(11), 7195–7211. https://doi.org/10.5194/acp-16-7195-2016

Hill, T. C. J., Moffett, B. F., DeMott, P. J., Georgakopoulos, D. G., Stump, W. L., & Franc, G. D. (2014). Measurement of Ice Nucleation-Active Bacteria on Plants and in Precipitation by Quantitative PCR. *Applied and Environmental Microbiology*, *80*(4), 1256–1267. https://doi.org/10.1128/AEM.02967-13

Hiranuma, N., Augustin-Bauditz, S., Bingemer, H., Budke, C., Curtius, J., Danielczok, A., Diehl, K., Dreischmeier, K., Ebert, M., Frank, F., Hoffmann, N., Kandler, K., Kiselev, A., Koop, T., Leisner, T., Möhler, O., Nillius, B., Peckhaus, A., Rose, D., … Yamashita, K. (2015). A comprehensive laboratory study on the immersion freezing behavior of illite NX particles: A comparison of 17 ice nucleation measurement techniques. *Atmospheric Chemistry and Physics*, *15*(5), 2489–2518. https://doi.org/10.5194/acp-15-2489-2015

Huang, S., Hu, W., Chen, J., Wu, Z., Zhang, D., & Fu, P. (2021). Overview of biological ice nucleating particles in the atmosphere. *Environment International*, *146*, 106197. https://doi.org/10.1016/j.envint.2020.106197

in ’t Zandt, M. H., Liebner, S., & Welte, C. U. (2020). Roles of Thermokarst Lakes in a Warming World. *Trends in Microbiology*, *28*(9), 769–779. https://doi.org/10.1016/j.tim.2020.04.002

Inoue, J., Tobo, Y., Taketani, F., & Sato, K. (2021). Oceanic Supply of Ice-Nucleating Particles and Its Effect on Ice Cloud Formation: A Case Study in the Arctic Ocean During a Cold-Air Outbreak in Early Winter. *Geophysical Research Letters*, *48*(16). https://doi.org/10.1029/2021GL094646

Intrieri, J. M. (2002). An annual cycle of Arctic surface cloud forcing at SHEBA. *Journal of Geophysical Research*, *107*(C10), 8039. https://doi.org/10.1029/2000JC000439

Irish, V. E., Hanna, S. J., Willis, M. D., China, S., Thomas, J. L., Wentzell, J. J. B., Cirisan, A., Si, M., Leaitch, W. R., Murphy, J. G., Abbatt, J. P. D., Laskin, A., Girard, E., & Bertram, A. K. (2019). Ice nucleating particles in the marine boundary layer in the Canadian Arctic during summer 2014. *Atmospheric Chemistry and Physics*, *19*(2), 1027–1039. https://doi.org/10.5194/acp-19-1027-2019

Irrgang, A. M., Bendixen, M., Farquharson, L. M., Baranskaya, A. V., Erikson, L. H., Gibbs, A. E., Ogorodov, S. A., Overduin, P. P., Lantuit, H., Grigoriev, M. N., & Jones, B. M. (2022). Drivers, dynamics and impacts of changing Arctic coasts. *Nature Reviews Earth & Environment*, *3*(1), 39–54. https://doi.org/10.1038/s43017-021-00232-1

Jansson, J. K., & Taş, N. (2014). The microbial ecology of permafrost. *Nature Reviews Microbiology*, *12*(6), 414–425. https://doi.org/10.1038/nrmicro3262

Jensen, L. Z., Glasius, M., Gryning, S.-E., Massling, A., Finster, K., & Šantl-Temkiv, T. (2022). Seasonal Variation of the Atmospheric Bacterial Community in the Greenlandic High Arctic Is Influenced by Weather Events and Local and Distant Sources. *Frontiers in Microbiology*, *13*, 909980. https://doi.org/10.3389/fmicb.2022.909980

Johansen, S. (1991). Airborne pollen and spores on the Arctic island of Jan Mayen. *Grana*, *30*(2), 373–379. https://doi.org/10.1080/00173139109431993

Johansen, S., & Hafsten, U. (1988). Airborne pollen and spore registrations at Ny-Ålesund, Svalbard, summer 1986. *Polar Research*, *6*(1), 11–17. https://doi.org/10.3402/polar.v6i1.6842

Jones, B. M., Grosse, G., Farquharson, L. M., Roy-Léveillée, P., Veremeeva, A., Kanevskiy, M. Z., Gaglioti, B. V., Breen, A. L., Parsekian, A. D., Ulrich, M., & Hinkel, K. M. (2022). Lake and drained lake basin systems in lowland permafrost regions. *Nature Reviews Earth & Environment*, *3*(1), 85–98. https://doi.org/10.1038/s43017-021-00238-9

Jorgenson, M. T. (2013). 8.20 Thermokarst Terrains. In *Treatise on Geomorphology* (pp. 313–324). Elsevier. https://doi.org/10.1016/B978-0-12-374739-6.00215-3

Jorgenson, M. T., Kanevskiy, M., Shur, Y., Moskalenko, N., Brown, D. R. N., Wickland, K., Striegl, R., & Koch, J. (2015). Role of ground ice dynamics and ecological feedbacks in recent ice wedge degradation and stabilization. *Journal of Geophysical Research: Earth Surface*, *120*(11), 2280–2297. https://doi.org/10.1002/2015JF003602

Kanevskiy, M., Shur, Y., Bigelow, N. H., Bjella, K. L., Douglas, T. A., Fortier, D., Jones, B. M., & Jorgenson, M. T. (2022). Yedoma Cryostratigraphy of Recently Excavated Sections of the CRREL Permafrost Tunnel Near Fairbanks, Alaska. *Frontiers in Earth Science*, *9*, 758800. https://doi.org/10.3389/feart.2021.758800

Kanevskiy, M., Shur, Y., Strauss, J., Jorgenson, T., Fortier, D., Stephani, E., & Vasiliev, A. (2016). Patterns and rates of riverbank erosion involving ice-rich permafrost (yedoma) in northern Alaska. *Geomorphology*, *253*, 370–384. https://doi.org/10.1016/j.geomorph.2015.10.023

Kanji, Z. A., Ladino, L. A., Wex, H., Boose, Y., Burkert-Kohn, M., Cziczo, D. J., & Krämer, M. (2017). Overview of Ice Nucleating Particles. *Meteorological Monographs*, *58*, 1.1-1.33. https://doi.org/10.1175/AMSMONOGRAPHS-D-16-0006.1

Kawai, K., Matsui, H., & Tobo, Y. (2023). Dominant Role of Arctic Dust With High Ice Nucleating Ability in the Arctic Lower Troposphere. *Geophysical Research Letters*, *50*(8), e2022GL102470. https://doi.org/10.1029/2022GL102470

Kervran, M., Vagner, C., Cochez, M., Ponçot, M., Saeb, M. R., & Vahabi, H. (2022). Thermal degradation of polylactic acid (PLA)/polyhydroxybutyrate (PHB) blends: A systematic review. *Polymer Degradation and Stability*, *201*, 109995. https://doi.org/10.1016/j.polymdegradstab.2022.109995

Knights, D., Kuczynski, J., Charlson, E. S., Zaneveld, J., Mozer, M. C., Collman, R. G., Bushman, F. D., Knight, R., & Kelley, S. T. (2011). Bayesian community-wide culture-independent microbial source tracking. *Nature Methods*, *8*(9), 761–763. https://doi.org/10.1038/nmeth.1650

Kokelj, S. V., & Jorgenson, M. T. (2013). Advances in Thermokarst Research: Recent Advances in Research Investigating Thermokarst Processes. *Permafrost and Periglacial Processes*, *24*(2), 108–119. https://doi.org/10.1002/ppp.1779

Kokelj, S. V., Tunnicliffe, J., Lacelle, D., Lantz, T. C., Chin, K. S., & Fraser, R. (2015). Increased precipitation drives mega slump development and destabilization of ice-rich

permafrost terrain, northwestern Canada. *Global and Planetary Change*, *129*, 56–68. https://doi.org/10.1016/j.gloplacha.2015.02.008

Kunert, A. T., Lamneck, M., Helleis, F., Pöschl, U., Pöhlker, M. L., & Fröhlich-Nowoisky, J. (2018). Twin-plate Ice Nucleation Assay (TINA) with infrared detection for high-throughput droplet freezing experiments with biological ice nuclei in laboratory and field samples. *Atmospheric Measurement Techniques*, *11*(11), 6327–6337. https://doi.org/10.5194/amt-11-6327-2018

Kunert, A. T., Pöhlker, M. L., Tang, K., Krevert, C. S., Wieder, C., Speth, K. R., Hanson, L. E., Morris, C. E., Schmale Iii, D. G., Pöschl, U., & Fröhlich-Nowoisky, J. (2019). Macromolecular fungal ice nuclei in <i>Fusarium</i>: Effects of physical and chemical processing. *Biogeosciences*, *16*(23), 4647–4659. https://doi.org/10.5194/bg-16-4647-2019

Kurek, J., Cwynar, L. C., & Vermaire, J. C. (2009). A late Quaternary paleotemperature record from Hanging Lake, northern Yukon Territory, eastern Beringia. *Quaternary Research*, *72*(2), 246–257. https://doi.org/10.1016/j.yqres.2009.04.007

Lachniet, M. S., Lawson, D. E., & Sloat, A. R. (2012). Revised ^{14} C dating of ice wedge growth in interior Alaska (USA) to MIS 2 reveals cold paleoclimate and carbon recycling in ancient permafrost terrain. *Quaternary Research*, *78*(2), 217–225. https://doi.org/10.1016/j.yqres.2012.05.007

Leck, C., Norman, M., & Bigg, E. K. (2002). Chemical composition and sources of the high Arctic aerosol relevant for cloud formation. *Journal of Geophysical Research*, *107*(D12), 4135. https://doi.org/10.1029/2001JD001463

Lohmann, U. (2002). A glaciation indirect aerosol effect caused by soot aerosols. *Geophysical Research Letters*, *29*(4), 1052. https://doi.org/10.1029/2001GL014357

Luo, J., Niu, F., Lin, Z., Liu, M., & Yin, G. (2015). Thermokarst lake changes between 1969 and 2010 in the Beilu River Basin, Qinghai–Tibet Plateau, China. *Science Bulletin*, *60*(5), 556–564. https://doi.org/10.1007/s11434-015-0730-2

Mackelprang, R., Burkert, A., Haw, M., Mahendrarajah, T., Conaway, C. H., Douglas, T. A., & Waldrop, M. P. (2017). Microbial survival strategies in ancient permafrost: Insights from metagenomics. *The ISME Journal*, *11*(10), 2305–2318. https://doi.org/10.1038/ismej.2017.93

Mason, R. H., Si, M., Chou, C., Irish, V. E., Dickie, R., Elizondo, P., Wong, R., Brintnell, M., Elsasser, M., Lassar, W. M., Pierce, K. M., Leaitch, W. R., MacDonald, A. M., Platt, A., Toom-Sauntry, D., Sarda-Estève, R., Schiller, C. L., Suski, K. J., Hill, T. C. J., … Bertram, A. K. (2016). Size-resolved measurements of ice-nucleating particles at six locations in North America and one in Europe. *Atmospheric Chemistry and Physics*, *16*(3), 1637–1651. https://doi.org/10.5194/acp-16-1637-2016

May, N. W., Axson, J. L., Watson, A., Pratt, K. A., & Ault, A. P. (2016). Lake spray aerosol generation: A method for producing representativeparticles from freshwater wave breaking. *Atmospheric Measurement Techniques*, *9*(9), 4311–4325. https://doi.org/10.5194/amt-9-4311-2016

McCluskey, C. S., Ovadnevaite, J., Rinaldi, M., Atkinson, J., Belosi, F., Ceburnis, D., Marullo, S., Hill, T. C. J., Lohmann, U., Kanji, Z. A., O'Dowd, C., Kreidenweis, S. M., & DeMott, P. J. (2018). Marine and Terrestrial Organic Ice-Nucleating Particles in Pristine Marine to

Continentally Influenced Northeast Atlantic Air Masses. *Journal of Geophysical Research: Atmospheres*, *123*(11), 6196–6212. https://doi.org/10.1029/2017JD028033

Miller, A., Brennan, K., Wieder, J., Mignani, C., Zipori, A., & Borduas-Dedekind, N. (2020). *Development of drop freezing ice nucleation chamber (FINC), validation using lignin, and application to organic matter samples* [Other]. oral. https://doi.org/10.5194/egusphere-egu2020-630

Moffett, B. F. (2016). Fresh water ice nuclei. *Fundamental and Applied Limnology*, *188*(1), 19–23. https://doi.org/10.1127/fal/2016/0851

Molnia, B. F. (Ed.). (1983). *Glacial-Marine Sedimentation*. Springer US. https://doi.org/10.1007/978-1-4613-3793-5

Moore, K. A., Alexander, S. P., Humphries, R. S., Jensen, J., Protat, A., Reeves, J. M., Sanchez, K. J., Kreidenweis, S. M., & DeMott, P. J. (2022). Estimation of Sea Spray Aerosol Surface Area Over the Southern Ocean Using Scattering Measurements. *Journal of Geophysical Research: Atmospheres*, *127*(22), e2022JD037009. https://doi.org/10.1029/2022JD037009

Morrison, H., de Boer, G., Feingold, G., Harrington, J., Shupe, M. D., & Sulia, K. (2012). Resilience of persistent Arctic mixed-phase clouds. *Nature Geoscience*, *5*(1), 11–17. https://doi.org/10.1038/ngeo1332

Mülmenstädt, J., Sourdeval, O., Delanoë, J., & Quaas, J. (2015). Frequency of occurrence of rain from liquid-, mixed-, and ice-phase clouds derived from A-Train satellite retrievals: RAIN FROM LIQUID- AND ICE-PHASE CLOUDS. *Geophysical Research Letters*, *42*(15), 6502–6509. https://doi.org/10.1002/2015GL064604

Murray, B. J., Carslaw, K. S., & Field, P. R. (2021). Opinion: Cloud-phase climate feedback and the importance of ice-nucleating particles. *Atmospheric Chemistry and Physics*, *21*(2), 665–679. https://doi.org/10.5194/acp-21-665-2021

Murray, B. J., O'Sullivan, D., Atkinson, J. D., & Webb, M. E. (2012). Ice nucleation by particles immersed in supercooled cloud droplets. *Chemical Society Reviews*, *41*(19), 6519. https://doi.org/10.1039/c2cs35200a

Nicolaus, M., Perovich, D. K., Spreen, G., Granskog, M. A., Von Albedyll, L., Angelopoulos, M., Anhaus, P., Arndt, S., Belter, H. J., Bessonov, V., Birnbaum, G., Brauchle, J., Calmer, R., Cardellach, E., Cheng, B., Clemens-Sewall, D., Dadic, R., Damm, E., De Boer, G., … Wendisch, M. (2022). Overview of the MOSAiC expedition: Snow and sea ice. *Elem Sci Anth*, *10*(1), 000046. https://doi.org/10.1525/elementa.2021.000046

Nielsen, D. M., Pieper, P., Barkhordarian, A., Overduin, P., Ilyina, T., Brovkin, V., Baehr, J., & Dobrynin, M. (2022). Increase in Arctic coastal erosion and its sensitivity to warming in the twenty-first century. *Nature Climate Change*, *12*(3), 263–270. https://doi.org/10.1038/s41558-022-01281-0

Niemand, M., Möhler, O., Vogel, B., Vogel, H., Hoose, C., Connolly, P., Klein, H., Bingemer, H., DeMott, P., Skrotzki, J., & Leisner, T. (2012). A Particle-Surface-Area-Based Parameterization of Immersion Freezing on Desert Dust Particles. *Journal of the Atmospheric Sciences*, *69*(10), 3077–3092. https://doi.org/10.1175/JAS-D-11-0249.1

Obu, J., Westermann, S., Bartsch, A., Berdnikov, N., Christiansen, H. H., Dashtseren, A., Delaloye, R., Elberling, B., Etzelmüller, B., Kholodov, A., Khomutov, A., Kääb, A., Leibman, M. O., Lewkowicz, A. G., Panda, S. K., Romanovsky, V., Way, R. G., Westergaard-Nielsen, A., Wu, T., … Zou, D. (2019). Northern Hemisphere permafrost

map based on TTOP modelling for 2000–2016 at 1 km2 scale. *Earth-Science Reviews*, *193*, 299–316. https://doi.org/10.1016/j.earscirev.2019.04.023

O′Sullivan, D., Murray, B. J., Ross, J. F., Whale, T. F., Price, H. C., Atkinson, J. D., Umo, N. S., & Webb, M. E. (2015). The relevance of nanoscale biological fragments for ice nucleation in clouds. *Scientific Reports*, *5*(1), 8082. https://doi.org/10.1038/srep08082

Ottoni, J. R., Oliveira, V. M. de, & Passarini, M. R. Z. (2022). Microbes in thawing permafrost: Contributions to climate change. In *Microbiome Under Changing Climate* (pp. 1–28). Elsevier. https://doi.org/10.1016/B978-0-323-90571-8.00001-8

Pady, S. M., & Kapica, L. (n.d.). *AIR-BORNE FUNGI IN THE ARCTIC AND OTHER PARTS OF CANADA*.

Parada, A. E., Needham, D. M., & Fuhrman, J. A. (2016). Every base matters: Assessing small subunit rRNA primers for marine microbiomes with mock communities, time series and global field samples: Primers for marine microbiome studies. *Environmental Microbiology*, *18*(5), 1403–1414. https://doi.org/10.1111/1462-2920.13023

Pedregosa, F., Varoquaux, G., Gramfort, A., Michel, V., Thirion, B., Grisel, O., Blondel, M., Prettenhofer, P., Weiss, R., Dubourg, V., Vanderplas, J., Passos, A., & Cournapeau, D. (2011). Scikit-learn: Machine Learning in Python. *MACHINE LEARNING IN PYTHON*.

Pereira Freitas, G., Adachi, K., Conen, F., Heslin-Rees, D., Krejci, R., Tobo, Y., Yttri, K. E., & Zieger, P. (2023). Regionally sourced bioaerosols drive high-temperature ice nucleating particles in the Arctic. *Nature Communications*, *14*(1), 5997. https://doi.org/10.1038/s41467-023-41696-7

Perkins, R. J., Gillette, S. M., Hill, T. C. J., & DeMott, P. J. (2020). The Labile Nature of Ice Nucleation by Arizona Test Dust. *ACS Earth and Space Chemistry*, *4*(1), 133–141. https://doi.org/10.1021/acsearthspacechem.9b00304

Philo, L. M., George, J. C., & Moulton. (1993). *The occurrence and description of anadromous fish in the Dease Inlet/Admiralty Bay*.

Pienitz, R., Smol, J. P., & Lean, D. R. S. (1997). *Physical and chemical limnology of 59 lakes located between the southern Yukon and the Tuktoyaktuk Peninsula, Northwest Territories (Canada)*. *54*, 17.

Pietsch, R. B., Grothe, H., Hanlon, R., Powers, C. W., Jung, S., Ross, S. D., & Schmale III, D. G. (2018). Wind-driven spume droplet production and the transport of *Pseudomonas syringae* from aquatic environments. *PeerJ*, *6*, e5663. https://doi.org/10.7717/peerj.5663

Polen, M., Brubaker, T., Somers, J., & Sullivan, R. C. (2018). Cleaning up our water: Reducing interferences from nonhomogeneous freezing of "pure" water in droplet freezing assays of ice-nucleating particles. *Atmospheric Measurement Techniques*, *11*(9), 5315–5334. https://doi.org/10.5194/amt-11-5315-2018

Pontes, A., Ruethi, J., Frey, B., Aires, A., Thomas, A., Overy, D., Halti, B., Kerr, R., & Sampaio, J. P. (2020). Cryolevonia gen. Nov. And Cryolevonia schafbergensis sp. Nov., a cryophilic yeast from ancient permafrost and melted sea ice. *International Journal of Systematic and Evolutionary Microbiology*, *70*(4), 2334–2338. https://doi.org/10.1099/ijsem.0.004040

Porter, G. C. E., Adams, M. P., Brooks, I. M., Ickes, L., Karlsson, L., Leck, C., Salter, M. E., Schmale, J., Siegel, K., Sikora, S. N. F., Tarn, M. D., Vüllers, J., Wernli, H., Zieger, P., Zinke, J., & Murray, B. J. (2022). Highly Active Ice-Nucleating Particles at the Summer

North Pole. *Journal of Geophysical Research: Atmospheres*, *127*(6). https://doi.org/10.1029/2021JD036059

Prenni, A. J., Harrington, J. Y., Tjernström, M., DeMott, P. J., Avramov, A., Long, C. N., Kreidenweis, S. M., Olsson, P. Q., & Verlinde, J. (2007). Can Ice-Nucleating Aerosols Affect Arctic Seasonal Climate? *Bulletin of the American Meteorological Society*, *88*(4), 541–550. https://doi.org/10.1175/BAMS-88-4-541

Previdi, M., Smith, K. L., & Polvani, L. M. (2021). Arctic amplification of climate change: A review of underlying mechanisms. *Environmental Research Letters*, *16*(9), 093003. https://doi.org/10.1088/1748-9326/ac1c29

Pummer, B. G., Bauer, H., Bernardi, J., Bleicher, S., & Grothe, H. (2012). Suspendable macromolecules are responsible for ice nucleation activity of birch and conifer pollen. *Atmospheric Chemistry and Physics*, *12*(5), 2541–2550. https://doi.org/10.5194/acp-12-2541-2012

Pummer, B. G., Budke, C., Augustin-Bauditz, S., Niedermeier, D., Felgitsch, L., Kampf, C. J., Huber, R. G., Liedl, K. R., Loerting, T., Moschen, T., Schauperl, M., Tollinger, M., Morris, C. E., Wex, H., Grothe, H., Pöschl, U., Koop, T., & Fröhlich-Nowoisky, J. (2015). Ice nucleation by water-soluble macromolecules. *Atmospheric Chemistry and Physics*, *15*(8), 4077–4091. https://doi.org/10.5194/acp-15-4077-2015

Pusz, W., & Urbaniak, J. (2021). Airborne fungi in Longyearbyen area (Svalbard, Norway)—Case study. *Environmental Monitoring and Assessment*, *193*(5), 290. https://doi.org/10.1007/s10661-021-09090-2

Quast, C., Pruesse, E., Yilmaz, P., Gerken, J., Schweer, T., Yarza, P., Peplies, J., & Glöckner, F. O. (2012). The SILVA ribosomal RNA gene database project: Improved data processing

and web-based tools. *Nucleic Acids Research*, *41*(D1), D590–D596. https://doi.org/10.1093/nar/gks1219

Rabe, B., Heuzé, C., Regnery, J., Aksenov, Y., Allerholt, J., Athanase, M., Bai, Y., Basque, C., Bauch, D., Baumann, T. M., Chen, D., Cole, S. T., Craw, L., Davies, A., Damm, E., Dethloff, K., Divine, D. V., Doglioni, F., Ebert, F., … Zhu, J. (2022). Overview of the MOSAiC expedition: Physical oceanography. *Elem Sci Anth*, *10*(1), 00062. https://doi.org/10.1525/elementa.2021.00062

Rantanen, M., Karpechko, A. Yu., Lipponen, A., Nordling, K., Hyvärinen, O., Ruosteenoja, K., Vihma, T., & Laaksonen, A. (2022). The Arctic has warmed nearly four times faster than the globe since 1979. *Communications Earth & Environment*, *3*(1), 168. https://doi.org/10.1038/s43247-022-00498-3

Raynolds, M. K., Walker, D. A., & Maier, H. A. (2006). *Alaska Arctic Tundra Vegetation Map* [Map]. U.S. Fish and Wildlife Service.

Ren, Z., Li, X., Zhang, C., Wang, Q., Fang, L., Cao, S., & Yu, J. (2022). From permafrost soil to thermokarst lake sediment: A view from C:N:P stoichiometry. *Frontiers in Environmental Science*, *10*, 986879. https://doi.org/10.3389/fenvs.2022.986879

Ren, Z., Zhang, C., Li, X., Ma, K., & Cui, B. (2022). Abundant and Rare Bacterial Taxa Structuring Differently in Sediment and Water in Thermokarst Lakes in the Yellow River Source Area, Qinghai-Tibet Plateau. *Frontiers in Microbiology*, *13*, 774514. https://doi.org/10.3389/fmicb.2022.774514

Rinke, A., Cassano, J. J., Cassano, E. N., Jaiser, R., & Handorf, D. (2021). Meteorological conditions during the MOSAiC expedition. *Elementa: Science of the Anthropocene*, *9*(1), 00023. https://doi.org/10.1525/elementa.2021.00023

Robeson, M. S., O'Rourke, D. R., Kaehler, B. D., Ziemski, M., Dillon, M. R., Foster, J. T., & Bokulich, N. A. (2020). *RESCRIPt: Reproducible sequence taxonomy reference database management for the masses* [Preprint]. Bioinformatics. https://doi.org/10.1101/2020.10.05.326504

Rogers, D. C., DeMott, P. J., & Kreidenweis, S. M. (2001). Airborne measurements of tropospheric ice-nucleating aerosol particles in the Arctic spring. *Journal of Geophysical Research: Atmospheres*, *106*(D14), 15053–15063. https://doi.org/10.1029/2000JD900790

Romanovsky, V. E. (2021). *Barrow 1 (N. Meadow Lake No.1 / NML-1)*. https://permafrost.gi.alaska.edu/site/br1

S. Ian Hartwell, Lomax, T., Dasher, D. H., Hoberg, M. K., Arny L. Blanchard, & Jewett, S. (2018). *Characterization of Benthic Habitats and Contaminant Assessment Arctic Lagoons and Estuaries*. https://doi.org/10.25923/A46E-TM48

Saliba, G., Chen, C.-L., Lewis, S., Russell, L. M., Rivellini, L.-H., Lee, A. K. Y., Quinn, P. K., Bates, T. S., Haëntjens, N., Boss, E. S., Karp-Boss, L., Baetge, N., Carlson, C. A., & Behrenfeld, M. J. (2019). Factors driving the seasonal and hourly variability of sea-spray aerosol number in the North Atlantic. *Proceedings of the National Academy of Sciences*, *116*(41), 20309–20314. https://doi.org/10.1073/pnas.1907574116

Salter, M. E., Nilsson, E. D., Butcher, A., & Bilde, M. (2014). On the seawater temperature dependence of the sea spray aerosol generated by a continuous plunging jet. *Journal of Geophysical Research: Atmospheres*, *119*(14), 9052–9072. https://doi.org/10.1002/2013JD021376

Sanchez, K. J., Roberts, G. C., Saliba, G., Russell, L. M., Twohy, C., Reeves, J. M., Humphries, R. S., Keywood, M. D., Ward, J. P., & McRobert, I. M. (2021). Measurement report:

Cloud processes and the transport of biological emissions affect southern ocean particle and cloud condensation nuclei concentrations. *Atmospheric Chemistry and Physics*, *21*(5), 3427–3446. https://doi.org/10.5194/acp-21-3427-2021

Šantl-Temkiv, T., Gosewinkel, U., Starnawski, P., Lever, M., & Finster, K. (2018). Aeolian dispersal of bacteria in southwest Greenland: Their sources, abundance, diversity and physiological states. *FEMS Microbiology Ecology*, *94*(4). https://doi.org/10.1093/femsec/fiy031

Šantl-Temkiv, T., Lange, R., Beddows, D., Rauter, U., Pilgaard, S., Dall'Osto, M., Gunde-Cimerman, N., Massling, A., & Wex, H. (2019). Biogenic Sources of Ice Nucleating Particles at the High Arctic Site Villum Research Station. *Environmental Science & Technology*, *53*(18), 10580–10590. https://doi.org/10.1021/acs.est.9b00991

Šantl-Temkiv, T., Sikoparija, B., Maki, T., Carotenuto, F., Amato, P., Yao, M., Morris, C. E., Schnell, R., Jaenicke, R., Pöhlker, C., DeMott, P. J., Hill, T. C. J., & Huffman, J. A. (2020). Bioaerosol field measurements: Challenges and perspectives in outdoor studies. *Aerosol Science and Technology*, *54*(5), 520–546. https://doi.org/10.1080/02786826.2019.1676395

Schiebel, T. (2017). *Ice Nucleation Activity of Soil Dust Aerosols*. Karlsruhe Institute of Technology.

Schmale, J., Sharma, S., Decesari, S., Pernov, J., Massling, A., Hansson, H.-C., Von Salzen, K., Skov, H., Andrews, E., Quinn, P. K., Upchurch, L. M., Eleftheriadis, K., Traversi, R., Gilardoni, S., Mazzola, M., Laing, J., & Hopke, P. (2022). Pan-Arctic seasonal cycles and long-term trends of aerosol properties from 10 observatories. *Atmospheric Chemistry and Physics*, *22*(5), 3067–3096. https://doi.org/10.5194/acp-22-3067-2022

Schmale, J., Zieger, P., & Ekman, A. M. L. (2021). Aerosols in current and future Arctic climate. *Nature Climate Change*, *11*(2), 95–105. https://doi.org/10.1038/s41558-020-00969-5

Schnell, R. C., & Vali, G. (1976). Biogenic Ice Nuclei: Part I. Terrestrial and Marine Sources. *Journal of the Atmospheric Sciences*, *33*(8), 1554–1564. https://doi.org/10.1175/1520-0469(1976)033<1554:BINPIT>2.0.CO;2

Schwidetzky, R., De Almeida Ribeiro, I., Bothen, N., Backes, A. T., DeVries, A. L., Bonn, M., Fröhlich-Nowoisky, J., Molinero, V., & Meister, K. (2023). Functional aggregation of cell-free proteins enables fungal ice nucleation. *Proceedings of the National Academy of Sciences*, *120*(46), e2303243120. https://doi.org/10.1073/pnas.2303243120

Sellegri, K., Harvey, M., Peltola, M., Saint-Macary, A., Barthelmeß, T., Rocco, M., Moore, K. A., Cristi, A., Peyrin, F., Barr, N., Labonnote, L., Marriner, A., McGregor, J., Safi, K., Deppeler, S., Archer, S., Dunne, E., Harnwell, J., Delanoe, J., … Law, C. S. (2023). Sea2Cloud: From Biogenic Emission Fluxes to Cloud Properties in the Southwest Pacific. *Bulletin of the American Meteorological Society*, *104*(5), E1017–E1043. https://doi.org/10.1175/BAMS-D-21-0063.1

Shakil, S., Tank, S. E., Kokelj, S. V., Vonk, J. E., & Zolkos, S. (2020). Particulate dominance of organic carbon mobilization from thaw slumps on the Peel Plateau, NT: Quantification and implications for stream systems and permafrost carbon release. *Environmental Research Letters*, *15*(11), 114019. https://doi.org/10.1088/1748-9326/abac36

Shannon, C. E. (1948). *A Mathematical Theory of Communication*. 55.

Shupe, M. D., & Intrieri, J. M. (2004). Cloud Radiative Forcing of the Arctic Surface: The Influence of Cloud Properties, Surface Albedo, and Solar Zenith Angle. *Journal of*

Climate, *17*(3), 616–628. https://doi.org/10.1175/1520-0442(2004)017<0616:CRFOTA>2.0.CO;2

Shupe, M. D., Matrosov, S. Y., & Uttal, T. (2006). Arctic Mixed-Phase Cloud Properties Derived from Surface-Based Sensors at SHEBA. *Journal of the Atmospheric Sciences*, *63*(2), 697–711. https://doi.org/10.1175/JAS3659.1

Shupe, M. D., Rex, M., Blomquist, B., Persson, P. O. G., Schmale, J., Uttal, T., Althausen, D., Angot, H., Archer, S., Bariteau, L., Beck, I., Bilberry, J., Bucci, S., Buck, C., Boyer, M., Brasseur, Z., Brooks, I. M., Calmer, R., Cassano, J., … Yue, F. (2022). Overview of the MOSAiC expedition: Atmosphere. *Elem Sci Anth*, *10*(1), 00060. https://doi.org/10.1525/elementa.2021.00060

Si, M., Irish, V. E., Mason, R. H., Vergara-Temprado, J., Hanna, S. J., Ladino, L. A., Yakobi-Hancock, J. D., Schiller, C. L., Wentzell, J. J. B., Abbatt, J. P. D., Carslaw, K. S., Murray, B. J., & Bertram, A. K. (2018). Ice-nucleating ability of aerosol particles and possible sources at three coastal marine sites. *Atmospheric Chemistry and Physics*, *18*(21), 15669–15685. https://doi.org/10.5194/acp-18-15669-2018

Slade, J. H., VanReken, T. M., Mwaniki, G. R., Bertman, S., Stirm, B., & Shepson, P. B. (2010). Aerosol production from the surface of the Great Lakes: GREAT LAKES AEROSOL PRODUCTION. *Geophysical Research Letters*, *37*(18), n/a-n/a. https://doi.org/10.1029/2010GL043852

Stopelli, E., Conen, F., Zimmermann, L., Alewell, C., & Morris, C. E. (2014). Freezing nucleation apparatus puts new slant on study of biological ice nucleators in precipitation. *Atmospheric Measurement Techniques*, *7*(1), 129–134. https://doi.org/10.5194/amt-7-129-2014

Streletskiy, D. A., Shiklomanov, N. I., Little, J. D., Nelson, F. E., Brown, J., Nyland, K. E., & Klene, A. E. (2017). Thaw Subsidence in Undisturbed Tundra Landscapes, Barrow, Alaska, 1962-2015: Barrow Subsidence. *Permafrost and Periglacial Processes*, *28*(3), 566–572. https://doi.org/10.1002/ppp.1918

Streletskiy, D., Anisimov, O., & Vasiliev, A. (2015). Permafrost Degradation. In *Snow and Ice-Related Hazards, Risks, and Disasters* (pp. 303–344). Elsevier. https://doi.org/10.1016/B978-0-12-394849-6.00010-X

Suski, K. J., Hill, T. C. J., Levin, E. J. T., Miller, A., DeMott, P. J., & Kreidenweis, S. M. (2018). Agricultural harvesting emissions of ice-nucleating particles. *Atmospheric Chemistry and Physics*, *18*(18), 13755–13771. https://doi.org/10.5194/acp-18-13755-2018

Sze, K. C. H., Wex, H., Hartmann, M., Skov, H., Massling, A., Villanueva, D., & Stratmann, F. (2023). Ice-nucleating particles in northern Greenland: Annual cycles, biological contribution and parameterizations. *Atmospheric Chemistry and Physics*, *23*(8), 4741–4761. https://doi.org/10.5194/acp-23-4741-2023

Tan, I., Barahona, D., & Coopman, Q. (2022). Potential Link Between Ice Nucleation and Climate Model Spread in Arctic Amplification. *Geophysical Research Letters*, *49*(4). https://doi.org/10.1029/2021GL097373

Tan, I., & Storelvmo, T. (2019). Evidence of Strong Contributions From Mixed-Phase Clouds to Arctic Climate Change. *Geophysical Research Letters*.

Taylor, P. C., Boeke, R. C., Li, Y., & Thompson, D. W. J. (2019). Arctic cloud annual cycle biases in climate models. *Atmospheric Chemistry and Physics*, *19*(13), 8759–8782. https://doi.org/10.5194/acp-19-8759-2019

Teeling, H., Fuchs, B. M., Bennke, C. M., Krüger, K., Chafee, M., Kappelmann, L., Reintjes, G., Waldmann, J., Quast, C., Glöckner, F. O., Lucas, J., Wichels, A., Gerdts, G., Wiltshire, K. H., & Amann, R. I. (2016). Recurring patterns in bacterioplankton dynamics during coastal spring algae blooms. *eLife*, *5*, e11888. https://doi.org/10.7554/eLife.11888

Testa, B., Hill, T. C. J., Marsden, N. A., Barry, K. R., Hume, C. C., Bian, Q., Uetake, J., Hare, H., Perkins, R. J., Möhler, O., Kreidenweis, S. M., & DeMott, P. J. (2021). Ice Nucleating Particle Connections to Regional Argentinian Land Surface Emissions and Weather During the Cloud, Aerosol, and Complex Terrain Interactions Experiment. *Journal of Geophysical Research: Atmospheres*, *126*(23). https://doi.org/10.1029/2021JD035186

Thiele, S., Vader, A., Thomson, S., Saubrekka, K., Petelenz, E., Armo, H. R., Müller, O., Olsen, L., Bratbak, G., & Øvreås, L. (2023). The summer bacterial and archaeal community composition of the northern Barents Sea. *Progress in Oceanography*, *215*, 103054. https://doi.org/10.1016/j.pocean.2023.103054

Thompson, L. R., Sanders, J. G., McDonald, D., Amir, A., Ladau, J., Locey, K. J., Prill, R. J., Tripathi, A., Gibbons, S. M., Ackermann, G., Navas-Molina, J. A., Janssen, S., Kopylova, E., Vázquez-Baeza, Y., González, A., Morton, J. T., Mirarab, S., Zech Xu, Z., Jiang, L., … Zhao, H. (2017). A communal catalogue reveals Earth's multiscale microbial diversity. *Nature*, *551*(7681), 457–463. https://doi.org/10.1038/nature24621

Tignat-Perrier, R., Dommergue, A., Thollot, A., Keuschnig, C., Magand, O., Vogel, T. M., & Larose, C. (2019). Global airborne microbial communities controlled by surrounding landscapes and wind conditions. *Scientific Reports*, *9*(1), 14441. https://doi.org/10.1038/s41598-019-51073-4

Tobo, Y. (2016). An improved approach for measuring immersion freezing in large droplets over a wide temperature range. *Scientific Reports*, *6*(1), 32930. https://doi.org/10.1038/srep32930

Tobo, Y., Adachi, K., DeMott, P. J., Hill, T. C. J., Hamilton, D. S., Mahowald, N. M., Nagatsuka, N., Ohata, S., Uetake, J., Kondo, Y., & Koike, M. (2019). Glacially sourced dust as a potentially significant source of ice nucleating particles. *Nature Geoscience*, *12*(4), 253–258. https://doi.org/10.1038/s41561-019-0314-x

Tobo, Y., DeMott, P. J., Hill, T. C. J., Prenni, A. J., Swoboda-Colberg, N. G., Franc, G. D., & Kreidenweis, S. M. (2014). Organic matter matters for ice nuclei of agricultural soil origin. *Atmospheric Chemistry and Physics*, *14*(16), 8521–8531. https://doi.org/10.5194/acp-14-8521-2014

Uetake, J., Hill, T. C. J., Moore, K. A., DeMott, P. J., Protat, A., & Kreidenweis, S. M. (2020). Airborne bacteria confirm the pristine nature of the Southern Ocean boundary layer. *Proceedings of the National Academy of Sciences*, *117*(24), 13275–13282. https://doi.org/10.1073/pnas.2000134117

Ullrich, R., Hoose, C., Möhler, O., Niemand, M., Wagner, R., Höhler, K., Hiranuma, N., Saathoff, H., & Leisner, T. (2017). A New Ice Nucleation Active Site Parameterization for Desert Dust and Soot. *Journal of the Atmospheric Sciences*, *74*(3), 699–717. https://doi.org/10.1175/JAS-D-16-0074.1

Vali, G. (1971). Quantitative evaluation of experimental results and the heterogeneous freezing nucleation of super cooled liquids. *Journal of the Atmospheric Sciences*, *28*, 402–409. https://doi.org/10.1175/1520-0469(1971)028<0402:QEOERA>2.0.CO;2

Vaulot, D., Del Campo, J., Burki, F., Jamy, M., Guillou, L., Santoferrara, L., Ganser, M., de Oliveira da Rocha Franco, A., Mertens, K., Gu, H., Hyeon Jang, S., Škaloud, P., Dünn, M., Gross, M., Seliuk, A., Sandin, M., Metz, S., Fiore-Donno, A. M., & Dorrell, R. (2023). *PR2 version 5.0.0* [dataset]. https://doi.org/10.5281/zenodo.7805244

Walter, K. M., Zimov, S. A., Chanton, J. P., Verbyla, D., & Chapin, F. S. (2006). Methane bubbling from Siberian thaw lakes as a positive feedback to climate warming. *Nature*, *443*(7107), 71–75. https://doi.org/10.1038/nature05040

Walters, W., Hyde, E. R., Berg-Lyons, D., Ackermann, G., Humphrey, G., Parada, A., Gilbert, J. A., Jansson, J. K., Caporaso, J. G., Fuhrman, J. A., Apprill, A., & Knight, R. (2016). Improved Bacterial 16S rRNA Gene (V4 and V4-5) and Fungal Internal Transcribed Spacer Marker Gene Primers for Microbial Community Surveys. *mSystems*, *1*(1), e00009-15. https://doi.org/10.1128/mSystems.00009-15

Wex, H., Huang, L., Zhang, W., Hung, H., Traversi, R., Becagli, S., Sheesley, R. J., Moffett, C. E., Barrett, T. E., Bossi, R., Skov, H., Hünerbein, A., Lubitz, J., Löffler, M., Linke, O., Hartmann, M., Herenz, P., & Stratmann, F. (2019). Annual variability of ice-nucleating particle concentrations at different Arctic locations. *Atmospheric Chemistry and Physics*, *19*(7), 5293–5311. https://doi.org/10.5194/acp-19-5293-2019

Wilson, T. W., Ladino, L. A., Alpert, P. A., Breckels, M. N., Brooks, I. M., Browse, J., Burrows, S. M., Carslaw, K. S., Huffman, J. A., Judd, C., Kilthau, W. P., Mason, R. H., McFiggans, G., Miller, L. A., Nájera, J. J., Polishchuk, E., Rae, S., Schiller, C. L., Si, M., … Murray, B. J. (2015). A marine biogenic source of atmospheric ice-nucleating particles. *Nature*, *525*(7568), 234–238. https://doi.org/10.1038/nature14986

Yang, H., Yan, R., Chen, H., Lee, D. H., & Zheng, C. (2007). Characteristics of hemicellulose, cellulose and lignin pyrolysis. *Fuel*, *86*(12–13), 1781–1788. https://doi.org/10.1016/j.fuel.2006.12.013

Yang, J. (2004). Storm-driven mixing and potential impact on the Arctic Ocean. *Journal of Geophysical Research*, *109*(C4), C04008. https://doi.org/10.1029/2001JC001248

Zaragotas, D., Liolios, N. T., & Anastassopoulos, E. (2016). Supercooling, ice nucleation and crystal growth: A systematic study in plant samples. *Cryobiology*, *72*(3), 239–243. https://doi.org/10.1016/j.cryobiol.2016.03.012

Zhou, L., Zhou, Y., Yao, X., Cai, J., Liu, X., Tang, X., Zhang, Y., Jang, K.-S., & Jeppesen, E. (2020). Decreasing diversity of rare bacterial subcommunities relates to dissolved organic matter along permafrost thawing gradients. *Environment International*, *134*, 105330. https://doi.org/10.1016/j.envint.2019.105330

Zinke, J., Nilsson, E. D., Zieger, P., & Salter, M. E. (2022). The Effect of Seawater Salinity and Seawater Temperature on Sea Salt Aerosol Production. *Journal of Geophysical Research: Atmospheres*, *127*(16). https://doi.org/10.1029/2021JD036005

A.1 Appendix for Chapter 2

Text A.1

The laboratory analysis methods are inherently different, as the DRUM samples are analyzed with the cold plate, while the polycarbonate filters are analyzed with the IS. The cold plate uses 100-2.5 µL drops laid out on a petroleum jelly covered copper plate, and cools at a variable rate, while the IS uses 32-50 µL drops (plus corresponding dilutions) in PCR trays, and cools at a constant rate. Yet, the methods used to analyze two water samples collected during MOSAiC produced data that agree well (Fig. A.1.3). A variable cooling rate, both within running a particular sample, and as a function of the time of year (when sample stages were not necessarily run on the same day) may have been a large factor (Fig. A.1.4). In early 2021, many other instruments were running in the laboratory, raising the ambient temperature and causing the cold plate (CP) to cool slowly. A liquid nitrogen dewar was placed near the Peltier cooling system in mid-February and by mid-March, the instrument was placed in a different space for the duration of the processed samples, generally kept between 15 and 18 °C. The cooling rate for all samples run on the CP varied between 0.036 and 7.70 °C min^{-1}.

Other potential factors for disagreement involve the collection time, as the polycarbonate filters were generally run for 72 hours, while the DRUM samples were run for 24 hours, and from the fact that the DRUM was sampling off of an inlet, while the polycarbonate filters did not. This difference is explored in Figure A.1.7, where a DRUM sample from within the same period as the polycarbonate filter collection were both run on the IS. The DRUM did not see the high concentrations that the polycarbonate filter saw (1.4 vs. 0.059 L^{-1} at -15 °C), but the underlying INP-temperature spectra are similar, with nearly identical freezing onsets. A nearby time period DRUM sample analyzed on the CP (July 2-3) only saw $1.1*10^{-3}$ L^{-1} at -15 °C. This

implies that there are periods where the DRUM is not efficiently collecting all particles due to inlet transmission efficiencies (see Creamean et al., 2022), or that particles are not always efficiently released from the substrate into liquid for analysis. For July 3-6, the period with the largest INP concentrations observed, 60% of the particles were larger than 1 µm at -15 °C (Fig. A.1.5), but this does not explain the entire discrepancy.

In conclusion, there are several potential reasons for the discrepancies: DRUM and polycarbonate sampling differences, ineffective substrate particle release, and variable cooling rates for the processed samples. Influences of these different factors may also change as a function of different seasonal airmasses, as different populations of INPs will be present. At this time, it cannot be advised to use the insensitive seasonal trend observed at colder temperatures measured with the DRUM and CP (including and below -20 °C), whereas at warmer temperatures, the general trends are similar to the polycarbonate filters. The average concentrations that were 1-3 orders of magnitude lower with the DRUM and CP versus the polycarbonate and IS is also concerning but are not able to be fully resolved here.

Table A.1.1: List of all potential source samples sequenced with Type (FT=Flowthrough seawater samples; CTD=seawater samples collected on a Conductivity, Temperature, and Depth rosette; SW=Surface or lead seawater samples; MP=Melt pond freshwater samples); Source tracking category; Collection date in UTC (12:00 given if no specific time recorded); Collection latitude in degrees, Collection longitude in degrees; and approximate collection depth in meters.

Type	Source Tracking Category	Collection Date (UTC)	Latitude (°)	Longitude (°)	Depth (m)
FT	Seawater	11/14/2019 6:30	86.188309	118.416527	11
CTD	Seawater	11/14/2019 12:00	86.153053	118.109711	100
CTD	Seawater	11/14/2019 12:00	86.153053	118.109711	10
CTD	Seawater	11/14/2019 12:00	86.153053	118.109711	200
CTD	Seawater	11/14/2019 12:00	86.153053	118.109711	20
CTD	Seawater	11/14/2019 12:00	86.153053	118.109711	2
FT	Seawater	11/14/2019 12:00	86.174263	118.245308	11
Ice	Ice-Melt Pond	11/18/2019 12:00	85.849571	120.581451	Bottom 0-5 cm
Ice	Ice-Melt Pond	11/18/2019 12:00	85.849571	120.581451	Bottom 5-10 cm
Snow	Snow	11/18/2019 12:00	85.849571	120.581451	0
SW	Seawater	11/18/2019 12:00	85.849571	120.581451	0

CTD	Seawater	12/6/2019 12:00	86.140556	122.196701	10
FT	Seawater	12/7/2019 10:00	86.161652	122.141006	11
FT	Seawater	12/9/2019 9:30	86.40139	120.931358	11
CTD	Seawater	1/23/2020 12:00	87.446587	94.088547	100
CTD	Seawater	1/23/2020 12:00	87.446587	94.088547	10
CTD	Seawater	1/23/2020 12:00	87.446587	94.088547	200
CTD	Seawater	1/23/2020 12:00	87.446587	94.088547	20
CTD	Seawater	1/23/2020 12:00	87.446587	94.088547	2
CTD	Seawater	1/23/2020 12:00	87.446587	94.088547	50
CTD	Seawater	1/23/2020 12:00	87.446587	94.088547	75
Snow	Snow	1/27/2020 12:00	87.445847	95.670288	0
SW	Seawater	1/27/2020 12:00	87.445847	95.670288	0
FT	Seawater	3/19/2020 19:38	86.46608	13.94327	11
FT	Seawater	3/20/2020 11:57	86.330116	14.79105	11
FT	Seawater	3/21/2020 18:42	86.246986	15.42696	11
FT	Seawater	4/7/2020 14:58	84.496758	14.54986	11
CTD	Seawater	4/17/2020 12:00	84.409119	13.65277	20
FT	Seawater	4/17/2020 18:58	84.428001	13.76142	11
CTD	Seawater	4/18/2020 12:00	84.409119	13.65277	2
FT	Seawater	5/1/2020 17:30	83.922569	17.61512	11
Ice	Ice-Melt Pond	5/4/2020 12:00	83.886208	18.24058	Top 0-10 cm
Ice	Ice-Melt Pond	5/4/2020 12:00	83.886009	18.314541	Top 30-40 cm
Snow	Snow	5/4/2020 12:00	83.886208	18.24058	0
SW	Seawater	5/4/2020 12:00	83.886208	18.24058	0
FT	Seawater	5/15/2020 16:30	83.392342	9.17819	11
FT	Seawater	6/15/2020 19:10	82.21862	8.21006	11
CTD	Seawater	6/27/2020 12:00	81.955391	9.90316	100
CTD	Seawater	6/27/2020 12:00	81.955391	9.90316	10
CTD	Seawater	6/27/2020 12:00	81.955391	9.90316	2
CTD	Seawater	6/27/2020 12:00	81.955391	9.90316	50
CTD	Seawater	6/27/2020 12:00	81.955391	9.90316	NA
CTD	Seawater	6/27/2020 12:00	81.955391	9.90316	150
FT	Seawater	6/27/2020 16:30	81.918716	9.77096	11
Ice	Ice-Melt Pond	6/30/2020 12:00	81.783981	8.94839	Bottom 0-5 cm
Ice	Ice-Melt Pond	6/30/2020 12:00	81.783981	8.94839	Bottom 5-10 cm
MP	Ice-Melt Pond	7/2/2020 12:00	NA	NA	0
MP	Ice-Melt Pond	7/4/2020 12:00	NA	NA	0
Ice	Ice-Melt Pond	7/6/2020 12:00	81.674088	5.19019	NA
Ice	Ice-Melt Pond	7/6/2020 12:00	81.673447	5.17166	Bottom 5-10 cm
Ice	Ice-Melt Pond	7/6/2020 12:00	81.673447	5.17166	Bottom 0-5 cm
MP	Ice-Melt Pond	7/7/2020 12:00	NA	NA	0
MP	Ice-Melt Pond	7/11/2020 12:00	NA	NA	0
MP	Ice-Melt Pond	7/13/2020 12:00	NA	NA	0

FT	Seawater	7/13/2020 21:02	81.406662	0.25795	11
CTD	Seawater	7/16/2020 12:00	81.230972	0.2981	2
CTD	Seawater	7/16/2020 12:00	81.230972	0.2981	11
MP	Ice-Melt Pond	7/16/2020 12:00	NA	NA	0
MP	Ice-Melt Pond	7/20/2020 12:00	NA	NA	0
MP	Ice-Melt Pond	7/23/2020 12:00	NA	NA	0
MP	Ice-Melt Pond	7/28/2020 12:00	NA	NA	0
Lead Ice	Ice-Melt Pond	8/30/2020 12:00	NA	NA	0
SW	Seawater	8/30/2020 12:00	NA	NA	0
CTD	Seawater	9/3/2020 12:00	88.560738	119.60759	100
CTD	Seawater	9/3/2020 12:00	88.560738	119.60759	10
CTD	Seawater	9/3/2020 12:00	88.560738	119.60759	200
CTD	Seawater	9/3/2020 12:00	88.560738	119.60759	2
CTD	Seawater	9/3/2020 12:00	88.560738	119.60759	50
CTD	Seawater	9/3/2020 12:00	88.560738	119.60759	20
FT	Seawater	9/3/2020 12:23	88.602692	120.106117	11
Lead Ice	Ice-Melt Pond	9/5/2020 12:00	NA	NA	0
Snow	Snow	9/5/2020 12:00	NA	NA	0
Ice	Ice-Melt Pond	9/7/2020 12:00	88.72242	112.05928	Top 0-10 cm
Ice	Ice-Melt Pond	9/7/2020 12:00	88.72242	112.05928	Top 10-20 cm
FT	Seawater	9/7/2020 13:30	88.688126	111.565254	11
FT	Seawater	10/2/2020 12:00	NA	NA	11

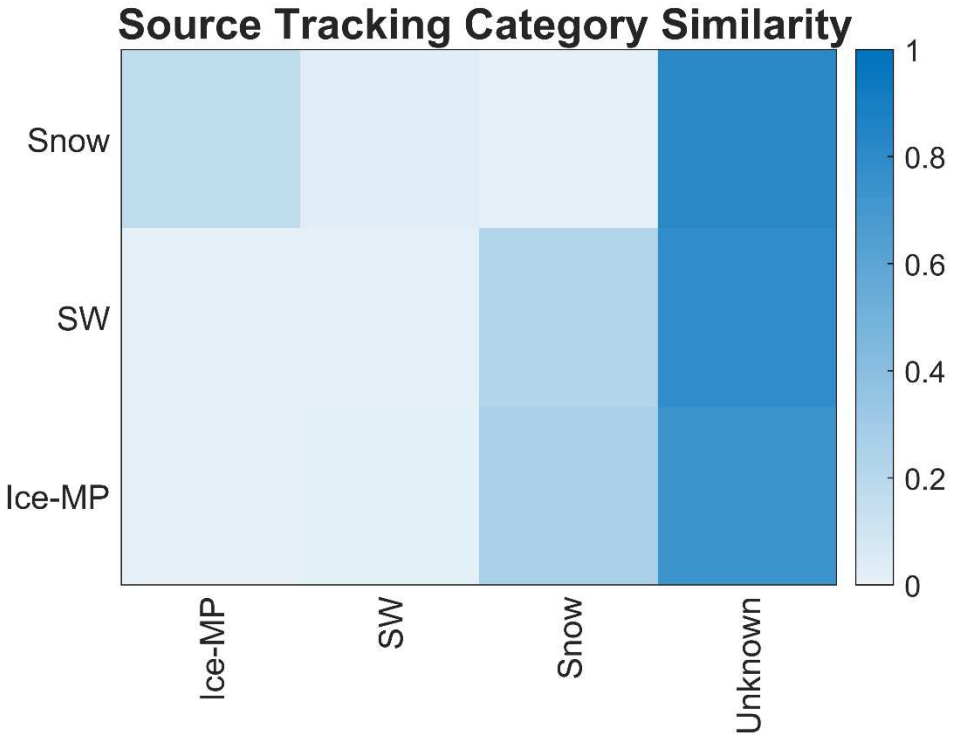

Figure A.1.1: Source tracking categories heatmap, using the leave-one-out option, that predicts the grouping (x-axis) based on the feature abundance of samples (y-axis). (SW=Seawater; MP=Melt Pond). Corresponding categories (e.g., Snow and Snow) are given 0.

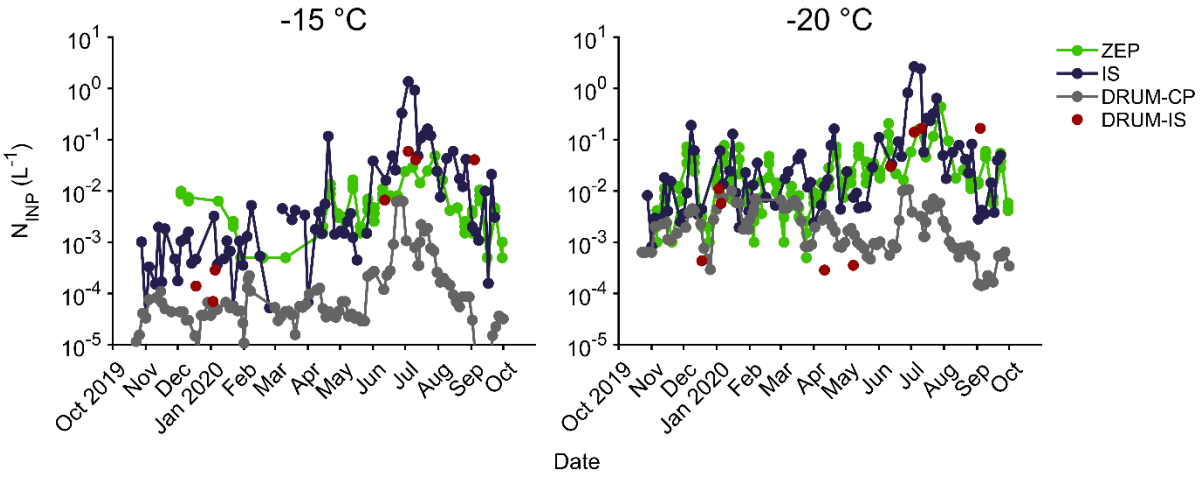

Figure A.1.2: INP concentration time series during the MOSAiC campaign at -15 °C (left) and -20 °C (right). ZEP (green) refers to data take at Zeppelin Observatory at Svalbard (Pereira Freitas et al., 2023); IS (blue) refers to filter samples analyzed with the Ice Spectrometer; DRUM-CP (gray) refers to the total DRUM samples analyzed on the cold plate; and DRUM-IS (red) refers to select total DRUM samples analyzed on the Ice Spectrometer.

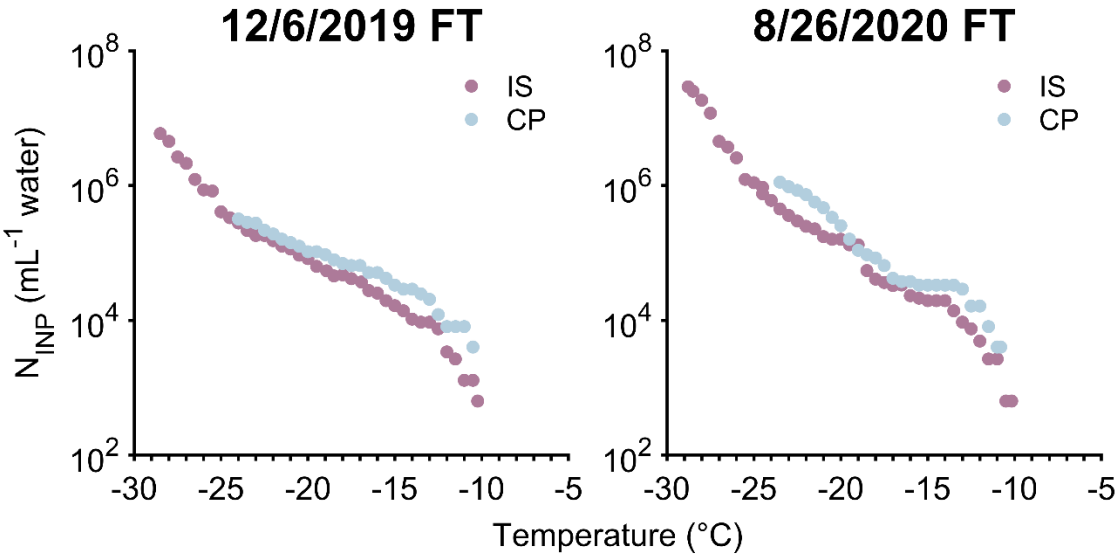

Figure A.1.3: Comparison of the same samples, Flowthrough water collected during MOSAiC, analyzed on the Ice Spectrometer (IS: purple) and Cold Plate (CP: Blue).

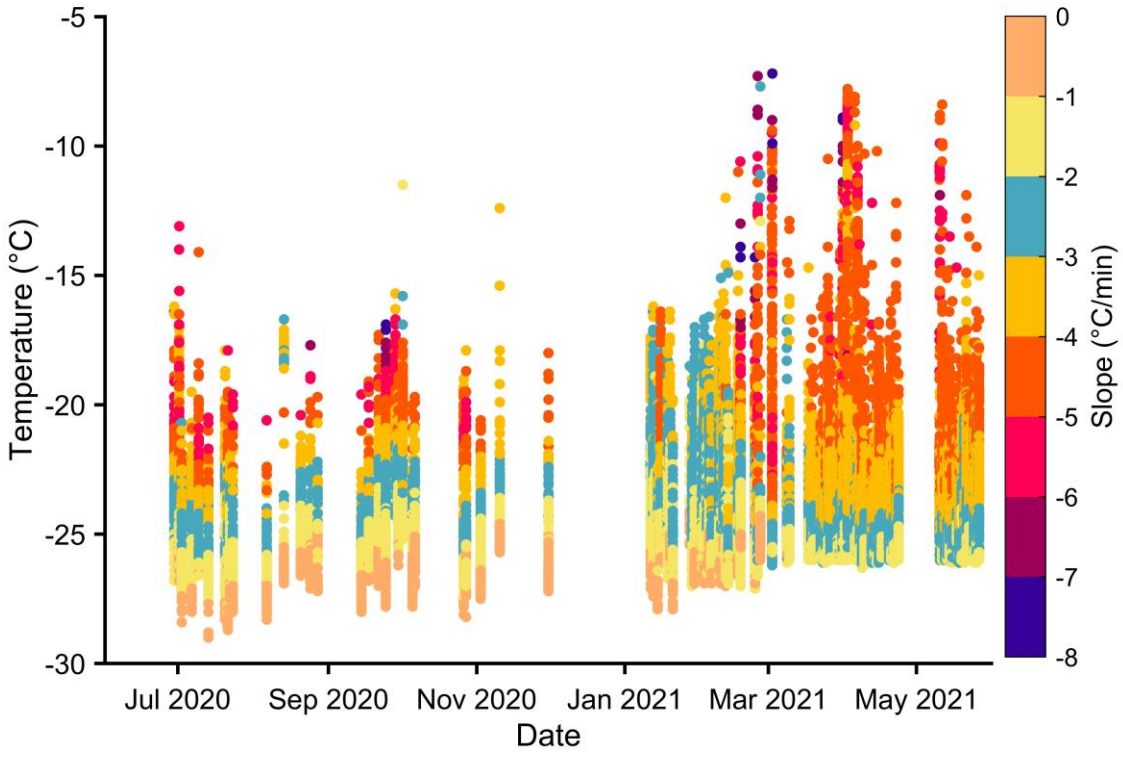

Figure A.1.4: Time series of the cooling rate of all the DRUM samples processed on the Cold Plate. Each dot represents a frozen drop and is colored by the corresponding cooling rate at the time of the manually detected freezing. Multiple samples and stages were ran on the same day, which is why there are overlapping points on the same day.

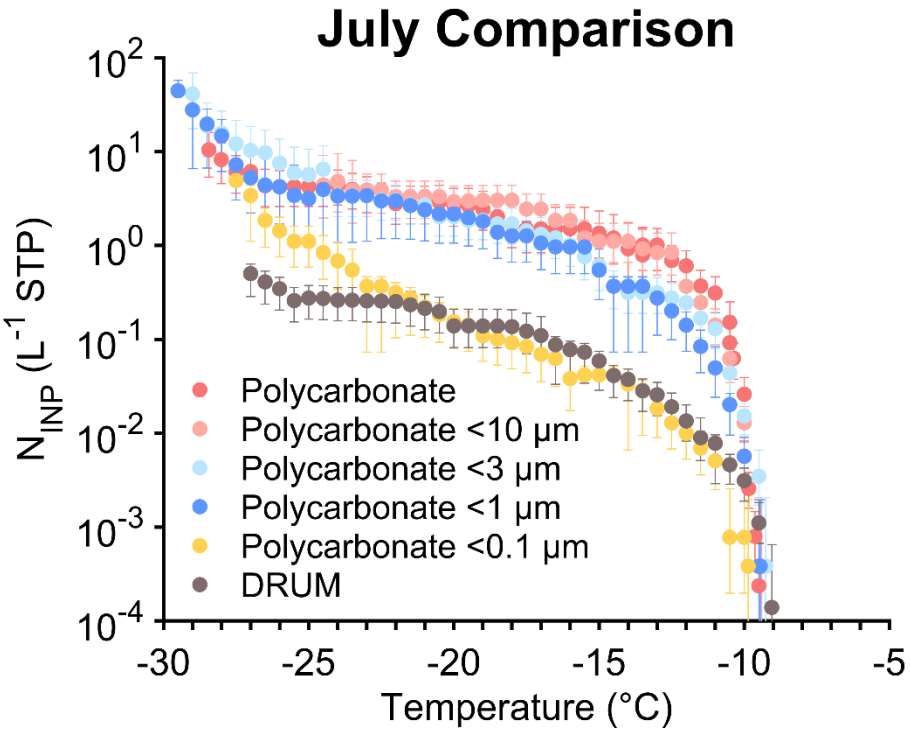

Figure A.1.5: Size filtering results for the July 3-6 polycarbonate filter and comparison to the July 4-5 DRUM sample (all stages combined), both run on the Ice Spectrometer (IS).

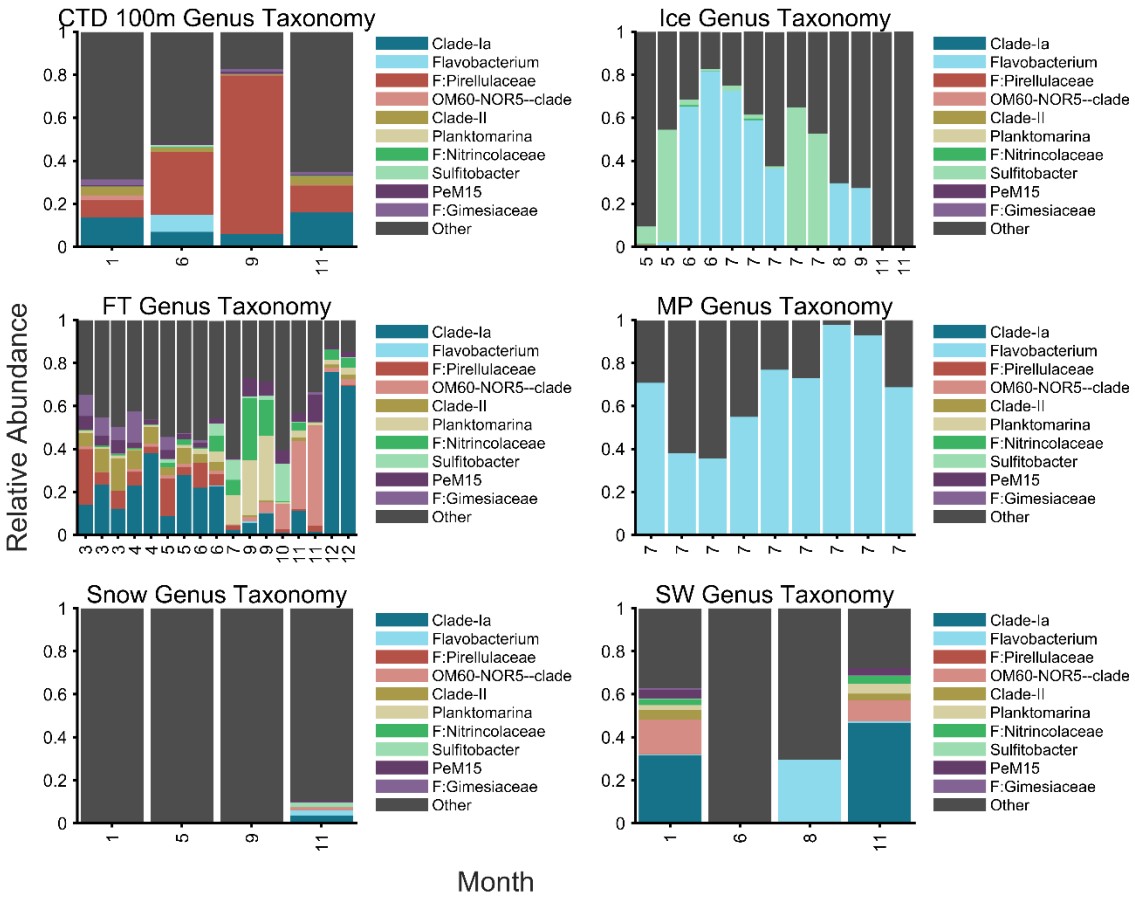

Figure A.1.6: Bacterial genus level relative abundance taxonomy for the different potential sources as a function of month collected. FT=Flowthrough; MP=Melt pond; SW=Lead water. The samples are colored by the top 10 genera for all sources combined.

A.2 Appendix for Chapter 3

Table A.2.1 Recipe used to make up the artificial freshwater for the tank experiments. Concentrations are given in millimolar (mM) as well as the total grams added to the 4 L of water in the tank.

	mM	g in 4L
$NaHCO_3$	0.6	0.202
$CaCO_3$	0.5	0.200
$MgCl_2$	0.3	0.244
K_2SO_4	0.03	0.0209

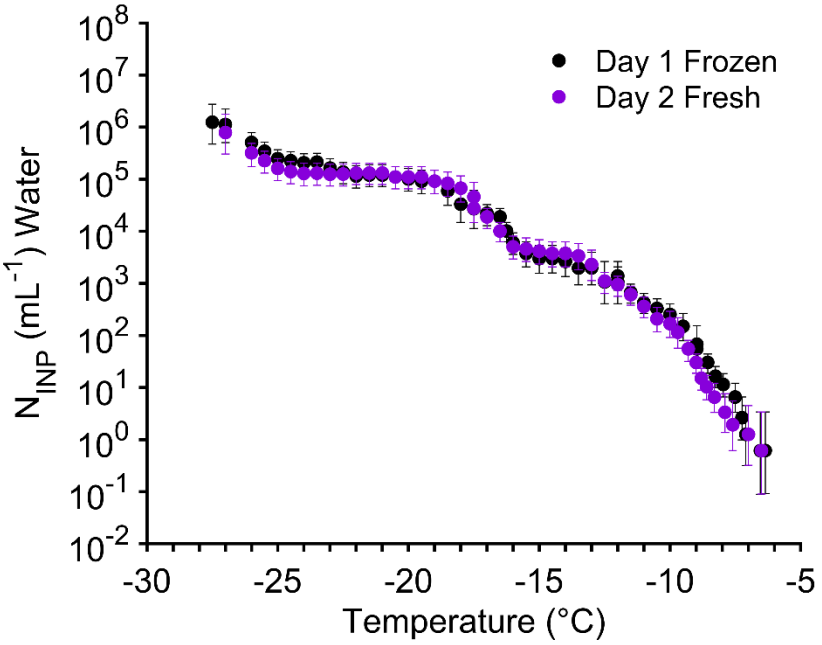

Figure A.2.1. Ice-nucleating particle (INP) temperature spectra for the 1000-year-old (S69CM) permafrost core experiment, which shows no difference in concentration in fresh or frozen samples (1 day after thawing).

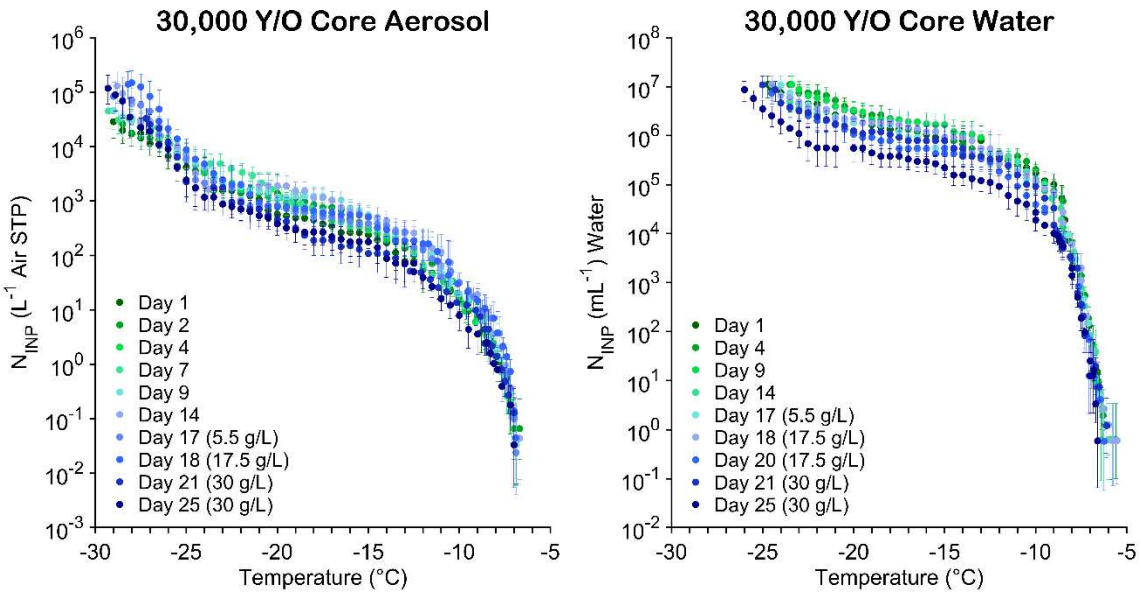

Figure A.2.2. Ice-nucleating particle (INP) temperature spectra for the 30,000-year-old (OT83L) permafrost core experiment. The aerosol is plotted on the left and water on the right. Points are colored by day of experiment. Salinity of tank water is listed in g/L in the legend starting at day 17, when artificial sea salts were added to the tank.

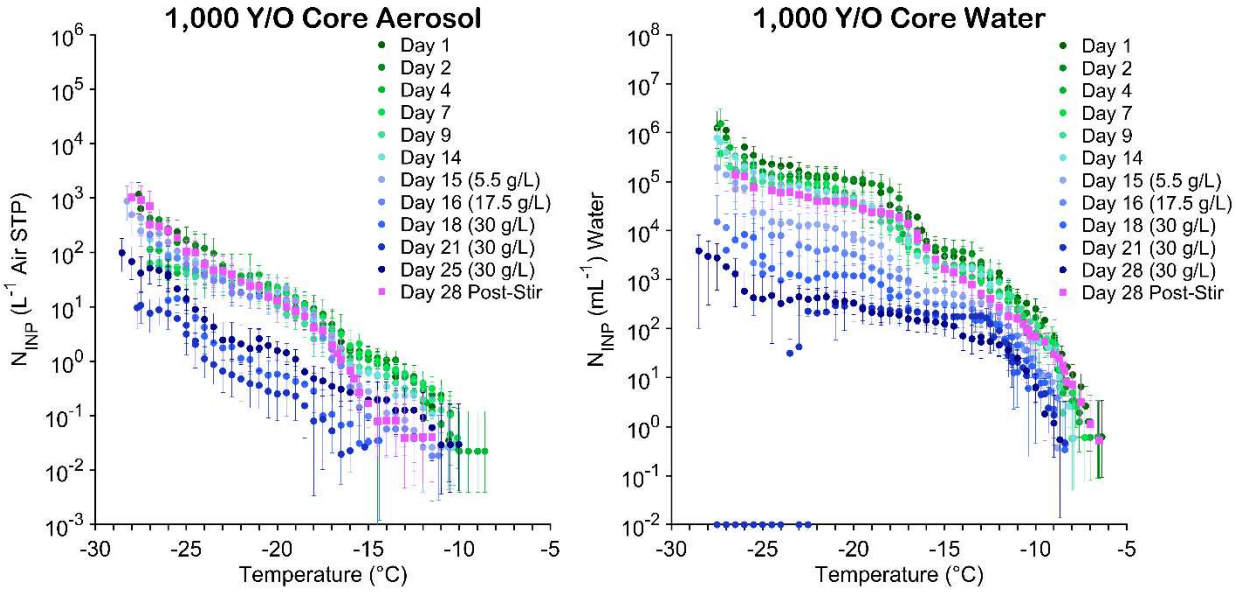

Figure A.2.3. Ice-nucleating particle (INP) temperature spectra for the 1000-year-old (S69CM) permafrost core experiment. The aerosol is plotted on the left and water on the right. Points are colored by day of experiment. Day 28 post-stir tests are given in pink squares. Salinity of tank water is listed in g/L in the legend starting at day 15, when artificial sea salts were added to the tank.

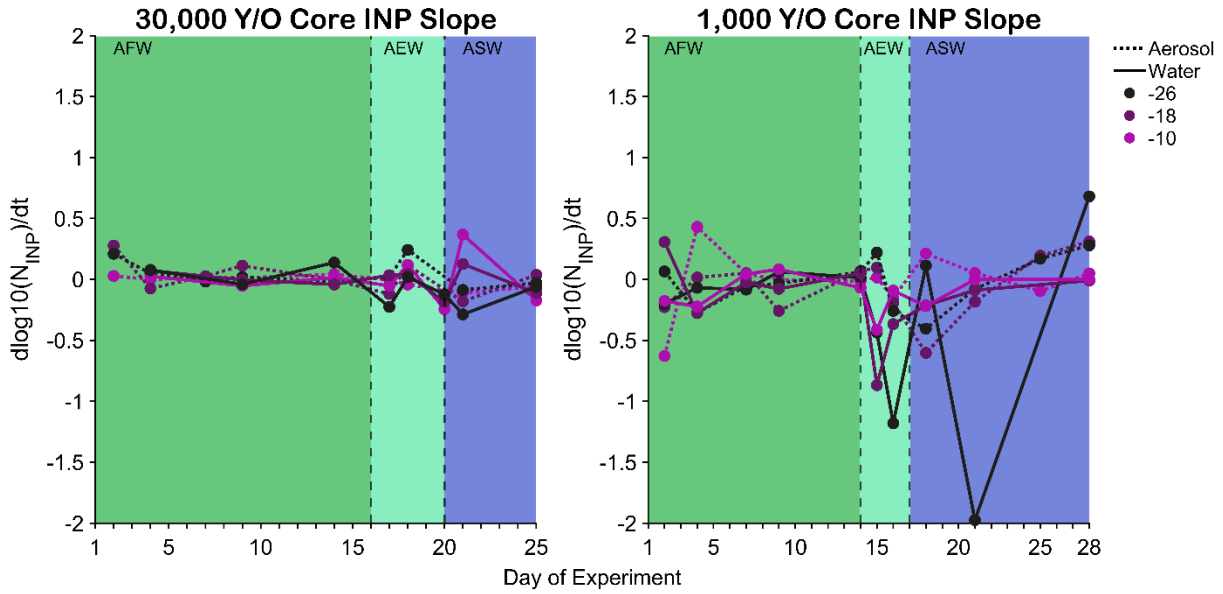

Figure A.2.4. The slope of the ice-nucleating particle (INP) concentrations for the aerosol (dotted lines) and water (solid lines) as a function of experiment day for T=-26 (black), -18 (purple), and -10 °C (magenta). The 30,000-year-old (OT83L) permafrost core experiment is plotted on the left and the 1000-year-old (S69CM) permafrost core experiment on the right. Background shading denotes salinity transitions (AFW=artificial freshwater; AEW=artificial estuary water; ASW=artificial seawater).

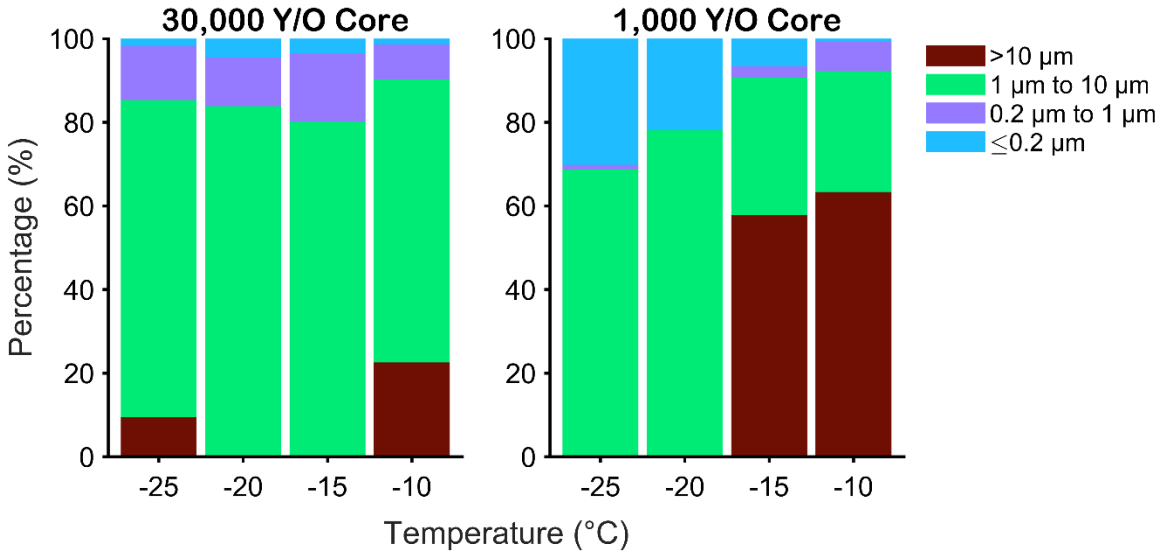

Figure A.2.5. Day 1 water ice-nucleating particle (INP) size histograms for the 30,000-year-old (OT83L: left) and 1000-year-old (S69CM: right) permafrost core experiments. The color denotes the size range of the INPs in each temperature bin.

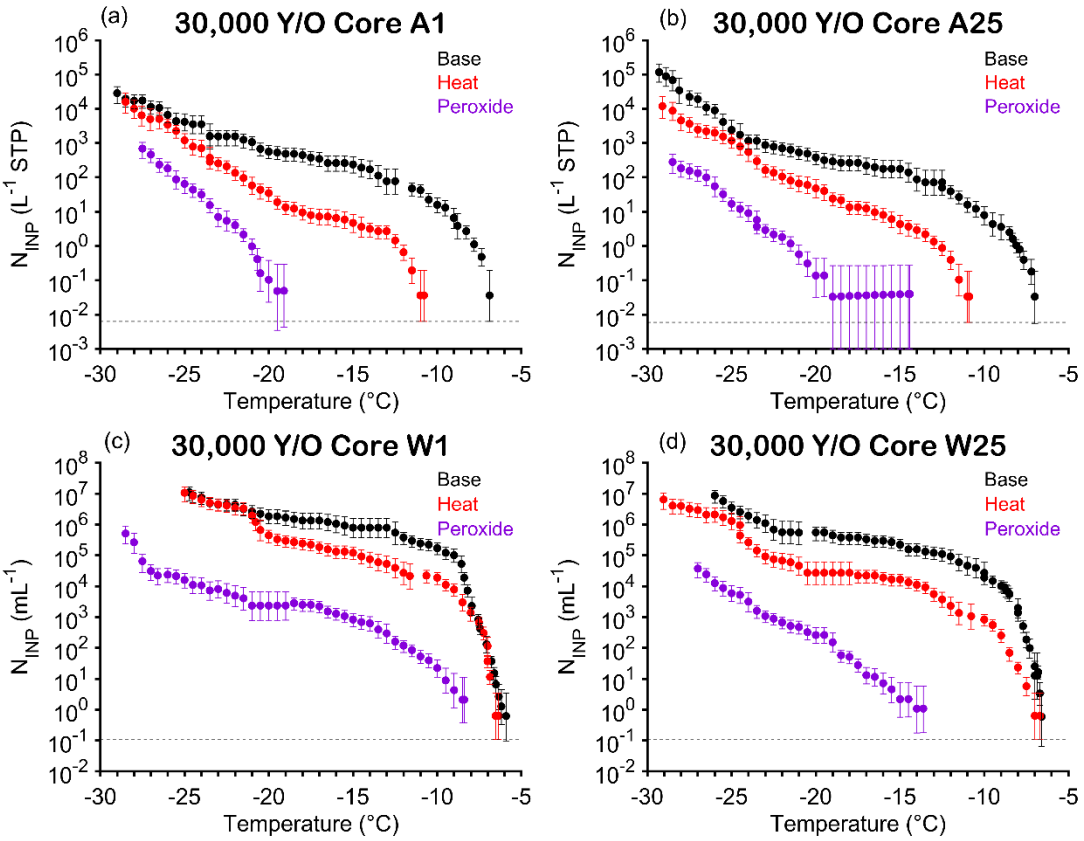

Figure A.2.6. Ice-nucleating particle (INP) treatment temperature spectra for the 30,000-year-old (OT83L) permafrost core experiment. Aerosol is given in panels a-b and water in panels c-d. Day 1 spectra are shown in panels a,c and day 25 spectra in panels b,d. Black denotes the untreated spectra, red denotes heat treated spectra, and purple is the peroxide digested spectra.

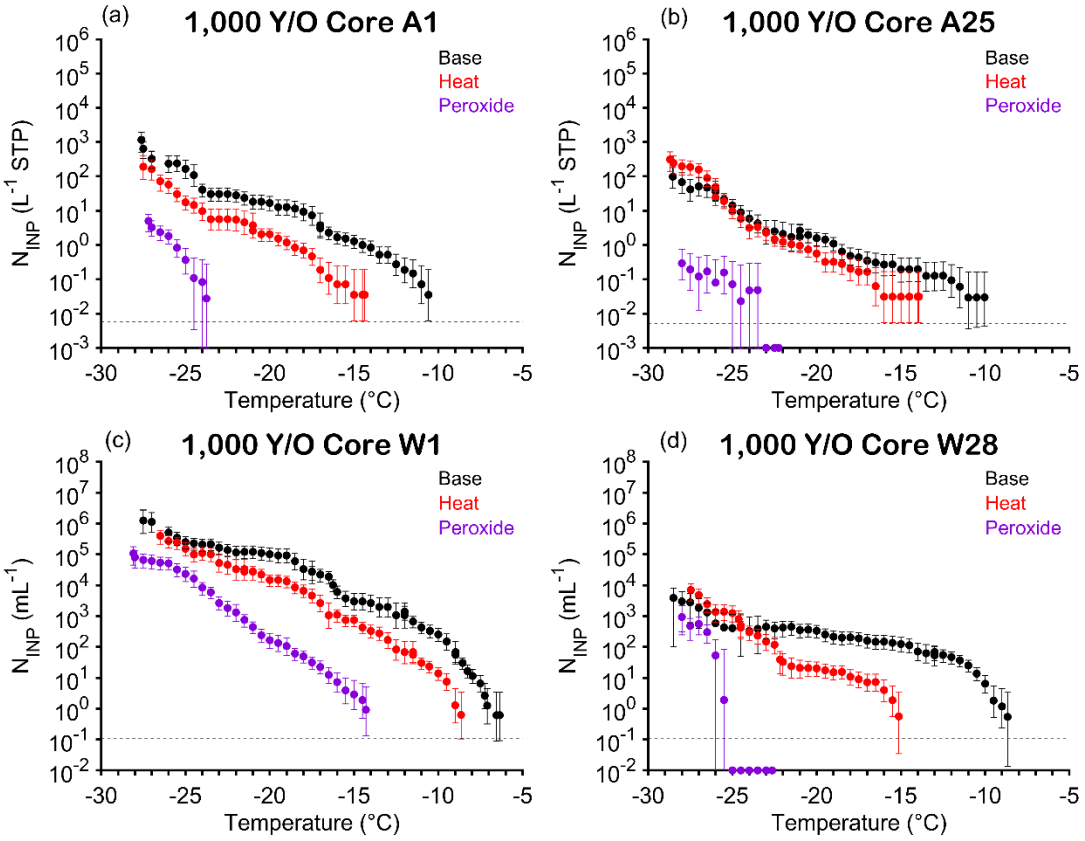

Figure A.2.7. Ice-nucleating particle (INP) treatment temperature spectra for the 1000-year-old (S69CM) permafrost core experiment. Aerosol is given in panels a-b and water in panels c-d. Day 1 spectra are shown in panels a,c, day 25 aerosol spectra in b, and day 28 water spectra in panel d. Black denotes the untreated spectra, red denotes heat treated spectra, and purple is the peroxide digested spectra.

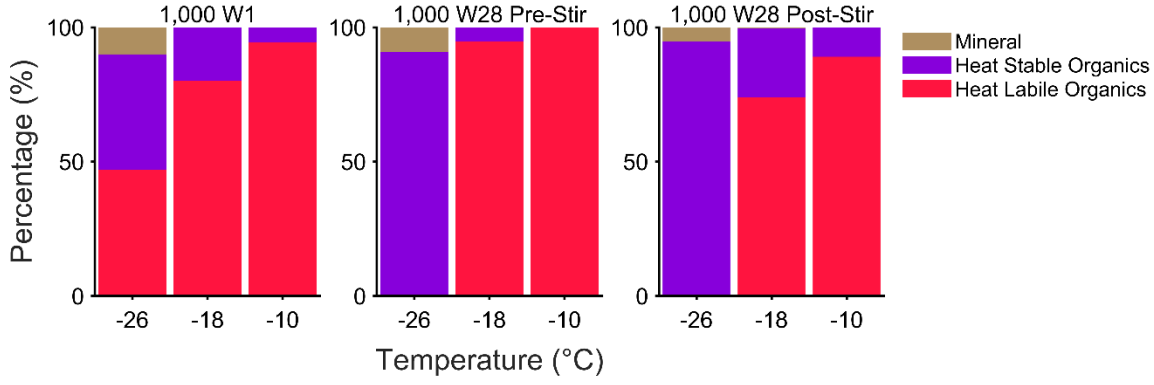

Figure A.2.8. Ice-nucleating particle (INP) compositional histograms for the 1000-year-old (S69CM) permafrost core experiment. Day 1 water (W) is shown on the left, pre-stir day 28 water in the center, and post-stir day 28 water on the right. Heat labile organics (INPs destroyed

after 95 °C heating) are in red, heat stable organics (INPs additionally destroyed after hydrogen peroxide digestion) are in purple, and the remainder (presumed mineral INPs) are shown in tan.

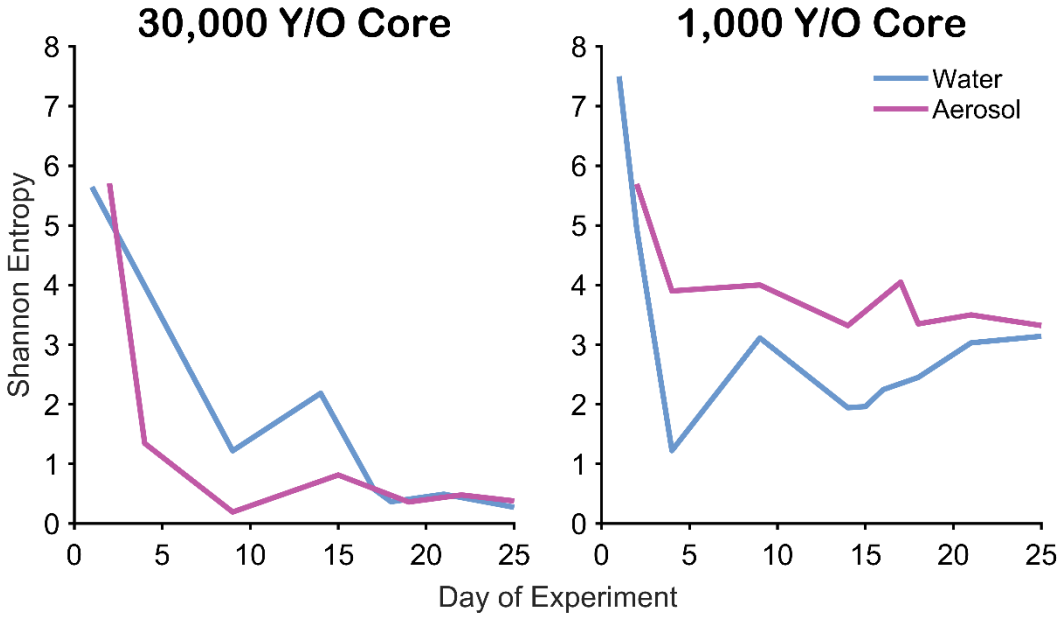

Figure A.2.9. Alpha diversity (Shannon Index) as a function of time for the 30,000-year-old (OT83L; left) and 1000-year-old (S69CM; right) permafrost core experiments. The colors of the lines denote sample type: water (blue) or aerosol (purple).

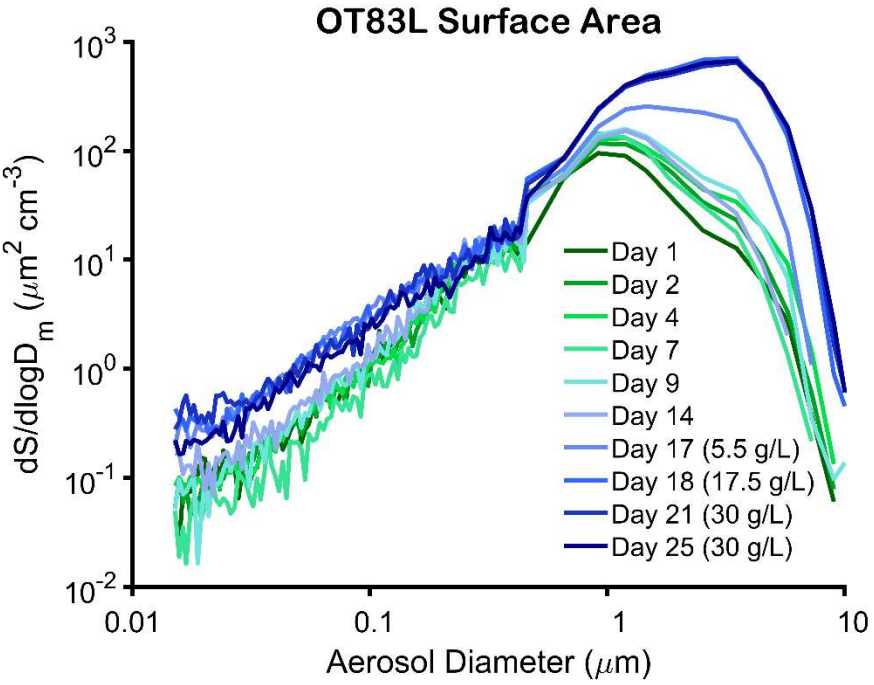

Figure A.2.10. Aerosol surface area size distributions for the 30,000-year-old (OT83L) permafrost core experiment. Points are colored by day of experiment. Salinity of tank water is listed in g/L in the legend starting at day 17, when artificial sea salts were added to the tank.

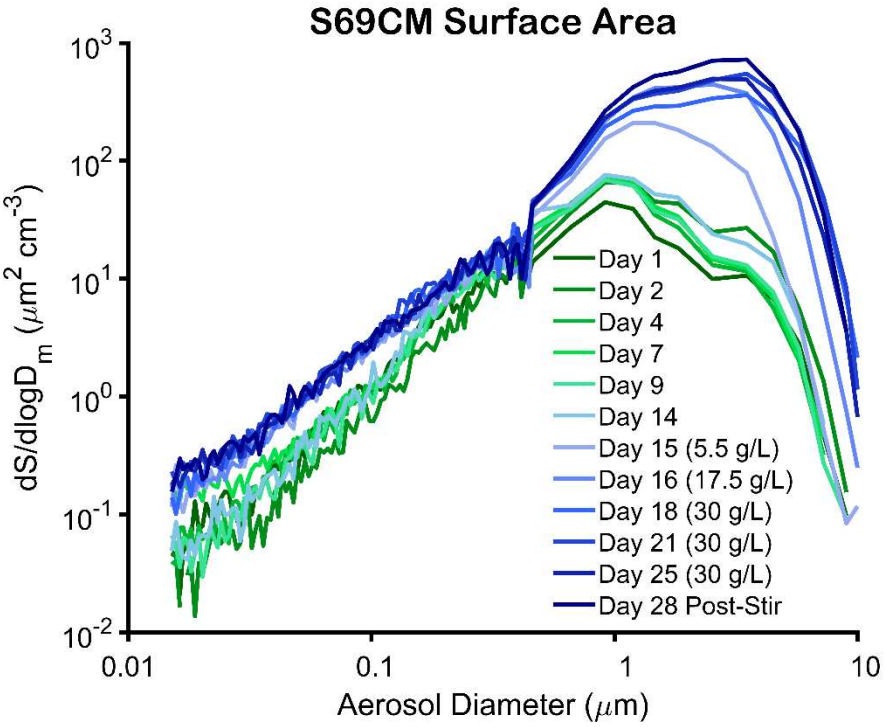

Figure A.2.11. Aerosol surface area size distributions for the 1000-year-old (S69CM) permafrost core experiment. Points are colored by day of experiment. Salinity of tank water is listed in g/L in the legend starting at day 15, when artificial sea salts were added to the tank.

A.3 Appendix for Chapter 4

Table A.3.1. Average INP concentration at -15 °C for all aerosol and potential source samples. TKL=Thermokarst lake.

Source	*Mean INP Concentration (-15 °C)*
Aerosol	$4.4*10^{-2}$ L^{-1}
TKL	$1.2*10^{5}$ mL^{-1}
Lagoon	$3.1*10^{4}$ mL^{-1}
Seawater	$1.7*10^{4}$ mL^{-1}
Active Layer	$3.6*10^{8}$ g^{-1}
Permafrost	$1.1*10^{8}$ g^{-1}
Sediment	$3.2*10^{7}$ g^{-1}
Vegetation	$2.0*10^{6}$ g^{-1}
Ice Wedge	$1.7*10^{5}$ g^{-1}

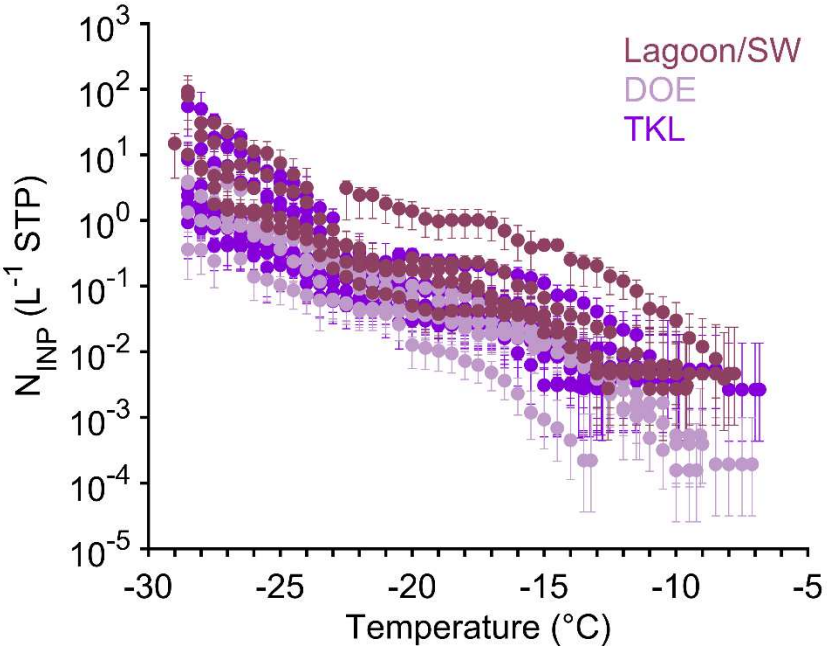

Figure A.3.1. Complete INP-temperature spectra for all aerosol samples, colored by environment collected (SW=seawater; DOE=fixed site; TKL=thermokarst lake). 95% confidence intervals are plotted (any confidence intervals overlapping with 0 are not shown).

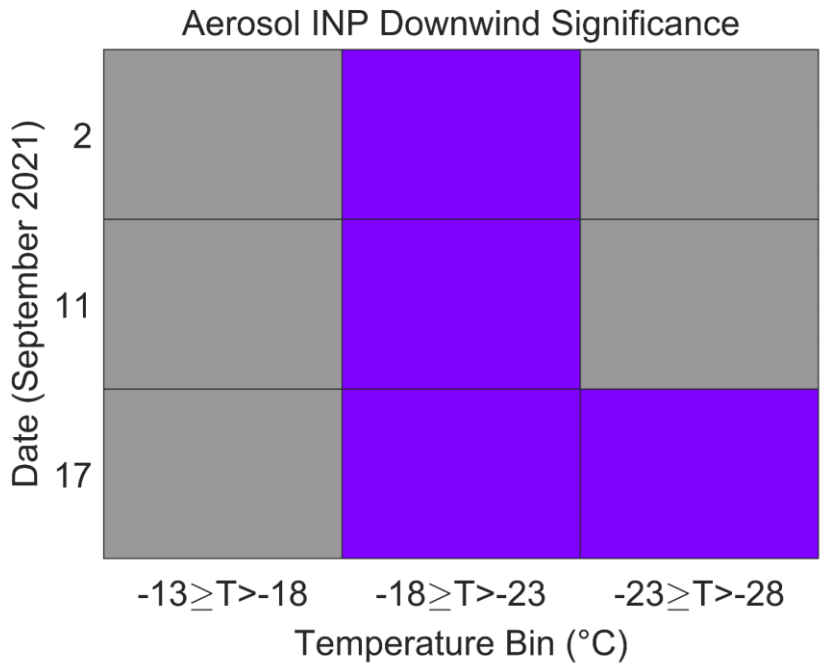

Figure A.3.2. A heatmap indicating results of statistical testing for downwind versus upwind aerosol INP concentrations. Purple represents an increase over upwind at 95% confidence, while gray represents no difference at 95% confidence.

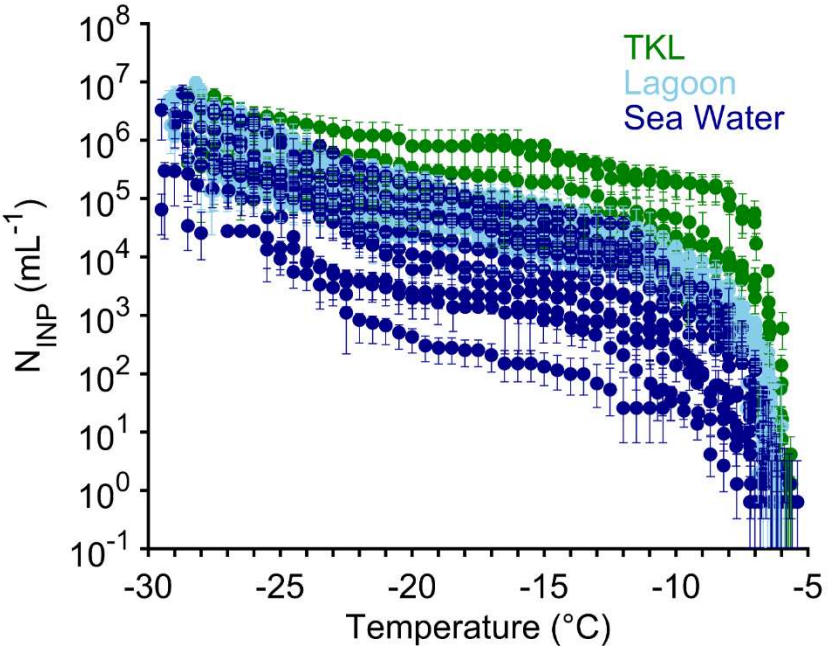

Figure A.3.3. Complete INP-temperature spectra for all water samples (thermokarst lake water: green; lagoon: light blue; seawater: dark blue). 95% confidence intervals are plotted (any confidence intervals overlapping with 0 are not shown).

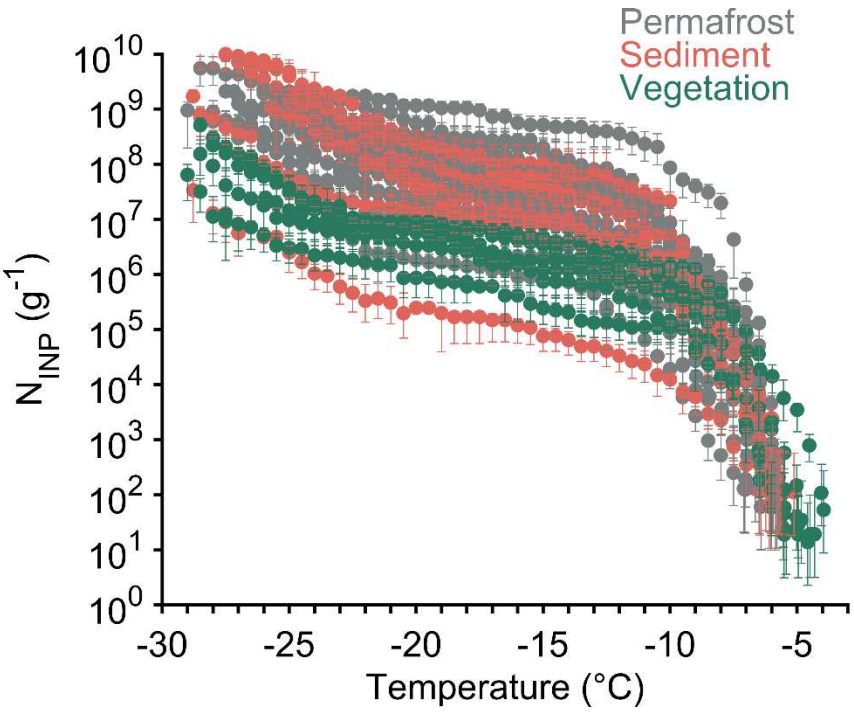

Figure A.3.4. Complete INP-temperature spectra for terrestrial samples (permafrost: gray; sediment: salmon; vegetation: dark green). 95% confidence intervals are plotted (any confidence intervals overlapping with 0 are not shown).

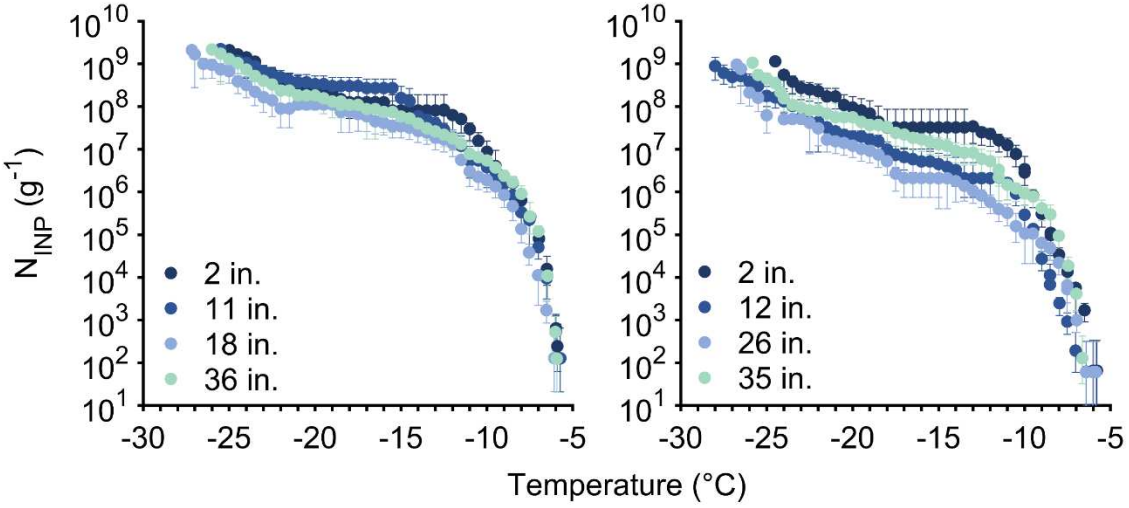

Figure A.3.5. Complete INP-temperature spectra from permafrost cores collected on September 11 (left) and September 17 (right). The different colors represent depth of sample taken in relation to the top of the permafrost core. 95% confidence intervals are plotted (any confidence intervals overlapping with 0 are not shown).

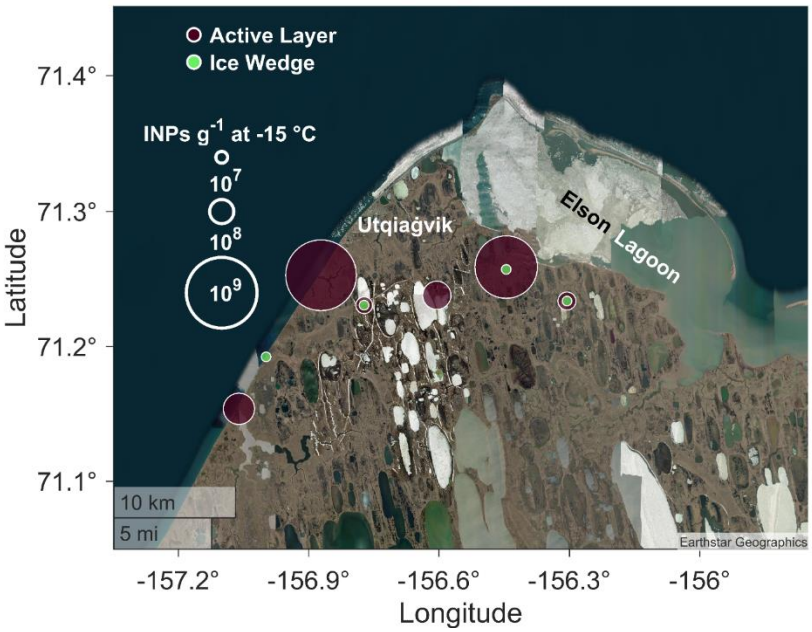

Figure A.3.6. INP concentration per g at -15 °C for active layer (maroon) and ice wedge (bright green) samples. The size of the markers corresponds to the INP concentration.

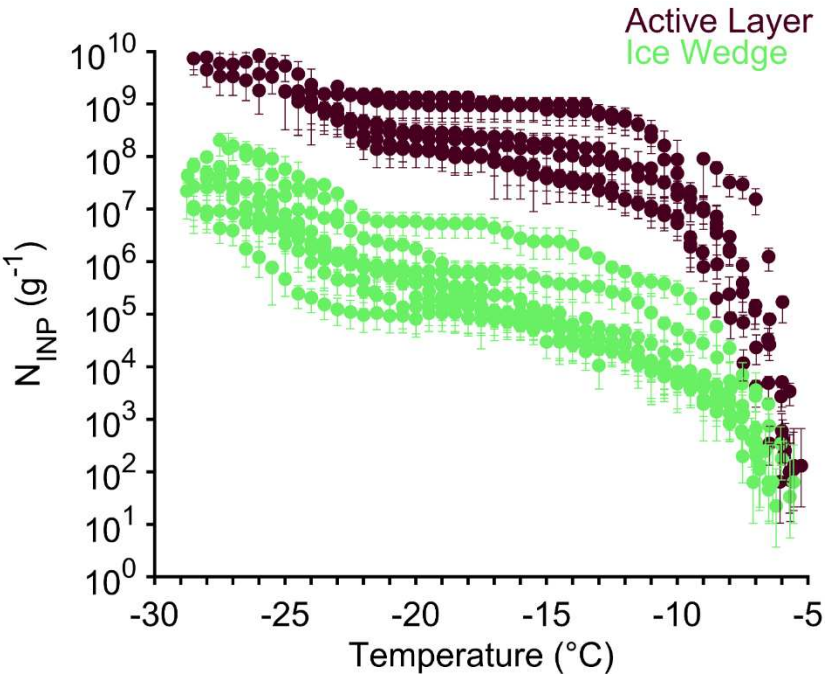

Figure A.3.7. Complete INP-temperature spectra for terrestrial samples (active layer: maroon; ice wedge: bright green). 95% confidence intervals are plotted (any confidence intervals overlapping with 0 are not shown).